

Rational Design of Two-Dimensional Transition Metal Carbide/Nitride (MXene) Hybrids and Nanocomposites for Catalytic Energy Storage and Conversion

Kang Rui Garrick Lim¹, Albertus D. Handoko¹, Srinivasa Kartik Nemani², Brian Wyatt², Hai-Ying Jiang³, Junwang Tang⁴, Babak Anasori^{2}, Zhi Wei Seh^{1*}*

¹ Institute of Materials Research and Engineering, Agency for Science, Technology and Research (A*STAR), 2 Fusionopolis Way, Innovis, Singapore 138634, Singapore

² Department of Mechanical and Energy Engineering, and Integrated Nanosystems Development Institute, Indiana University-Purdue University Indianapolis, Indianapolis, 46202, USA

³ Key Lab of Synthetic and Natural Functional Molecule Chemistry of Ministry of Education, the Energy and Catalysis Hub, College of Chemistry and Materials Science, Northwest University, Xi'an 710127, P. R. China

⁴ Department of Chemical Engineering, University College London, Torrington Place, London, WC1E 7JE, UK

Corresponding Authors

*Z. W. Seh: sehzw@imre.a-star.edu.sg

*B. Anasori: banasori@iupui.edu

ABSTRACT

Electro-, photo-, and photoelectrocatalysis play a critical role toward the realization of a sustainable energy economy. They facilitate numerous redox reactions in energy storage and conversion systems, enabling the production of chemical feedstock and clean fuels from abundant resources like water, carbon dioxide, and nitrogen. One major obstacle for their large-scale implementation is the scarcity of cost-effective, durable, and efficient catalysts. A family of two-dimensional transition metal carbides, nitrides, and carbonitrides (MXenes) has recently emerged as promising earth-abundant candidates for large-area catalytic energy storage and conversion due to their unique properties of hydrophilicity, high metallic conductivity, and ease of production by solution processing. To take full advantage of these desirable properties, MXenes have been combined with other materials to form MXene hybrids with significantly enhanced catalytic performances beyond the sum of their individual components. MXene hybridization tunes the electronic structure towards optimal binding of redox active species to improve intrinsic activity, while increasing the density and accessibility of active sites. This review outlines recent strategies in the design of MXene hybrids for industrially relevant electrocatalytic, photocatalytic, and photoelectrocatalytic applications such as water splitting, metal-air/sulfur batteries, carbon dioxide reduction, and nitrogen reduction. By clarifying the roles of individual material components in the MXene hybrids, we provide design strategies to synergistically couple MXenes with associated materials for highly efficient and durable catalytic applications. We conclude by highlighting key gaps in the current understanding of MXene hybrids to guide future MXene hybrid designs in catalytic energy storage and conversion applications.

KEYWORDS: MXenes, hybrid material, electrocatalysis, photocatalysis, water splitting, CO₂ reduction, N₂ reduction, energy conversion, batteries, energy storage

The advancement of our energy economy using cost-effective, accessible, and environmentally responsible means is critical to ensure a sustainable supply to meet the burgeoning global energy demand.^{1,2} In this regard, catalysts play a critical role in enabling efficient energy conversion of earth-abundant resources such as water, carbon dioxide, and nitrogen to clean fuels and chemical feedstock precursors such as hydrogen, hydrocarbons, and ammonia.³⁻⁵ Durable and active catalysts are also required to facilitate long-term energy storage in H₂ fuel cells and batteries of varying architectures.⁶⁻⁸ Presently, precious platinum group metals (PGMs) such as Pt, their alloys, and related structures (PtIr, IrO₂, RuO₂, *etc.*) are widely regarded as the most effective catalysts for the hydrogen evolution reaction (HER), oxygen reduction reaction (ORR), and oxygen evolution reaction (OER), respectively.⁹⁻¹¹ The widespread commercialization and adoption into energy storage and conversion devices however, can only be realized with alternative earth-abundant and cost-effective catalysts with high catalytic activity and stability.^{3,4}

Since their discovery in 2011, more than 30 different compositions belonging to a family of two-dimensional (2D) transition metal carbides, nitrides, and carbonitrides (MXenes) have been successfully synthesized, with many other stable compositions predicted theoretically.¹²⁻¹⁴ MXenes have attracted significant attention as promising catalysts due to their unique combination of physical and chemical properties.¹³⁻¹⁵ They possess high metallic electrical conductivity with hydrophilicity similar to graphene oxide, and mechanical strength of transition metal (TM) carbides/nitrides. MXenes can be easily scaled, because of their solution processible top-down synthesis, into stable colloidal solutions or flexible films for energy applications (electrocatalysts, batteries, and supercapacitors) and beyond (flexible electronics, sensors, and electromagnetic shielding).^{13,14,16} In addition to their high metallic conductivity to facilitate efficient electronic charge transport at the electrode-electrolyte interface, the large-area 2D basal planes of MXenes

are HER-active,^{17–19} unlike the widely studied semiconducting 2H-MoS₂ with HER activity restricted only to their edges.²⁰ Separate theoretical calculations have also predicted a variety of MXenes for efficient photocatalytic (PC), electrocatalytic (EC), and photoelectrocatalytic (PEC) reactions such as the hydrogen evolution (HER), oxygen evolution (OER), oxygen reduction (ORR), carbon dioxide reduction (CO₂RR), and nitrogen reduction (N₂RR) reactions.^{21–25} MXenes have a general formula of M_{n+1}X_nT_x where n = 1–4, M = early transition metal such as Ti, V and Mo, X = C and/or N and T_x = surface termination groups such as –O, –OH, –F, and –Cl, which are formed on the outer M basal plane during the synthesis process.^{26–28} For consistency, a standardized notation of M_{n+1}X_nT_x will be used to describe MXenes throughout this review.

MXenes are most commonly produced through the top-down separation of layered MXene sheets from their parent layered ternary TM carbide MAX phase materials (“A” = group 13 or 14 elements such as Al, Si, and Ga) by aqueous wet selective etching and removal of A-group atom layers.^{12,27} The A-group atom layers are preferentially etched away as the M-A bonds binding the MXene layers together in the MAX structure are chemically more active than the stronger M-X bonds within the MXene sheets.^{29–31} This scalable top-down etching process to produce MXenes is most commonly conducted under ambient conditions with gentle heating using hydrofluoric acid (HF) directly, or HF produced *in-situ* from F-containing etchants.^{32–35} After etching away the A-group atom layers, the exposed outer M basal planes of the etched MXene sheets are functionalized with hydrophilic surface termination groups (T_x) such as –O, –OH, –F and –Cl due to the aqueous F- or Cl-containing etchants.^{14,31,36} The surface chemistry of MXenes can be controlled to some extent by the selective wet etching conditions or through post-etch processing to optimize binding toward specific electroactive species for efficient catalysis.^{18,37} Subsequent delamination and exfoliation separates the weakly bound MXene sheets into single- or few-layered MXenes using

intercalants,^{38,39} exposing large MXene surface areas for catalysis and to serve as a conductive support for co-catalysts.

Most recently, organic and inorganic materials such as TM compounds (carbides, phosphides, chalcogenides, oxides, *etc.*), layered double hydroxides (LDHs), metal-organic frameworks (MOFs), carbon-based (C-based) materials such as graphitic carbon nitride (*g*-C₃N₄) and carbon nanotubes (CNTs), quantum dots (QDs), metallic alloys, and polymers have been combined with MXenes to form MXene hybrids and composites.^{40–45} These MXene hybrids exhibit significantly enhanced catalytic activities and stability beyond the sum of their individual components, due to synergistic coupling between MXenes and the secondary materials. The strong and intimate coupling increases the density of catalytically active sites, and optimizes these active sites toward binding of electrochemically active species for efficient catalysis.^{40–45} The hybrid mix can perform a variety of functions such as a large-area, electronically conductive support, electronic structure modulator, and co-catalyst,^{40–45} as we discuss in this review. Indeed, MXene hybrids have garnered significant traction since 2014, with the number of papers published doubling year-on-year, and more than half (168) of the publications on MXene hybrids in 2019 (312) focused on catalysis and energy storage (**Figure 1a**). The breakdown of the many different secondary materials integrated with MXenes to form MXene hybrids also illustrates the versatility of MXene hybrids to meet the demands of a wide spectrum of applications (**Figure 1b**), especially in the many important catalytic reactions of interest (**Figure 1c**).

In this review, we summarize recent strategies in the design of MXene hybrids for industrially relevant EC, PC, and PEC applications in energy storage (metal-air/sulfur batteries catalyzed by OER, ORR, and sulfur redox reactions) and conversion (water splitting catalyzed by OER and HER). We clarify the roles of each material component in the MXene hybrids for their

intended applications to provide a set of rational design rules to synergistically couple MXenes with the relevant secondary materials for highly efficient and durable catalysis. The feasibility of MXene hybrids for important emerging catalytic applications such as CO₂RR and N₂RR is then discussed. The review concludes by highlighting key gaps in the current fundamental understanding of MXene hybrids and provides an outlook to inform forthcoming MXene hybrid designs in catalytic energy storage and conversion applications.

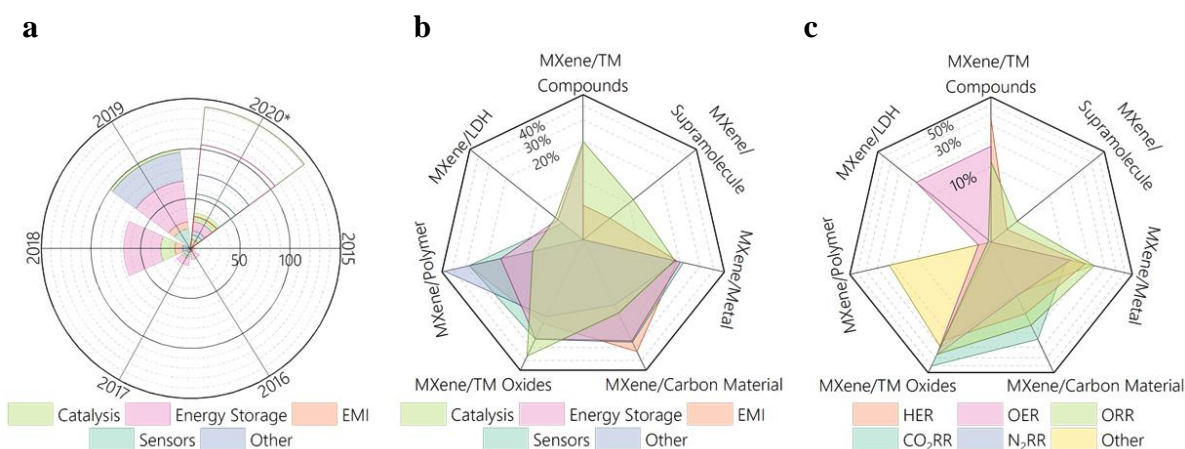


Figure 1. (a) Graphical representation of the total publications to date (*March 2020) on MXene hybrids for various applications on Web of Science. Color filled radial bars represent different applications, while uncolored radial bars are the projected number of publications for the rest of 2020. (b) Spider plot survey of all MXene hybrid publications to date, illustrating the type of MXene hybrids most used for specific applications. For example, 31% of all published MXene hybrid papers for catalysis used MXene/TM oxides hybrids. (c) Spider plot survey of all MXene hybrid publications for catalysis to date, illustrating the type of MXene hybrids most used for various catalytic reactions of interest. For instance, MXene/TM compound hybrids account for 32% of all HER-related papers using MXene hybrids. Raw data used for each plot is provided in **Tables S1a–S1c** respectively.

DESIGN STRATEGIES FOR MXENE HYBRIDS AND COMPOSITES

The layered nature and variety in surface T_x groups of MXenes³⁰ afford a high degree of tuneability in their properties^{13–15} and hence, strong compatibility with a wide range of secondary materials to produce MXene hybrids with high catalytic performances. MXene hybrids with precise and well-formed interfaces have been reported to improve charge transfer,^{46–48} mitigate volumetric expansion in batteries^{49,50} and resist secondary material agglomeration through confinement effects.^{51–53} In this review, we define a MXene hybrid/composite as a material comprising MXenes and at least one other non-MXene material, either organic or inorganic. This is a more general term than MXene heterostructures, which are produced when a material is grown onto MXenes in a repetitive layered manner (see **Vocabulary** for full definition of MXene hybrid/composite and MXene heterostructures).

A growing number of MXenes have been integrated with non-MXene secondary materials to form MXene hybrids, realizing unique material properties and enhanced performance. These MXenes include, but are not limited to, Ti_2CT_x ,⁵⁴ $Ti_3C_2T_x$,^{55,56} Ti_3CNT_x ,⁵⁶ V_2CT_x ,^{57,58} $V_4C_3T_x$,^{59,60} Nb_2CT_x ,^{61,62} Nb_4CT_x ,⁶² $Mo_{1.33}CT_x$,⁶³ Mo_2CT_x ,^{64–66} $Mo_2TiC_2T_x$,⁶⁷ and $Ta_4C_3T_x$.⁶⁸ Since rapid electronic charge transfer is crucial to efficient electrocatalysis, $Ti_3C_2T_x$ is most extensively incorporated into MXene hybrids for electrocatalytic applications, due to their high electrical conductivity (up to 15000 S cm^{-1})⁶⁹ as compared to other MXenes. The wide diversity in MXene-compatible secondary materials (TM compounds, supramolecular structures, C-based materials, and metals), coupled with the many different synthetic methods to form these hybrids (**Figure 2**), illustrates the boundless potential for MXene hybrids and composites to meet the various demands in energy-related applications and beyond.^{40–44}

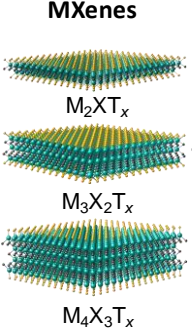
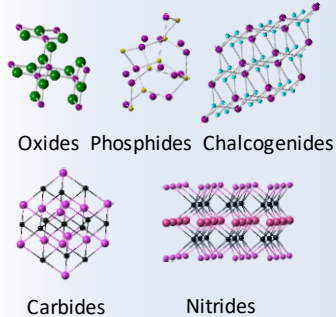
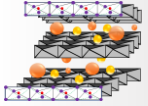
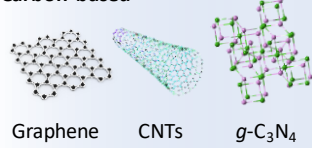
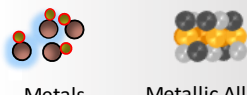
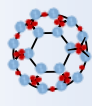
	Secondary Materials	Processing method	Applications
MXenes 	Transition Metal Compounds  Oxides Phosphides Chalcogenides Carbides Nitrides	<i>In situ</i> oxidation/sulfidation Hydro/solvothermal synthesis Solution processing Electrostatic self-assembly Electrodeposition Dropcasting	Water splitting: HER/OER Metal-air battery: OER/ORR Metal-S battery: S cathode CO ₂ RR, N ₂ RR
	Layered Double Hydroxides 	Hydro/solvothermal synthesis Electrostatic self-assembly	Water splitting: HER/OER Metal-air battery: OER CO ₂ RR
	Carbon-based  Graphene CNTs g-C ₃ N ₄	Solution processing Electrostatic self-assembly Physical deposition (CVD, ALD)	Water splitting: OER Metal-air battery: OER/ORR Metal-S battery: S cathode CO ₂ RR, N ₂ RR
	Element/ Multi-element  Metals Metallic Alloys	Electrostatic self-assembly Solution processing (self-reduction stabilization)	Water splitting: HER/OER Metal-air battery: OER/ORR CO ₂ RR, N ₂ RR
	Supramolecular Structures  MOFs	Solution processing Electrostatic self-assembly	Water splitting: OER CO ₂ RR

Figure 2. Three different MXene types combined with secondary materials to form MXene hybrids. Cyan, dark grey and yellow spheres represent M, X, and T_x respectively. Common processing methods to fabricate the MXene hybrids and their catalytic applications are also listed.

The first step to designing efficient and durable MXene hybrids for energy storage and conversion is the deliberate choice of secondary material and the processing method. Highly interconnected charge transfer networks for electronic transport, a large-area/hierarchical/porous network for mass transfer of electroactive species, and an abundance of catalytically active sites, are all highly desirable properties in MXene hybrids for catalytic applications.^{40–44} Additionally, a

strongly and chemically coupled MXene hybrid synergistically increases the hybrid's intrinsic activity, while secondary material dislodgement or degradation during electrocatalysis is prevented, especially at large applied potentials.⁷⁰ MXene hybrids are synthesized through three main routes: (1) *in-situ* conversion of the MXenes' surface structure through oxidation (*e.g.* $\text{Ti}_3\text{C}_2\text{T}_x$ to TiO_2)⁵⁵ or sulfidation (*e.g.* $\text{Mo}_2\text{TiC}_2\text{T}_x$ to MoS_2),⁶⁷ (2) reactive chemical formation of secondary materials on MXenes, using methods such as hydro/solvothermal synthesis,^{47,71,72} solution processing,⁷³ or deposition,⁷⁴⁻⁷⁹ and (3) non-reactive assembly of secondary materials by drop-casting⁸⁰ and adsorption processes.⁵⁶ In this section, we summarize the common and unique features for each of these three synthetic routes for MXene hybrid formation, highlighting their suitability, advantages, and shortfalls (and how they have been overcome).

***In-situ* conversion of MXene surfaces to form MXene hybrids.** The layered structure of MXenes leaves the TM atomic layers exposed on their outer basal planes (left schematics in **Figure 2**). These TM layers are highly oxophilic^{81,82} and hence prone to surface reactions such as oxidation (*e.g.* Ti to TiO_2 in $\text{Ti}_3\text{C}_2\text{T}_x$)⁵⁵ or sulfidation (*e.g.* Mo to MoS_2 in $\text{Mo}_2\text{TiC}_2\text{T}_x$).⁶⁷ In these processes, the MXenes' surface is transformed, either partially or fully, to form a second material. We thus refer to this process as an *in-situ* conversion of the MXenes' surface. The advantage of surface conversion is clear: the second material is strongly integrated with MXenes, forming a hybrid interface.⁶⁷ Since the MXene surfaces are directly involved in the conversion, no additional TM source is required for the secondary material growth. Consequently, this process is self-limited by the MXenes' surface exposure,⁶⁷ minimizing the issue of excessive secondary material nucleation and growth that would otherwise restrict access of reactants to catalytically active sites.

Most surface conversions involve the treatment of MXenes with gases such as O_2 or CO_2 for oxidation, or H_2S for sulfidation. These processes are typically conducted at elevated

temperatures to form highly crystalline secondary materials on MXene surfaces.^{67,83} Hence, there exists a delicate balance between the extent of MXene conversion, and preserving the MXenes' structural integrity that can be compromised in oxidizing environments at high temperatures.⁸³ The range of secondary materials that can be grown through MXene surface conversion is also limited by the chemical identity and reactivity of the MXenes' TM surface exposed. For instance, the Ti surface of $\text{Ti}_3\text{C}_2\text{T}_x$ implies that only Ti-based secondary materials can be grown through this conversion route. In this regard, we anticipate that disordered solid solution MXenes such as $(\text{Ti},\text{V})_2\text{CT}_x$ and $(\text{Mo},\text{V})_4\text{C}_3\text{T}_x$, denoted by the chemical formula $(\text{M}',\text{M}'')_{n+1}\text{C}_n\text{T}_x$, will be interesting for growth of secondary materials through this surface conversion route, since they possess two different TMs at the surface in a random distribution.⁸⁴

Thermally-assisted oxidation is an efficient one-step method to produce MXene/TM oxide hybrids.^{41,43} MXene surface oxidation is most commonly employed in Ti-based MXenes to form TiO_2 photocatalysts,⁵⁵ although oxidation can be also applied to V, Nb, and Mo-based MXenes to form their respective oxides.^{58,62,82} *In-situ* oxidation is achieved through flash oxidation (1150 °C, 30 s),⁵⁵ prolonged oxidation from calcination (350–650 °C),^{85–87} hydro/solvothermal processes (120–220 °C),^{47,78,88–91} or CO_2 oxidation (500–900 °C).^{62,83} Control over the MXenes' surface T_x groups prior to oxidation is crucial, since different surface terminations have resulted in morphological differences in the oxides formed. Li *et al.* reported that calcining untreated $\text{Ti}_3\text{C}_2\text{T}_x$ with –O, –F, and –OH terminations resulted in larger anatase TiO_2 nanoparticles (NPs) with exposed (001) planes, compared to the smaller and more spherical anatase TiO_2 NPs formed by calcining $\text{Ti}_3\text{C}_2\text{T}_x$ with primarily –OH terminations.⁸⁷ With precise control and optimization over the heat treatment conditions, a variety of functional TiO_2 /MXene hybrids can be formed with high PC activity toward water splitting, CO_2RR , and N_2RR .^{87,89}

For example, $\text{Ti}_3\text{C}_2\text{T}_x$ has been oxidized to varying degrees to produce hybrids ranging from $\text{Ti}_3\text{C}_2\text{T}_x/\text{TiO}_2$ (partial MXene surface oxidation) to C/TiO_2 (complete MXene oxidation).^{83,92,93} While controlled partial oxidation retained some of the Ti-C layered structure from the MXene precursor,⁹² complete oxidation degraded the entire MXene structure.⁸³ The latter resulted in a Ti-O structure supported by C-C bonded layers, in the form of TiO_2 on 2D carbon sheets (C/TiO_2).^{83,94} The morphology and phase of the resulting TiO_2 NPs was also highly dependent on the treatment conditions.^{83,95} This is important as the identity and quantity of exposed facets, together with the distribution and phase of TiO_2 formed, directly influences PC activity.^{47,93} Ghassemi *et al.* utilized *in-situ* environmental transmission electron microscopy (TEM) and Raman spectroscopy to elucidate the oxidation mechanism of $\text{Ti}_3\text{C}_2\text{T}_x$ under various conditions (**Figure 3a**).⁹⁶ In flash oxidation, the exposed Ti basal planes serve as nucleating sites to form a thin 2D anatase TiO_2 film. Subsequently, the 2D TiO_2 nuclei grew vertically to form 3D TiO_2 anatase NPs from the outward migration of inner Ti layer atoms. Conversely, a slower heating process yielded rutile TiO_2 NPs without the formation of the intermediate anatase phase. Experimentally, anatase TiO_2 was formed from partial $\text{Ti}_3\text{C}_2\text{T}_x$ oxidation at lower temperatures,^{47,62,83} while rutile TiO_2 was mostly formed through near-complete oxidation of $\text{Ti}_3\text{C}_2\text{T}_x$, often resulting in degradation of the Ti-C MXene interior.^{83,97}

MXene/TM chalcogenides hybrids have also been formed through *in-situ* sulfidation of MXene surfaces.⁶⁷ Although TM chalcogenides are HER-active, they are less electrically conductive than MXenes. Thus, MXene/TM chalcogenides hybrids benefit from (1) significantly improved charge transfer kinetics due to the metallic MXenes, and (2) an increased number of active sites with TM chalcogenides acting as co-catalysts in the hybrid structure.^{70,89} In ordered double TM (Mo, Ti) MXenes such as $\text{Mo}_2\text{TiC}_2\text{T}_x$ and $\text{Mo}_2\text{Ti}_2\text{C}_3\text{T}_x$, Mo atoms preferentially

occupy the surface (outer) basal planes.^{98,99} This led to a follow-up study on the *in-situ* sulfidation of the Mo-rich surface of $\text{Mo}_2\text{TiC}_2\text{T}_x$ to form the $\text{MoS}_2@\text{Mo}_2\text{TiC}_2\text{T}_x$ hybrid.⁶⁷ After an initial liquid mixing process to incorporate sulfur on and within the $\text{Mo}_2\text{TiC}_2\text{T}_x$ sheets, heat treatment in an inert Ar atmosphere with additional elemental sulfur converted the surface Mo-O motifs to 2H- MoS_2 to form the final $\text{MoS}_2@\text{Mo}_2\text{TiC}_2\text{T}_x$ hybrid (**Figure 3b**). The $\text{Mo}_2\text{TiC}_2\text{T}_x$: MoS_2 ratio was also tuned from 1 : 0.62 and 1 : 2.19 by adjusting the treatment temperature from 500 to 700 °C. Furthermore, the intimate interfacial relationship was evident in the stacking of thin 2H- MoS_2 on the MXenes (**Figures 3c and 3d**). This 2H- MoS_2 on MXene hybrid exhibited an increased specific capacity when used as a lithium ion anode, which was attributed to the incorporation of MoS_2 . We speculate that ordered double TM MXenes with a Mo-rich surface, such as $\text{Mo}_2\text{TiC}_2\text{T}_x$ and $\text{Mo}_2\text{Ti}_2\text{C}_3\text{T}_x$, might be better suited for sulfidation compared to single TM MXenes (Mo_2CT_x), due to the presence of a conductive inner Ti layer after surface Mo sulfidation to MoS_2 .^{98–100}

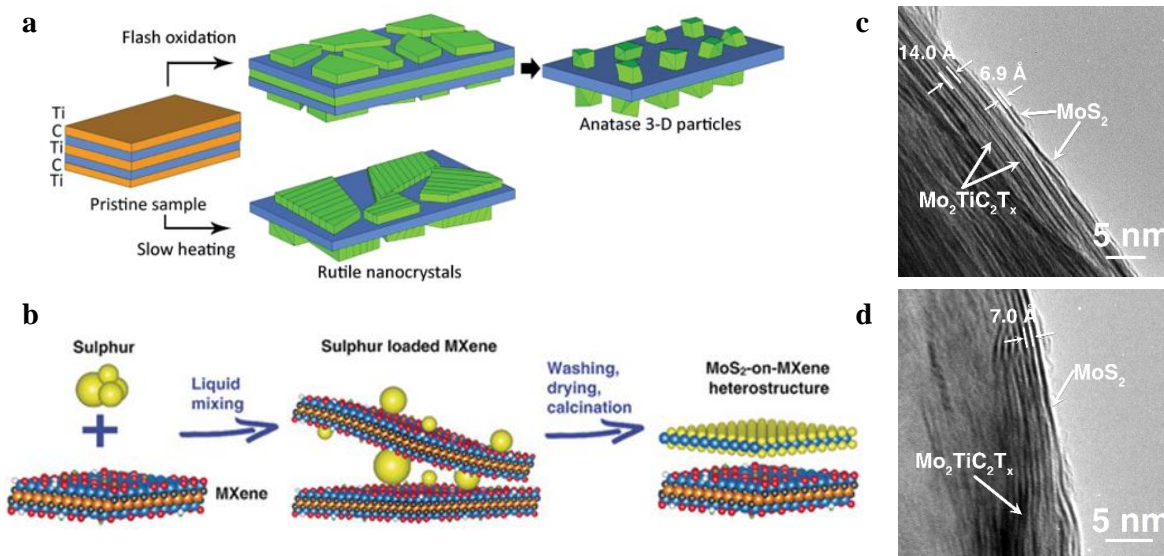


Figure 3. *In-situ* conversion of MXene surfaces to form MXene hybrids. (a) Oxidation mechanism of $\text{Ti}_3\text{C}_2\text{T}_x$ to form TiO_2 under different oxidation conditions. Adapted with permission from ref ⁹⁶. Copyright 2014 Royal Society of Chemistry. (b) *In-situ* sulfidation of $\text{Mo}_2\text{TiC}_2\text{T}_x$ and cross-sectional TEM image of the resulting $\text{MoS}_2@\text{Mo}_2\text{TiC}_2\text{T}_x$ hybrid heat treated at (c) 500 °C and (d) 700 °C. Adapted with permission from ref ⁶⁷. Copyright 2018 Wiley-VCH.

***In-situ* reactive formation of secondary materials onto MXenes to form MXene hybrids.** Compared to *in-situ* conversion of MXene surfaces, this approach allows for the incorporation of wider material compositions, independent of the MXenes' TM surface identity. Here, MXenes can be viewed as substrates, not reactants, for secondary material growth. The main advantage of *in-situ* reactive formation is the preservation of the MXenes' integrity in the synthesis process, as virtually any precursors (cationic, anionic, or metallic) can be utilized for the nucleation and growth of the secondary material. With this process, it is possible to form hybrids with high secondary material to MXene ratios as reported for Bi₂WO₆/Ti₃C₂T_x (Bi₂WO₆ : MXene layer height ≈3:1)¹⁰¹ or MoSe₂/Ti₃C₂T_x.¹⁰² Thus, this strategy is most useful if the secondary material is catalytically active, since large quantities can be grown on the large surface area of MXenes. Typical synthesis routes available for this strategy include hydro/solvothermal synthesis,^{47,72,103–105} solution processing,⁷³ and deposition (physical or electro/photo-induced).^{74–79} Most of these synthetic routes, except physical deposition, rely on the van der Waals⁵³ or ionic/electrostatic¹⁰⁶ interactions between the negatively charged MXene surfaces (from the T_x groups) and positively charged secondary material precursors.⁴¹ After initial adsorption, the secondary materials are formed *in-situ* onto the MXenes' surface through chemical processing with additional reactants and/or heat treatment.^{101,107}

Hydro/solvothermal synthesis exploits the interactions between the liquid solvent, mineralizer (*e.g.* base), and precursor moieties at elevated temperatures and pressures, mimicking the processes occurring at the Earth's crust.¹⁰⁸ This synthesis route is a simple and scalable way to synthesize many different types of secondary materials (**Figure 2**) in various morphologies,^{109–111} and is versatile enough to yield solid solution mixtures¹¹² or different material allotropes¹¹³ by carefully tuning the processing conditions. Although hydrothermal synthesis is typically directed

at bulk material synthesis, heterogeneous nucleation and epitaxial films can be achieved by adding suitable substrates.^{114,115} A major challenge in this route is aggressive corrosion by water molecules or –OH moieties at elevated temperatures and pressures, which may induce undesired damage to the MXenes.⁷⁰ This can be partially alleviated by replacing water with non-aqueous solvents, thus the term solvothermal.¹¹⁶ Wu *et al.* proposed the addition of glucose to the solvent to protect MXenes from oxidative damage.⁷⁰ During the reaction, glucose molecules were adhered on MXene surfaces *via* hydrogen bonding and converted to a simple hydrocarbon coating (**Figure 4a**), which was subsequently converted to carbon with thermal treatment. The carbon coating was shown to improve charge transport characteristics and prevent secondary material aggregation.¹¹⁷

Solution processing at ambient pressure is an alternative to hydro/solvothermal treatment, since the gentler reaction conditions can reduce unwanted MXene damage.⁷³ To achieve controlled growth, metallic precursors are first adsorbed onto MXenes *via* a mixing process. Thereafter, anionic precursors are introduced to chemically react and form the desired secondary materials on the MXene surface. An additional annealing step is usually required to complete the reaction and enhance the integration of the secondary material on MXenes.^{118–120} A variety of inorganic materials such as TM oxides,¹²¹ phosphides,¹²² chalcogenides,¹¹⁸ nitrides,¹²³ MOFs,¹²⁴ perovskites,¹²⁵ and LDHs^{109,126} have been hybridized with MXenes this way (**Figure 2**). Yu *et al.* prepared FeNi-LDH@Ti₃C₂T_x hybrids by the co-precipitation of Fe³⁺ and Ni²⁺ cations on negatively charged Ti₃C₂T_x sheets for EC OER (**Figure 4b**).¹²⁶ The abundance of –OH and –F surface groups facilitated the initial electrostatic nucleation and subsequent growth of LDH sheets on MXenes with minimal oxidation. Additionally, secondary materials that are initially electrostatically adsorbed and formed on MXene surfaces, can be chemically converted to other more catalytically active materials.^{119,120} For instance, zeolitic imidazolate framework-67 (ZIF-67)

self-assembled on $\text{Ti}_3\text{C}_2\text{T}_x$ was etched to NiCo-LDH by ultrasonication after the addition of Ni^{2+} precursors. Then, heat treatment and sulfidation of the mildly OER-active NiCo-LDH/ $\text{Ti}_3\text{C}_2\text{T}_x$ yielded NiCoS/ $\text{Ti}_3\text{C}_2\text{T}_x$ MXene hybrids with significantly enhanced OER activity (**Figure 4c**).¹²⁰

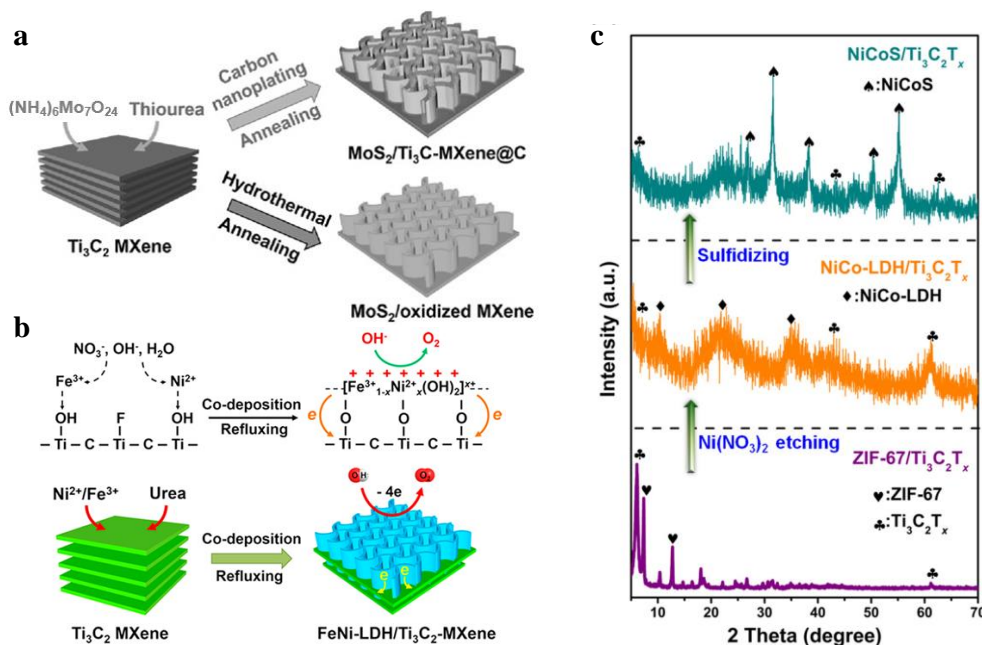


Figure 4. *In-situ* formation of secondary materials on MXenes to form MXene hybrids. (a) Carbon nanoplating to resist MXene oxidation during hydrothermal treatment. Adapted with permission from ref ⁷⁰. Copyright 2017 Wiley-VCH. (b) *In-situ* electrostatic self-assembly of FeNi-LDH/ $\text{Ti}_3\text{C}_2\text{T}_x$ hybrid. Adapted with permission from ref ¹²⁶. Copyright 2017 Elsevier Ltd. (c) X-ray diffraction (XRD) spectra showing the conversion of $\text{ZIF-67}/\text{Ti}_3\text{C}_2\text{T}_x$ to $\text{NiCoS}/\text{Ti}_3\text{C}_2\text{T}_x$ hybrid. Adapted with permission from ref ¹²⁰. Copyright 2018 American Chemical Society.

Finally, MXene hybrids can be formed *via* various deposition methods. Deposition methods are generally non-invasive, controlled, and a more conformal way of fabricating MXene hybrids and heterostructures as compared to the random assembly methods of *in-situ* conversion and self-assembly. Secondary materials have been deposited on MXene surfaces through atomic layer deposition (ALD),^{79,127–130} electro-,^{76,77,131,132} or photodeposition.^{78,133} MXenes have been used as substrates for ALD and chemical vapor deposition (CVD) of secondary material precursors to grow TM oxides,⁷⁹ metal NPs,¹²⁷ CNTs,¹²⁸ and inorganic NPs.¹²⁹ These techniques promote strong interfacial bonding due to *in-situ* hybrid formation at elevated temperatures,^{128,129} which

promotes charge transfer for electrocatalysis.¹³⁰ While ALD and CVD are useful for atomic-scale studies at the MXene hybrid interface,⁶⁵ these methods may not be viable to produce hybrids for electrocatalysis at larger scales due to the cost and difficulty in scaling up.

MXene hybrids comprising TM phosphides,⁷⁴ oxides,¹³¹ metals,⁷⁶ and C-based materials^{77,132} have also been formed through electrodeposition. Electrodeposition can be used to produce MXene hybrid coatings or electrodes without the use of binders or additives, which can potentially hinder charge and mass transport during electrocatalysis.¹³² In one study, the conductive $\text{Ti}_3\text{C}_2\text{T}_x$ film was directly used as a cathode for the deposition of secondary material precursors.⁷⁶ Alternatively, other electrodeposition studies disperse both the MXenes and secondary material precursors in the electrolyte, and deposit the hybrid onto a conductive electrode such as nickel foam,¹³¹ graphite paper¹³² or nickel plate.⁷⁴ Specifically, $-\text{OH}$ surface groups on $\text{Ti}_3\text{C}_2\text{T}_x$ have been demonstrated to improve the adsorption of Sn^{4+} and Pb^{2+} ,^{134,135} which presents the possibility of tuning the T_x composition to selectively favor the electrodeposition of specific metallic precursors. Complementary to electrodeposition, photodeposition was used to reduce metallic ions to deposit metallic NPs such as Cu^{78} and Pt^{133} *in-situ* onto MXene surfaces. Photodeposition possesses an advantage over other deposition methods in that it can be used to target specific areas or facets where photo-generated electrons accumulate.¹³⁶ However, the light intensity must be controlled carefully, as very intense light irradiation has been shown to oxidize and degrade MXenes.^{137,138}

Non-reactive assembly of secondary materials onto MXenes to form MXene hybrids.

Secondary materials with a positive surface charge can also be easily combined with MXenes to form MXene hybrids through physical processes such as drop-casting⁸⁰ and adsorption.⁵⁶ This method also relies on the same electrostatic/van der Waals self-assembly principle as the previous

method (reactive chemical formation of secondary materials on MXenes). However, in this non-reactive method, the secondary materials are in the final forms *prior* to integration with MXenes. Hence, the MXenes are typically not subjected to high temperature treatment steps such as hydro/solvothermal treatment for secondary material integration. This method is most suitable for ambient-stable secondary materials that can be easily solution-processed.

Adsorption of C-based materials such as *g*-C₃N₄,^{133,139} CNTs,^{56,140,141} graphene oxide (GO), and reduced graphene oxide (rGO)^{61,142} is commonly used for the assembly of MXene/C-based material hybrids. CNTs are often mixed with MXenes by sonication,^{56,140} while *g*-C₃N₄, GO, and rGO are electrostatically adsorbed.^{143,144} MXene hybrids with CNTs, *g*-C₃N₄, and GO/rGO are then traditionally filtered to yield free standing films for electrode applications and capacitors.^{139,141,145} After the adsorption process, MXene hybrids with CNTs and GO/rGO can be further freeze-dried to form conductive aerogel networks for capacitors.^{61,140,142} Generally, MXene/*g*-C₃N₄ hybrids promote electron transfer at the interface to augment the catalytic activity of *g*-C₃N₄,^{133,143} while CNTs, GO, and rGO on MXenes serve as additional conductive and/or structural supports.¹⁴⁶ Other secondary materials such as TM oxides,¹²¹ phosphates,¹²² chalcogenides,¹¹⁸ nitrides,¹²³ MOFs¹⁰⁷ and LDHs¹⁰⁹ can also be combined with MXenes this way.

MXene hybrids have also been formed by drop-casting MXenes onto the secondary material (or *vice versa*).^{80,147} For example, TiO₂ nanorods were grown hydrothermally on a fluorine-doped tin oxide (FTO) substrate, and then coated with Ti₃C₂T_x through solution drop casting to produce the Ti₃C₂T_x/TiO₂/FTO photoanode for PEC water splitting.⁸⁰ While drop-casting is a less-intensive process, post-processing steps such as annealing may be required to optimize MXene-secondary material interfacial chemical bonding and charge transfer.

Summary, specific challenges, and outlook for processing of MXene hybrids. We have described how MXene hybrids can be formed through (1) *in-situ* conversion by using MXene surfaces as reactants, (2) direct chemical growth of secondary materials on MXenes, and (3) deposition of secondary materials on MXenes. The processing method employed for MXene hybrids formation is highly dependent on their intended catalytic application. For instance, PC applications require semiconducting photo-absorbers, which can be formed *via in-situ* oxidation or hydro/solvothermal treatment of Ti-based MXenes.⁸⁹ In contrast, oxide formation on MXenes is detrimental to electrocatalysis, as oxides are less conductive and limit charge transport properties,¹⁴⁸ so a self-assembly process may be more appropriate. MXene hybrids should also be carefully designed to optimize chemical coupling at the MXene-secondary material interfaces toward catalytic activity enhancement. For example, strong chemical coupling between $\text{Ti}_3\text{C}_2\text{T}_x$ with *g*- C_3N_4 afforded a highly OER-active hybrid.¹³⁹ A strongly coupled MXene hybrid also reduces the probability of hybrid disintegration during electrocatalysis.¹⁴⁹ Finally, the surface chemistry of MXene T_x groups play an important role in determining the morphology, phase, and growth characteristics of secondary materials in the various synthesis methods.^{83,87,95} Since the presence of termination groups on MXene surfaces is dependent on the synthesis processes,¹⁵⁰ it is thus crucial to carefully select the route of MXene synthesis, as well as the subsequent treatment steps, to develop MXene hybrids with high catalytic activity and structural stability.

MXENE HYBRIDS FOR WATER SPLITTING REACTIONS

MXenes' unique set of physical and electronic properties make them excellent candidates for catalytic water splitting.^{13–15} High hydrophilicity and solution processability allow MXenes to be robust and durable in aqueous electrolytes such as acids, bases, and seawater.¹⁵¹ Metallic electronic conductivity enables MXenes to facilitate efficient electronic charge transport at the electrode-electrolyte interface as a large-area conductive 2D substrate when coupled to other highly active but less conductive co-catalysts.^{42,152} This combination of properties circumvent the limitations of conventional C-based supports such as graphene whose hydrophobicity restricts their use in aqueous electrocatalysis, and GO whose conductivity is reduced because of hydroxyl functionalization.^{126,153} Hybridization also creates additional catalytically active motifs at the interface¹³⁹ and modulates the electronic structure to augment intrinsic catalytic activity.^{126,153} With precise control over the MXene hybrid's interfaces and growth of secondary materials, bifunctional non-PGM MXene hybrid couples have outperformed full PGM couples (Pt/C as HER cathode, RuO₂ or IrO₂ as OER anode) in both activity and stability.^{102,149} Here, we highlight highly active and non-PGM HER, OER, and bifunctional water splitting MXene hybrid catalysts, clarifying the roles played by each material component in the overall catalyst design. For the reader's benefit, a summary table of performance metrics for various MXene hybrids in EC HER/OER and PC/PEC HER is provided in **Tables S2 and S3** respectively.

MXene hybrids and composites for electrocatalytic (EC) HER. MXenes have garnered significant attention after they were theoretically predicted^{154–156} and then demonstrated to be HER-active.¹⁷ Unlike other 2D materials like 2H-MoS₂ that exhibit higher catalytic activity on the edges,²⁰ the 2D basal planes of MXenes are more HER active,^{17–19} allowing for more efficient catalyst utilization. HER activity in bare MXenes was reported experimentally using Mo₂CT_x and

Ti₂CT_x by Seh *et al.*, with the –O T_x surface groups determined as active sites on the MXenes' basal planes.¹⁷ Due to the modest EC HER activity of bare MXenes, initial efforts were directed at improving their HER activity through physically increasing the density of electrochemically active surface area (ECSA) by nanostructuring,^{157,158} or by modulating the MXene electronic structure to achieve a more thermoneutral *H adsorption free energy ($\Delta G_H \rightarrow 0$), a common predictor for HER activity.^{154–156} Effective binding energy tuning may be achieved through T_x control,^{18,154} and doping with other TMs^{127,159–162} and/or non-metals (such as N, S, and P).^{163–165}

The effect of TM doping in changing *H binding energy was recently illustrated by Djire *et al.* using scanning electrochemical microscopy (SECM) on Ti₄N₃T_x MXenes.¹⁹ SECM is a unique tool capable of generating high-resolution local conductivity and EC activity maps of the catalyst surface. In the feedback mode, ferrocene (Fc), a redox mediator, is included to probe the surface conductivity. A higher tip current (i_T) will be observed on a more conductive surface due to a faster rate of Fc⁺ reduction. As the MXene flakes are placed on top of a conductive substrate like indium tin oxide (ITO), i_T contrast also demarcates the boundaries of the MXene flake edges. The HER activity can be mapped by applying a negative bias to the substrate, referred to as the substrate generation/tip collection (SG/TC) mode.

Alloying Ti₄N₃T_x with V, which produced V-alloyed Ti₄N₃T_x (denoted as y M V-Ti₄N₃T_x, where y = molar concentration of aqueous VOSO₄ dopant used for alloying), did not improve the surface conductivity, as shown by the negligible i_T in 0.3 M V-Ti₄N₃T_x, similar to bare Ti₄N₃T_x (**Figures 5a** and **5c**). However, the HER activity in V-alloyed Ti₄N₃T_x increased very significantly compared to the bare MXenes (**Figures 5b** and **5d**). Improved conductivity in V-Ti₄N₃T_x was also be achieved by increasing the concentration of VOSO₄ dopant used (**Figure 5e**) and was accompanied by a slight improvement in HER activity (**Figure 5f**). This study by Djire *et al.* is

experimental proof of basal plane HER activity in MXenes, as inferred from the lower i_T around the flake edges in the SG/TC mode. Furthermore, it demonstrates that the conductivity and HER activity in MXenes may be decoupled, possibly due to the self-gating phenomenon, reported previously on the basal planes of a variety of semiconducting 2D materials, including 2H-MoS₂.¹⁶⁶

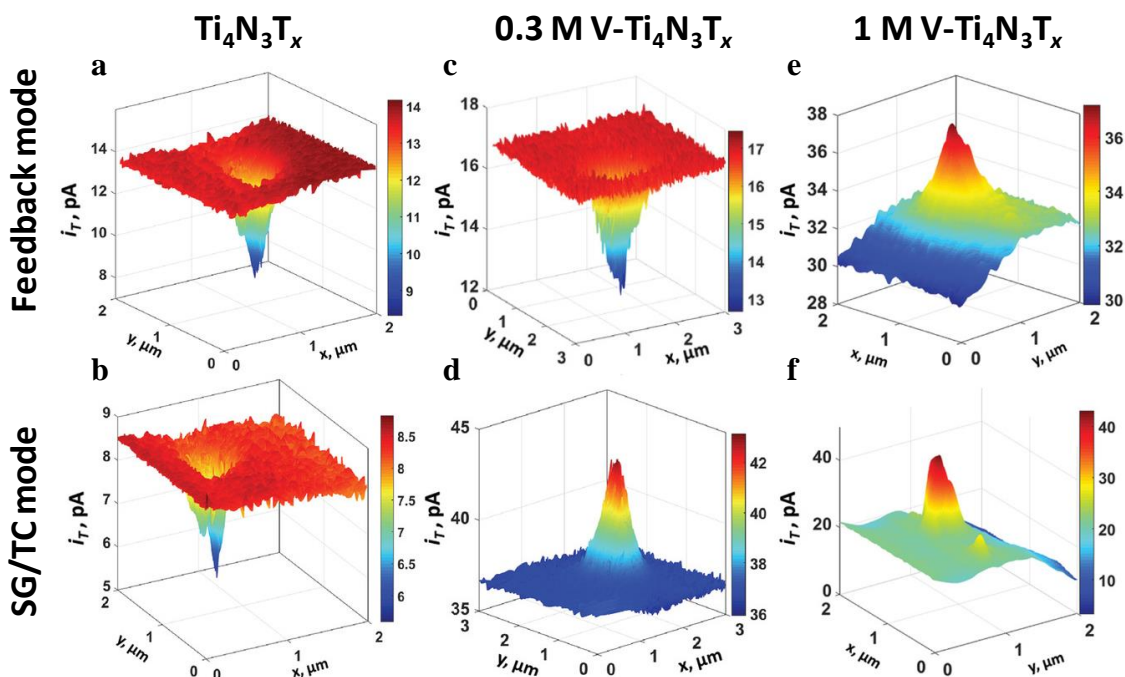


Figure 5. SECM feedback mode and SG/TC mapping of (a, b) bare Ti₄N₃T_x and V-alloyed Ti₄N₃T_x, using (c, d) 0.3 M or (e, f) 1.0 M aqueous VOSO₄ dopant for alloying. Adapted with permission from ref¹⁹. Copyright 2020 WILEY-VCH.

Coupling MXenes with other HER-active co-catalysts such as TM chalcogenides,^{102,167} phosphides,^{168–170} carbides,^{151,171} and QDs (metallic alloys and black phosphorus, BP) are common ways to enhance HER activity.^{52,53} Here, MXenes serve as a large-area conductive and mechanical support to facilitate charge transfer, act as a HER co-catalyst, and modulate the hybrid's electronic structure to optimize for H⁺ adsorption and HER activity. With significantly higher HER activities than the sum of their individual material components, intimately coupled MXene hybrids benefit from synergistic HER enhancement to achieve PGM-like activities.

Coupling MXenes with TM chalcogenides for EC HER was reported by Wu *et al.* in a hierarchical MoS₂/Ti₃C₂T_x@C architecture (**Figure 4a**).⁷⁰ The MXene support constrained 2H-MoS₂ to grow vertically,^{172,173} maximizing ECSA and mass transport of gaseous products (**Figure 6a**). The strong interfacial and chemical relationship between Ti₃C₂T_x and 2H-MoS₂ was verified by the Mo (MoS₂)-C (MXene) X-ray photoelectron spectroscopy (XPS) peak, which would be absent in a physical mixture of Ti₃C₂T_x and 2H-MoS₂. With a small charge transfer resistance of 1.28 Ω, MoS₂/Ti₃C₂T_x@C required a small overpotential ($\eta_{j=10}$) of 135 mV at a current density of -10 mA cm⁻² in 0.5 M H₂SO₄, 217 mV smaller than the MoS₂/rGO@C hybrid when rGO is used as the substrate (curves 1 and 2, **Figure 6b**, see **Vocabulary** for a definition of overpotential and Tafel slope).⁷⁰ The nanohybrids were also durable in acid for 20 h of operation at -130 mV (*vs.* reversible hydrogen electrode, RHE), due to the protective carbon nanoplating surrounding the hybrid. Additionally, coupling other TM chalcogenides such as MoS₂,¹¹⁸ MoSe₂,¹⁰² NiS₂,¹⁷⁴ NiSe₂,¹⁷⁵ and VS₂¹⁷⁶ to various MXenes have also achieved synergistically enhanced HER activity.

TM carbides^{151,171} and phosphides¹⁶⁸⁻¹⁷⁰ have also been integrated into MXene hybrids for EC HER. TM phosphides will be discussed in the next sub-section due to their HER and OER bifunctionality. A collaborative catalytic interface was formed between the cobalt-doped β-Mo₂C co-catalyst, Ti₃C₂T_x, and N-doped carbon (NC) to enhance electrical conductivity and expose ECSA, while improving H⁺ and water absorption kinetics for efficient HER in a wide pH range, including in seawater.¹⁵¹ Theoretical calculations revealed that the Co_xMo_{2-x}C/NC interface reduced the H⁺ absorption barrier to 0.05 eV, and the water dissociation barrier to 0.78 eV. Notably, the water dissociation barrier was lower than Pt (111) at 0.89 eV. With accelerated water dissociation and HER kinetics, the optimized Co_{0.31}Mo_{1.69}C/MXene/NC hybrid exhibited Pt-like HER activity with an $\eta_{j=10}$ and Tafel slope of 75 mV and 32 mV dec⁻¹, respectively, in 1 M KOH

(curve 2, **Figure 6c**), outperforming the individual β -Mo₂C and MXene components (curves 4 and 6, **Figure 6c**). This corroborated with a separate report on Mo₂C/Ti₃C₂T_x@NC, whose exchange current density (j_0) in acid was four-fold higher than Mo₂C@NC without the MXene support.¹⁷¹ These works demonstrate the synergistic co-operation between material components, with β -Mo₂C and NC providing favorable H⁺ adsorption sites,¹⁵¹ while MXenes facilitated charge transport.¹⁷¹

QDs have also been anchored on MXenes to modulate the electronic structure or alter the adsorption kinetics of intermediates. Du *et al.* modified the Ti₃C₂T_x surface with Ni/Co alloyed QDs to reduce the overly strong Ti-H interaction.¹⁷⁷ Nb was also doped into Ti₃C₂T_x to raise the Fermi level to the conduction band, improving the electronic conductivity of the Ti₃C₂T_x support. The optimized Ni_{0.9}Co_{0.1}@Ti_{2.5}Nb_{0.5}C₂T_x hybrid showed $\eta_{j=10}$ of 43 mV for HER, a significant improvement compared to the 516 mV required for Ti_{2.5}Nb_{0.5}C₂T_x without the alloyed QDs. Critically, the HER enhancement was intrinsic, given that the HER improvement trends were still valid after normalization for ECSA. Separately, BP QDs were decorated on Ti₃C₂T_x to similarly reduce Ti₃C₂T_x surface binding to H⁺ from -1.01 eV to as low as -0.17 eV (**Figure 6d**).⁵³ Beneficially, the MXene support physically confined the growth of BP to discrete 0D QDs, which prevented agglomeration, and maximized ECSA and mass transport for electrocatalysis.^{52,53}

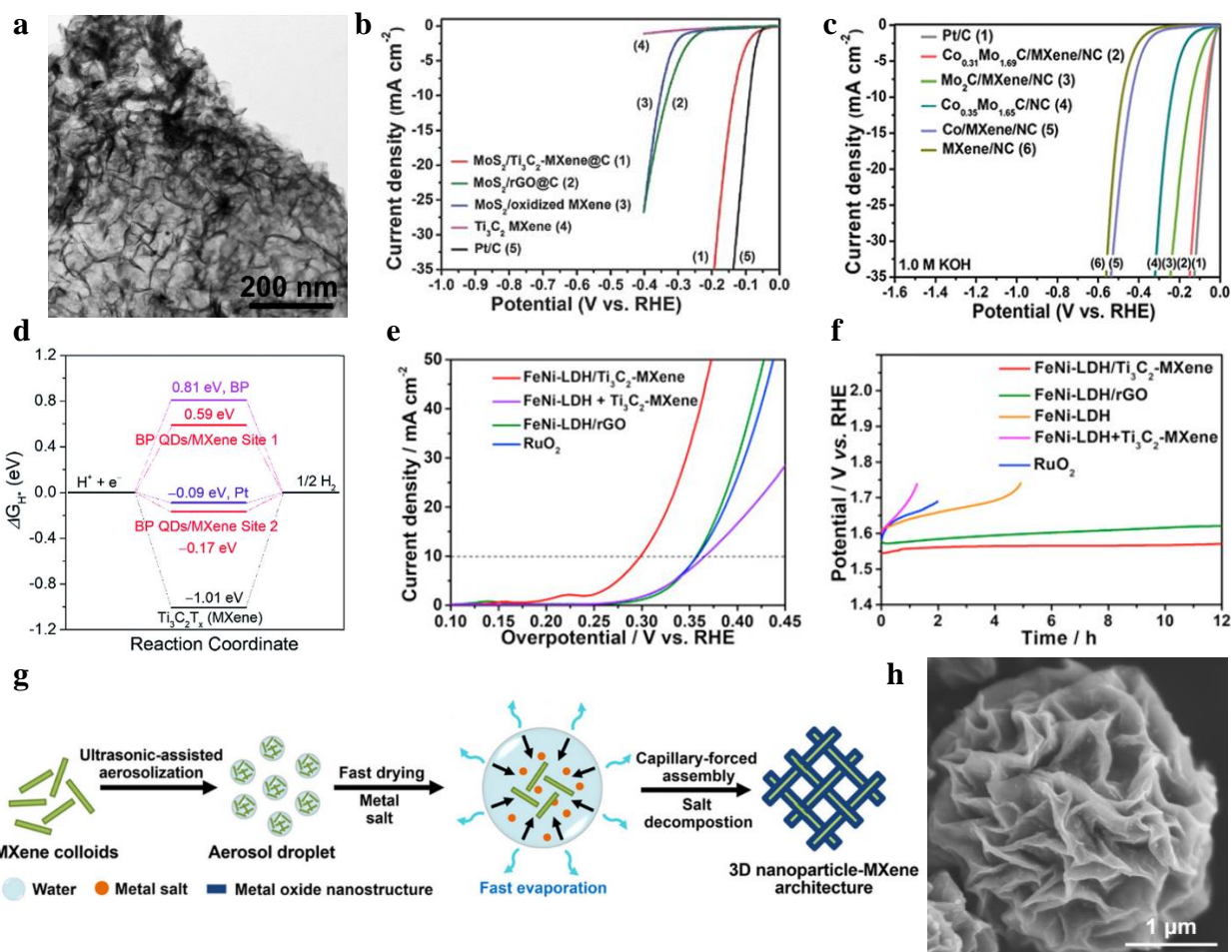


Figure 6. MXene hybrids for EC water splitting. (a) TEM image and (b) polarization curves of MoS₂/Ti₃C₂T_x-MXene@C, showing vertical growth of MoS₂ on Ti₃C₂T_x. Adapted with permission from ref ⁷⁰. Copyright 2017 WILEY-VCH. (c) Polarization curves of Co_xMo_{2-x}C/MXene/NC. Adapted with permission from ref ¹⁵¹. Copyright 2019 WILEY-VCH. (d) Free energy diagram of BP QDs/Ti₃C₂T_x. Adapted with permission from ref ⁵³. Copyright 2018 Royal Society of Chemistry. (e) Polarization curves and (f) Constant current (-10 mA cm⁻²) stability test of FeNi-LDH/Ti₃C₂T_x-MXene. Adapted with permission from ref ¹²⁶. Copyright 2017 Elsevier Ltd. (g) Assembly and (h) Scanning electron microscope (SEM) image of 3D CoP-MXene. Adapted with permission from ref ¹⁶⁹. Copyright 2018 American Chemical Society.

MXene hybrids and composites for electrocatalytic (EC) OER and water splitting.

Compared to HER, OER is a more complex reaction as it involves a four-electron transfer process and multiple reaction intermediates. Achieving efficient and durable OER often require electrocatalysts with intricate heterostructuring and design.¹⁷⁸ Although bare MXenes are not efficient OER catalysts,⁴⁵ they can serve as electrically conductive supports, modulate the

electronic density of their coupled OER co-catalyst, and even create additional OER-active motifs to greatly enhance OER activity.^{44,139} For instance, coupling $\text{Ti}_3\text{C}_2\text{T}_x$ with $g\text{-C}_3\text{N}_4$ created a highly OER-active Ti (MXene)- N_x ($g\text{-C}_3\text{N}_4$) motif at the interface for PGM-like OER activity.¹³⁹ Many OER-active materials such as TM chalcogenides,^{102,120} oxides,^{131,179} nitrides,¹⁸⁰ phosphides,^{168–170} MOFs,¹⁰⁷ LDHs,^{126,153,181} C-based materials,^{139,182} and QDs^{53,183} have been coupled with MXenes to augment OER activity. More significantly, these strategies have yielded non-PGM MXene hybrids that have outperformed PGM-based electrocatalysts for EC OER and water splitting.

Heterostructured and hybrid materials are often subject to lattice mismatch and strain at the interface, which has been exploited in phase engineering to alter electronic states near the interface and stabilize metastable material phases.^{184,185} Li *et al.* stabilized a mixture of metastable 1T (23%) and stable 2H (77%) MoSe_2 on $\text{Ti}_3\text{C}_2\text{T}_x$ as a bifunctional HER and OER electrocatalyst.¹⁰² The 1T/2H $\text{MoSe}_2/\text{MXene}$ hybrid (HER $\eta_{j=10} = 95$ mV) outperformed their individual components and other phases (2H $\text{MoSe}_2/\text{MXene}$ HER $\eta_{j=10} = 123$ mV) for both HER and OER. The non-PGM 1T/2H $\text{MoSe}_2/\text{MXene}$ couple also required a modest 1.64 V (*vs.* RHE) to maintain a current density of -10 mA cm^{-2} for 50 h while retaining a high 1T phase content. The activity improvement was attributed to the use of conductive MXenes to improve charge transfer and confine the 1T/2H MoSe_2 nanostructures to prevent aggregation. The intrinsic activity of MoSe_2 was also boosted by the abundance of MoSe_2 active sites, particularly from the more catalytically active and now stabilized 1T phase. This work illustrates the potential of using MXenes to stabilize metastable phases that are highly electrocatalytically active, as co-catalysts to achieve higher activities.¹⁰²

Although LDHs are excellent candidates for alkaline OER and water splitting, they are poor electrical conductors and aggregate easily.^{126,153,181} Previously, LDHs were used with C-based supports such as graphene to improve charge transport. These C-based supports, however, had to

be first functionalized to rGO/GO before they could be integrated with LDHs, compromising the support's structural integrity and conductivity. Therefore, Yu *et al.* exploited the negatively charged surface T_x groups of MXenes to electrostatically self-assemble FeNi-LDH nanostructures vertically on $Ti_3C_2T_x$ in a 3D array (**Figure 4b**).¹²⁶ The vertical growth of LDH atop MXenes reduced repulsion and aggregation between positively charged LDH sheets while maximizing ECSA for catalysis.^{153,181} The benefits of strong chemical coupling within the hybrid was evident in their OER performance (**Figure 6e**) and stability (**Figure 6f**), which are far superior to the physical mixture (FeNi-LDH + $Ti_3C_2T_x$) or when the FeNi-LDH OER catalyst was hybridized with a less conductive substrate (FeNi-LDH/rGO) instead of MXenes. The reasoning for the enhanced OER is attributed to the increased oxidation state of Ni and Fe centers after hybridization, as shown in the +0.5 eV shift of the Ni and Fe 2p XPS peaks.¹²⁶ A follow-up work integrated the FeNi-LDH/ $Ti_3C_2T_x$ structure with a 3D nickel foam network to further maximize ECSA and mass transport, achieving a high current density of 500 mA cm⁻² at very low overpotentials for alkaline OER (300 mV), HER (205 mV), and bifunctional water splitting (1.75 V vs. RHE).¹⁴⁹ Separately, extensive growth of Co-LDH on $Ti_3C_2T_x$ was successful in arresting $Ti_3C_2T_x$ surface oxidation during OER, which would have impeded both charge transfer at the MXene-LDH interface, and overall electronic conductivity in the hybrid.¹⁸⁶

The LDH-MXene hybrids can also be processed further to form bifunctional catalysts like phospho-sulfides. For example, FeNi-LDH/MXenes can be converted to 2D bimetallic $Ni_xFe_{1-x}PS_3$ (MPS_3)/MXenes hybrid *via* thermal annealing with red phosphorus in a vacuum sealed ampule.¹⁶⁷ The resulting MPS_3 /MXenes hybrid possess a broken-up nanomosaic morphology with high ECSA, possibly due to the thermal stress. More importantly, the MPS_3 /MXenes composition can be easily tailored by tuning the starting Fe : Ni ratio in the FeNi-LDH/MXenes precursor.

Interestingly, the catalytic reaction preference of MPS₃ hybrids depends on its Fe : Ni ratio – Ni_{0.9}Fe_{0.1}PS₃/Ti₃C₂T_x was found to be most proficient in catalyzing HER ($\eta_{j=10} = 196$ mV) in 1 M KOH, while Ni_{0.7}Fe_{0.3}PS₃/Ti₃C₂T_x exhibited excellent OER activity ($\eta_{j=10} = 282$ mV). The Ni_{0.7}Fe_{0.3}PS₃/Ti₃C₂T_x (OER) || Ni_{0.9}Fe_{0.1}PS₃/Ti₃C₂T_x (HER) couple can deliver -10 mA cm⁻² of complete water splitting at a lower potential (1.65 V vs. RHE) than the full-PGM IrO₂ || Pt/C reference standard (1.71 V vs. RHE). The MPS₃/MXenes couple was also stable for over 50 h at the said potential. This work demonstrates strain engineering for ECSA maximization, and the added flexibility of tuning multi-metal compounds to optimize toward different electrochemical reactions of interest as multi-functional electrocatalysts.

TM phosphides have also been integrated with MXenes as bifunctional HER and OER electrocatalysts.^{168–170} Xiu *et al.* reported a hierarchical CoP@3D Ti₃C₂T_x-MXene architecture to significantly enhance EC activity for water splitting.¹⁶⁹ After nebulizing MXene colloids containing cobalt salts into tiny droplets, the droplets were dried rapidly at 600 °C. Solvent evaporation induced an inward capillary force on the droplets to cause isotropic compression of MXene sheets into aggregation-resistant Co₃O₄@3D Ti₃C₂T_x-MXene hybrids (**Figure 6g**). Further phosphorization converted Co₃O₄ in the hybrids into OER-active CoP. The highly porous and interconnected 3D MXene architecture (**Figure 6h**) provided a large surface area for catalysis and facilitated long-range electrical charge transport. An efficient bifunctional HER and OER electrocatalyst, CoP@3D Ti₃C₂T_x-MXene required only 1.565 V (vs. RHE) to supply -10 mA cm⁻² of current density and remained stable (< 25 mV degradation) for 150 h at a high current density of -100 mA cm⁻². Combining TM phosphides with MXenes is also reported to shift the TM *d*-band center to higher energies, resulting in reduced occupancy of antibonding states from the TM and adsorbed O intermediate, for enhanced OH⁻ adsorption and OER.¹⁶⁸ Additionally, 1D CoP

nanorods grown on top of $\text{Ti}_3\text{C}_2\text{T}_x$ sheets was also reported to induce tensile stress and bending of $\text{Ti}_3\text{C}_2\text{T}_x$ to expose higher ECSA for improved OER activity.¹⁷⁰

MXene hybrids and composites for photocatalytic (PC) and photoelectrocatalytic (PEC) water splitting. Given the close alignment of the MXenes' Fermi energy (E_F) position to the H^+/H_2 reduction potential,¹⁸⁷ efficient H^+ adsorption, and respectable EC water splitting performances as described earlier, MXene hybrids are a logical choice for PC/PEC water splitting to harvest sunlight as a renewable energy driving source. Unlike EC, PC reactions require semiconductor photo-absorbers, where electron-hole pairs are generated. Since most MXenes are metallic and not semiconducting,¹⁵² other materials are necessarily drafted to harvest light and promote the separation of photo-generated carriers.¹⁸⁸ A few works feature MXene hybrids as multi-functional PEC HER, OER, and water splitting catalysts. Lin *et al.* reported a $\text{Ti}_3\text{C}_2\text{T}_x/\text{InGaN}$ photo-anode with a 10-fold improvement in HER photocurrent density after MXene hybridization, verifying the high HER activity on the MXene surface.¹⁸⁹ $\text{Ti}_3\text{C}_2\text{T}_x/\text{TiO}_2/\text{NiFeCo-LDH}$ was also tested for PEC OER, with the MXene and NiFeCo-LDH acting as the conductive support and OER catalyst, respectively.¹⁸¹ Yu *et al.* reported $\text{Ti}_3\text{C}_2\text{T}_x/\text{TiO}_2$ as an OER photo-anode with a six-fold increment in applied bias photon-to-current efficiency compared to a bare TiO_2 photoanode.⁸⁰ Here, PEC OER occurred on the MXene surface, which served as a hole scavenger and OER active site.

As discussed previously, MXenes generally exhibit only modest OER activity and hence rely on hybridization with OER-active catalysts (such as TM chalcogenides¹⁰² and LDHs^{126,149}), with the MXenes serving primarily as conductive supports and electronic modulators.^{44,139} Thus, most PC/PEC applications of MXenes and their hybrids are directed at HER instead of OER to take advantage of MXenes' HER activity. In this endeavor, MXenes, especially Ti-based MXenes, have

been employed as precursors to TM oxides with rich vacancies, which are widely considered as stable, efficient, and robust HER photocatalysts.^{83,97,100}

Yuan *et al.* oxidized $\text{Ti}_3\text{C}_2\text{T}_x$ in CO_2 at high temperatures to produce a 2D MXene-derived C/ TiO_2 hybrid.⁸³ Since the Ti and C atoms were already alternately arranged in the MXene structure ($\text{Ti}_3\text{C}_2\text{T}_x$), calcination is likely to result in alternating TiO_2 and 2D carbon sheets, while retaining the large-area 2D-layered structure of MXenes, which is suitable for PC HER (**Figure 7a**). After optimizing for calcination temperature and CO_2 flow rates, C/ TiO_2 -700-150 hybrid exhibited the highest PC H_2 generation rate of $24 \mu\text{mol g}^{-1} \text{h}^{-1}$, representing an 89-fold enhancement from TiO_2 . This was credited to the thin carbon layers facilitating charge transport, whose high electrical conductivity improved photo-carrier separation efficiency and reduced their recombination rate, in agreement with other works.^{100,190,191} The thin carbon layers also provided a high degree of transparency for visible light penetration to the TiO_2 photo-absorber. This method was also employed to synthesize S-doped TiO_2 NPs/C (**Figure 7b**) from S-doped $\text{Ti}_3\text{C}_2\text{T}_x$, whereby S doping further optimized H^+ binding energy for efficient HER.⁹⁷ The strategy of using MXenes as precursors to synthesize MXene/TM oxide hybrids has also been applied to other MXenes, given the relative ease in oxidizing MXenes,^{192,193} such as in the oxidation of Nb_2CT_x to $\text{Nb}_2\text{CT}_x/\text{C}/\text{Nb}_2\text{O}_5$,¹⁹⁴ Mo_2CT_x to $\text{Mo}_2\text{C}/\text{MoO}_x$,¹⁴⁸ and V_2CT_x to $\text{V}_2\text{CT}_x/\text{V}_2\text{O}_x$.^{57,195}

Apart from acting as TM oxide precursors, MXenes can also serve as efficient PC/PEC HER co-catalysts themselves to promote photo-generated charge carrier separation when coupled to semiconductors.^{133,196–199} The most widely studied MXene, $\text{Ti}_3\text{C}_2\text{T}_x$, has been applied as a PC HER co-catalyst and successfully coupled to a variety of semiconducting photocatalysts such as TM oxides,^{191,196} sulfides,^{124,187} perovskites,^{197,198} and $g\text{-C}_3\text{N}_4$.^{133,199}

For instance, Ran *et al.* investigated the use of $\text{Ti}_3\text{C}_2\text{T}_x$ as a HER co-catalyst, with CdS acting as a photo-absorber for PC HER.¹⁸⁷ The electrostatic self-assembly of CdS NPs on $\text{Ti}_3\text{C}_2\text{T}_x$ NPs produced cauliflower-structured sub-microspheres (referred to as CTX, where X refers to the mass ratio of MXenes : CdS) with distinct and well-formed $\text{Ti}_3\text{C}_2\text{T}_x/\text{CdS}$ interfaces (**Figure 7c**). An optimal 2.5 wt% MXene incorporation (CT2.5) resulted in a substantial 136-fold improvement in H_2 production rate compared to bare CdS (CT0, **Figure 7d**). In fact, the strongly coupled $\text{Ti}_3\text{C}_2\text{T}_x/\text{CdS}$ (CT2.5) hybrid outperformed other hybrids such as 2.5 wt% Pt-CdS, NiS-CdS, Ni-CdS and MoS_2 -CdS (**Figure 7d**). The outstanding PC HER activity of CT2.5 was attributed to a reduction in interfacial charge transfer resistance arising from intimate chemical coupling at the $\text{Ti}_3\text{C}_2\text{T}_x/\text{CdS}$ interface, and high metallic conductivity of $\text{Ti}_3\text{C}_2\text{T}_x$. Furthermore, the photo-carrier separation efficiency was enhanced by deliberately matching the energy bands of $\text{Ti}_3\text{C}_2\text{T}_x$ and CdS in a Schottky junction to trap photo-generated electrons and limit carrier recombination. This was observed in the suppression of both the radiative recombination photoluminescence (PL, $\lambda \approx 560$ nm, **Figure 7e**), and defect level recombination (red-shifted tail from 650–700 nm in **Figure 7e**) peaks, resulting in a longer overall photo-carrier lifetime (**Figure 7f**). Finally, theoretical calculations revealed that $-\text{O}$ terminations in $\text{Ti}_3\text{C}_2\text{T}_x$ served as active HER sites due to their favorable E_F position and efficient H^+ adsorption. $\text{Ti}_3\text{C}_2\text{T}_x$ was also further hybridized with other semiconductor photocatalysts such as ZnS and $\text{Zn}_{0.8}\text{Cd}_{0.2}\text{S}$ and similar trends in improved PC HER activity was observed. This work thus demonstrates the use of O-terminated $\text{Ti}_3\text{C}_2\text{T}_x$ as efficient and durable PC HER co-catalysts for synergistic coupling with a variety of earth-abundant semiconductor photocatalysts (*e.g.* CdS, ZnS, $\text{Zn}_{1-x}\text{Cd}_x\text{S}$) to achieve significantly improved PC HER performances for PC water splitting.

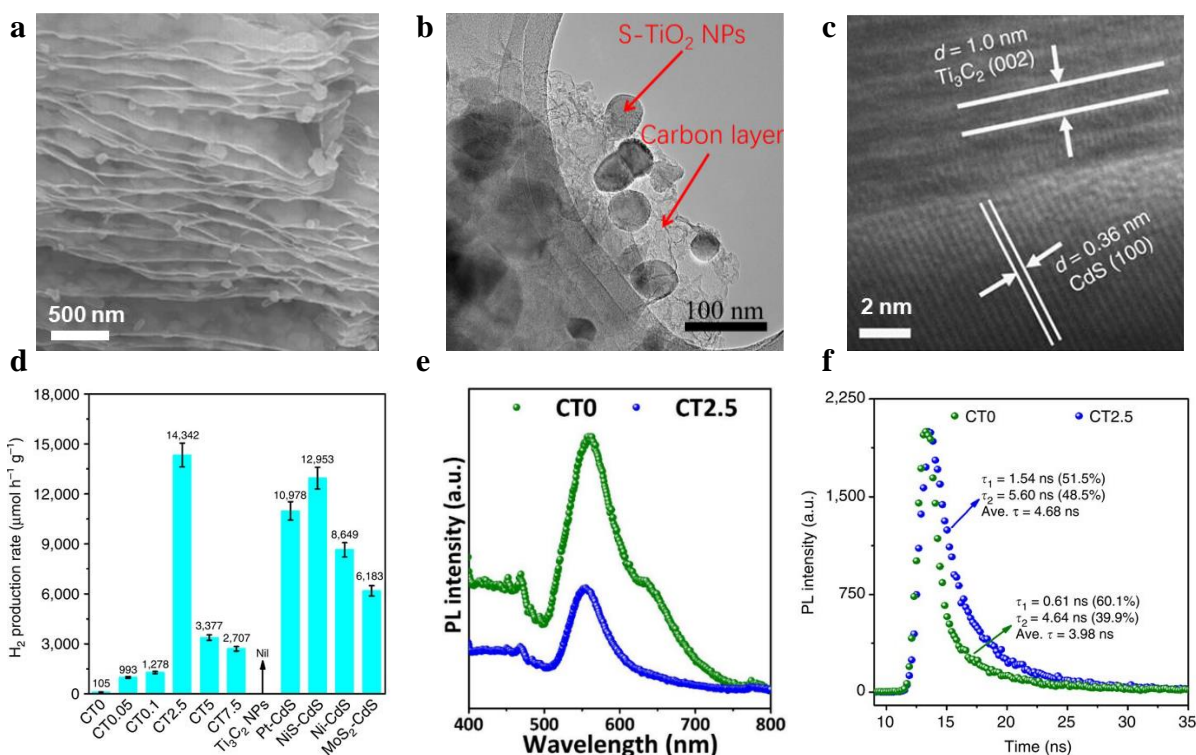


Figure 7. MXene hybrids for PC HER. (a) SEM of $\text{Ti}_3\text{C}_2\text{T}_x$ -derived 2D-layered C/ TiO_2 . Adapted with permission from ref ⁸³. Copyright 2017 WILEY-VCH. (b) High resolution TEM (HRTEM) of $\text{Ti}_3\text{C}_2\text{T}_x$ -derived S- TiO_2 /C. Adapted with permission under a Creative Commons CC-BY license from ref ⁹⁷. Copyright 2018 The Authors. (c) HRTEM of 2.5%- $\text{Ti}_3\text{C}_2\text{T}_x$:CdS hybrid (CT2.5). (d) PC HER activity of various co-catalysts hybridized with CdS. (e) PL and (f) time-resolved PL spectrum of bare CdS (CT0), and CT2.5 MXene hybrids. Adapted with permission under a Creative Commons CC-BY license from ref ¹⁸⁷. Copyright 2017 The Author(s).

Summary, specific challenges, and outlook for EC, PC, and PEC water splitting. In this section, we reviewed the various materials hybridized with MXenes for EC/PC/PEC HER, OER, and water splitting. A summary table of performance metrics ($\eta_{j=10}$, Tafel slope, and turnover rate) for various MXene hybrids in EC HER/OER and PC/PEC HER is provided in **Tables S2 and S3** respectively. In summary, MXenes play various critical roles: (1) providing a large-area conductive and structural support, (2) acting as a HER co-catalyst, (3) confining, stabilizing, and thus preventing the hybridized material from aggregating on the MXene support, and (4) inducing charge transfer to modulate the electronic band structure of the hybrid material to optimize H^+ , OH^- , and water adsorption kinetics when strongly and chemically coupled to other materials.

Lattice strain induced at the MXene-secondary material interfaces can also alter electronic density and stabilize metastable co-catalyst material phases through strain and phase engineering. Apart from activity enhancement, MXene hybrids also benefit from improved stability in acidic and alkaline electrolytes (**Figure 5f**).¹²⁶ A strong and chemically coupled MXene hybrid, especially at the hybrid interface, is important for prolonged cycling and operational stability, particularly at higher current densities.¹⁴⁹ The NiFe-LDH/Ti₃C₂T_x/3D nickel foam hybrid was stable for 200 h of continuous water splitting in 1 M KOH at a high current density of 100 mA cm⁻² due to the strong chemical integration between the LDH, MXenes, and 3D nickel foam network.¹⁴⁹ Conversely, Mo₂CT_x/2H-MoS₂ hybrid suffered a significant ≈50% loss in operating current density after a short 8 h of HER.²⁰⁰ This was due to crack formation within the hybrid, and MoS₂ dislodgement during HER, possibly due to poor chemical integration between Mo₂CT_x and 2H-MoS₂.

Presently, non-PGM MXene hybrid couples have outperformed full-PGM couples (IrO₂ and RuO₂ for OER, Pt/C for HER) for EC water splitting due to the exceptional OER activity from the non-MXene OER-active components (TM phosphides, LDHs). From an activity standpoint, more work should thus be done on improving non-PGM MXene hybrids for HER, and this begins by working with Mo-based MXenes, which possess a higher intrinsic HER activity compared to Ti-based MXenes.¹⁷ Concurrently, further improvement in the OER competitiveness of MXene hybrids can be realized through the theory-guided development of MXenes with higher intrinsic OER activities such as nitride MXenes.²⁰¹ Lastly, the use of *operando* and localized electrochemical/physical characterization techniques such as scanning electrochemical cell microscopy (SECCM) can elucidate more information on catalytic activity at different areas of the MXene hybrid, of which regions near and at the hybrid interface is of particular interest for further

investigation.^{19,202} These investigations are of particular importance to MXene hybrids for OER, since MXenes can be readily oxidized to TM oxides under the applied oxidizing potentials.

MXENE HYBRIDS AS ELECTROCATALYSTS FOR METAL-AIR AND METAL-SULFUR BATTERIES

Aside from their high HER and OER catalytic activity for water splitting, MXene hybrids are also similarly efficient in catalyzing the OER/ORR redox couple^{203,204} to serve as cathodes for metal-air batteries.^{180,205–207} With high metallic conductivity, MXene hybrids are well-positioned to facilitate rapid electronic transfer for sulfur redox reactions at the sulfur cathode in lithium-sulfur (Li-S) batteries as well.^{56,208} MXene hybrids have recently been demonstrated to possess a high binding affinity toward deleterious lithium polysulfide (LiPS) side products when used as a separator, extending the cycle life and reducing the capacity fade of Li-S batteries.^{209,210} In this section, we review the catalytic role of MXene hybrids towards realizing the industrial potential of metal-air and metal-sulfur batteries (see **Vocabulary** for full definition) as next-generation battery architectures to complement existing lithium ion batteries (LIBs).

MXene hybrids and composites for electrocatalytic (EC) OER and ORR in metal-air batteries. A post-LIB technological prospect, metal-air batteries comprise of design elements from both traditional batteries (using a metal anode) and fuel cells (using a cathode exposed to air).⁸ Metal-air batteries have attracted widespread interest due to their compact size, lightweight composition,²¹¹ and high theoretical energy density.²¹² For instance, Zn-air batteries have a theoretical energy density (1350 Wh kg⁻¹, excluding oxygen) about five times that of LIBs,²¹² and can be produced at significantly lower costs (<\$10 kW⁻¹ h⁻¹) than LIBs (≈\$400–800 kW⁻¹ h⁻¹).²¹³

Unfortunately, the theoretical promise of metal-air batteries has yet to be practically realized due to their poor air cathode performance. The complex, multi-step, four-electron OER/ORR redox couple is severely hampered by sluggish kinetics as the rate-determining step.²¹¹

Even though MXenes are not OER or ORR-active as previously discussed, MXenes have been utilized as conductive supports for other ORR-active electrocatalysts.^{182,206} Hybridizing MXenes with other materials also resulted in electronic structure modulation, and the creation of catalytic motifs to exhibit enhanced OER, ORR, and bifunctional OER/ORR activity comparable to PGMs such as Pt/C (for ORR) and IrO₂/RuO₂ (for OER).^{123,139,180} Since MXene hybrids for EC OER have been described previously for water splitting, we focus our discussions here on MXene hybrids for EC ORR, bifunctional EC OER/ORR, and their use in Zn-air batteries.^{180,205–207} A summary of EC ORR performances for various MXene hybrids is provided in **Table S2c**.

Iron-nitrogen-carbon (Fe-N-C) materials are one of the most promising class of PGM-free ORR catalysts due to their highly active FeN₄ motifs.^{123,203,214} To further augment the intrinsic ORR activity of iron phthalocyanine (FePc), Li *et al.* hybridized FePc on Ti₃C₂T_x support and obtained a significant two-fold activity enhancement in FePc, which was also five times higher than Pt/C.¹²³ Two-electron ORR was also virtually suppressed with a calculated electron number of ≈ 4 and an ultralow H₂O₂ yield (<1%). The authors posit that the negatively charged –OH/–F T_x groups of Ti₃C₂T_x interacted strongly with the Fe²⁺ center through intermolecular van der Waals forces or hydrogen bonding to reduce the local Fe²⁺ electron density, which induced a transition to a higher spin state to optimize O₂ binding for ORR. A follow-up work synthesized Fe(phen)₂/Ti₃C₂T_x hybrids through pyrolysis, using the MXene as a large-area 2D conductive support to prevent aggregation of the rugged Fe(phen)₂ coating.²¹⁴ Separately, positively charged 2D Fe-N-C sheets were produced by decorating g-C₃N₄ sheets with Fe NPs.²⁰³ By manipulating the Fe/g-C₃N₄ precursor ratio, the positive zeta potential (from Fe²⁺) per unit area of Fe-N-C sheets was adjusted to +30.4 mV to match the negative zeta potential (from MXenes' T_x groups) per unit area of Ti₃C₂T_x sheets (-39.7 mV). This allowed both sheets to be electrostatically self-assembled

in a 2D/2D layered superlattice-like heterostructure in aqueous solutions with enhanced ORR activity. This work can potentially be further extended to manipulate the positive sheet charges of other 2D materials using TM NP clusters to achieve the wet chemical, electrostatic self-assembly of 2D material/MXene layered heterostructures, circumventing the use of small-scale and energy intensive physical deposition methods such as CVD and ALD.

TM oxide²⁰⁷ and chalcogenide²⁰⁶ NPs have also been incorporated onto MXene scaffolds to synergistically enhance ORR activity for Zn-air batteries (**Figure 8a**). For example, 3D N-CoSe₂/MXene architecture can be obtained with the aid of a poly(vinylalcohol) (PVA) cross-linker, followed by thermal annealing in NH₃.²⁰⁶ The 3D architecture separates the MXene layers and prevents them from aggregation, thus maximizing ECSA and mass transport properties. Theoretical calculations revealed that N-CoSe₂/MXene hybridization increases the activity at Co sites, by virtue of significant electron transfer from Ti₃C₂T_x to CoSe₂, while N-doping reduces the thermodynamic barrier to the potential-limiting steps for both OER and ORR. This resulted in a highly efficient bifunctional OER/ORR electrocatalyst, with a higher specific capacity (751 mAh g_{Zn}⁻¹) than the RuO₂+Pt/C OER/ORR benchmark (690 mAh g_{Zn}⁻¹) when discharged at 5 mA cm⁻². The discharge characteristics and maximum power density of N-CoSe₂/3D Ti₃C₂T_x (142 mW cm⁻² at 232 mA cm⁻²) also outperforms the full PGM standard reference of RuO₂ + Pt/C (119 mW cm⁻² at 168 mA cm⁻²), as seen in **Figure 8b**. The high cycling stability (500 cycles, 166 h at 10 mA cm⁻²) was attributed to the preservation of the 3D MXene architecture and strong integration of CoSe₂ NPs into the MXene network, which prevented CoSe₂ NPs from dislodging during cycling.

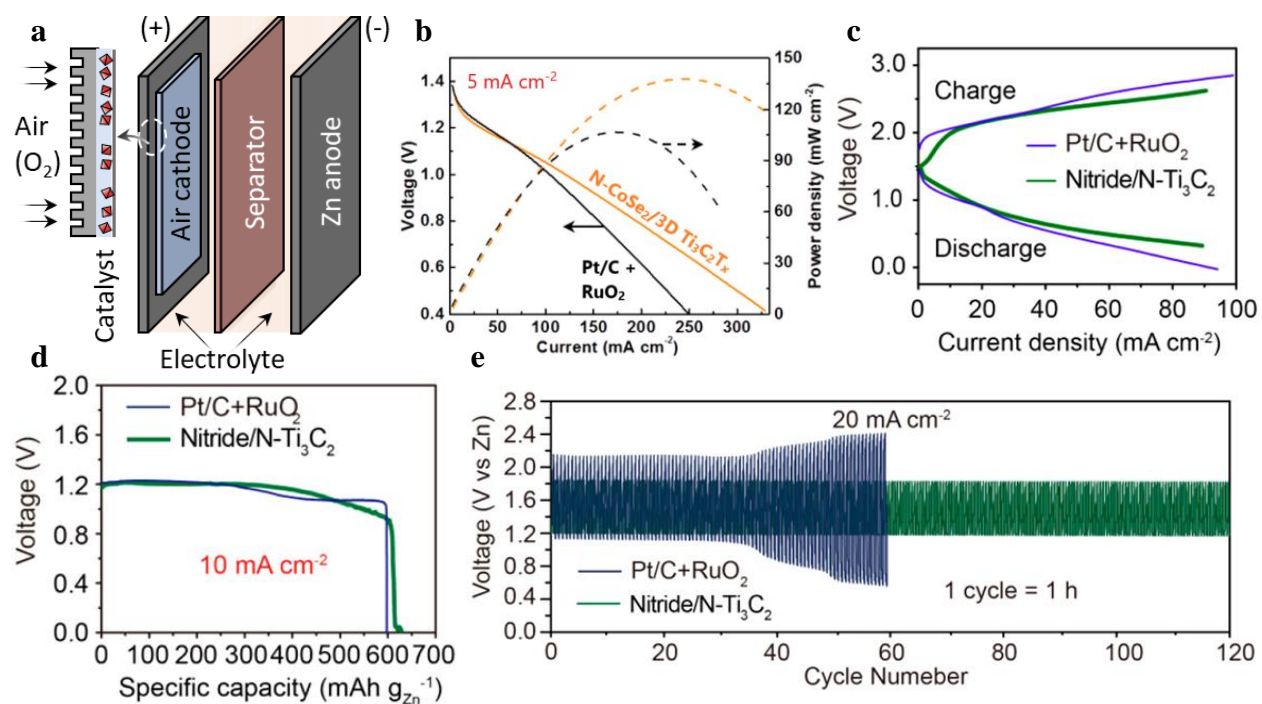


Figure 8. MXene hybrids as air cathodes for (a) Zn-air batteries. (b) Discharge and power density curves of N-CoSe₂/3D Ti₃C₂T_x cathode, compared against Pt/C + RuO₂. Adapted with permission from ref ²⁰⁶. Copyright 2019 American Chemical Society. (c) Charge-discharge polarization curves, (d) specific capacities (calculated with Zn mass consumed) and (e) galvanostatic charge-discharge cycling of NiFeMn nitride/N-Ti₃C₂T_x cathode, compared against Pt/C + RuO₂. Adapted with permission from ref ¹⁸⁰. Copyright 2020 American Chemical Society.

Recently, fiber-shaped flexible Zn-air batteries were developed with molecularly thin trimetallic NiFeMn nitride sheets stabilized by Ti₃C₂T_x, exhibiting bifunctionality toward both OER and ORR.¹⁸⁰ The stabilization effect was supported by theoretical calculations, while strong interfacial coupling between the nitride and Ti₃C₂T_x sheets was marked by the formation of ORR-active motifs (Ni/Fe/Mn-N-Ti) from the Ti (MXene)-N (trimetallic nitride) peak in the Ti 2p XPS spectrum. The ECSA for ORR/OER was maximized by stabilizing the 2D nitride sheets atop the MXene sheets, which facilitated efficient charge transport for electrocatalysis. This resulted in synergistic OER and ORR activity enhancement of the nitride/N-Ti₃C₂T_x hybrid after Ti₃C₂T_x incorporation, despite standalone Ti₃C₂T_x being practically OER and ORR-inactive. The potential difference between the OER $\eta_{j=10}$ and ORR half-wave potential ($E_{1/2}$) was smaller for the nitride/N-

Ti₃C₂T_x hybrid (0.68 V) than RuO₂ + Pt/C (0.80 V), illustrating the hybrid's superior OER/ORR bifunctionality without the use of PGMs. When used in Zn-air battery applications, the bifunctional nitride/N-Ti₃C₂T_x air cathode operated with a smaller charge-discharge voltage gap (hence better rechargeability, **Figure 8c**), and higher specific capacity (**Figure 8d**, 630 mAh g_{Zn}⁻¹) than RuO₂ + Pt/C. The hybrid also demonstrated long-term cycling stability for 120 cycles (120 h at 20 mA cm⁻²) with no appreciable voltage fade, in comparison to the large voltage increase and hence instability of the RuO₂ + Pt/C air cathode during the same cycling test (**Figure 8e**). After being incorporated into a unique fibrous design, the flexible Zn-air battery operated durably for more than 3 h under various mechanical deformation states for wearable technology applications.

Summary, specific challenges, and outlook for metal-air batteries. MXene hybrid metal-air batteries are still in their early stages of development, with predominantly Ti₃C₂T_x-based MXene hybrids being explored for Zn-air batteries. Theoretically, a high efficiency for MXene-derived catalyst supports has been predicted for Li-air batteries due to the MXenes' ability to adsorb Li species to facilitate interfacial charge transfer and redox reactions.²¹⁵ We thus expect MXene hybrids to be explored for other metal-air chemistries such as Li, Na, Mg and Al, using other highly conductive MXenes apart from Ti₃C₂T_x.

Beyond metal-air batteries, the high ORR activity of MXene hybrids can also be translated to effective PC pollutant degradation and environmental remediation, an essential application that can be readily deployed in remote and less developed areas. For example, Ti₃C₂T_x/TiO₂,⁴⁷ Ti₃C₂T_x/Ag₃PO₄,¹²² and In₂S₃/TiO₂@Ti₃C₂T_x⁴⁸ hybrids have demonstrated very high activity and durability for PC removal of organic dyes and inorganic pollutants.^{42,44} By combining strategies for designing efficient water splitting photocatalysts in the previous section (maximizing photo-carrier separation and minimizing carrier recombination) with the strategies discussed here in

designing efficient ORR electrocatalysts, we anticipate further strides to be made in MXene hybrid photocatalysts for broad-based pollutant remediation applications too.

MXene hybrids and composites for metal-sulfur batteries. Li-S batteries have been touted as the next-generation energy storage device for decades due to their unique conversion mechanism and high theoretical energy density (2500 Wh kg⁻¹).²¹⁶ During discharge, the Li anode is oxidized to Li⁺ ions which travel to the S cathode, reacts with it, and forms Li₂S through a series of lithiation steps and intermediate LiPS species ($n \text{Li}^+ + \text{S}_8 + n \text{e}^- \rightarrow \text{soluble Li}_2\text{S}_8 \rightarrow \text{Li}_2\text{S}_6 \rightarrow \text{Li}_2\text{S}_4 \rightarrow \dots \rightarrow \text{solid Li}_2\text{S}$). In reality, the majority of the intermediate LiPS species (Li₂S₄ to Li₂S₈) dissolves readily into the electrolyte before reaching the insoluble Li₂S phase, resulting in a lower discharge capacity and rapid capacity decay.²¹⁶ The soluble LiPS species can further diffuse to the Li anode to be chemically reduced to shorter-chain LiPS before diffusing back to the cathode to be re-oxidized in an internal short circuit/self-discharge (shuttling effect).²¹⁶ Furthermore, the poor ionic and electrical conductivity of the S cathode, coupled with a large volumetric expansion in the cathode upon lithiation ($\approx 80\%$), imposes structural stress and inhibits electrochemical performance at the S cathode.²¹⁶ To address these issues, S cathodes have been hybridized with C-based materials to improve conductivity, while polymeric binders, TM oxides and chalcogenides have been incorporated to improve LiPS adsorption.²¹⁶ Separator membranes, commonly coated with conductive polymers, TM oxides, or C-based materials, have also been placed in the electrolyte between the electrodes to capture the shuttling LiPS.²¹⁶

With a unique combination of metallic conductivity and polar T_x groups, MXenes have been employed as S-host materials for both the S cathode^{56,208} and separator,^{209,210} as they can chemically interact with LiPS and facilitate efficient electronic transport at the cathode.¹⁴ Experimentally, highly conductive MXenes (Ti₂CT_x,^{56,217} Ti₃C₂T_x,^{56,218} Ti₃CNT_x,⁵⁶ and V₂CT_x⁵⁸)

have been investigated as cathode materials. Theoretical studies have also revealed various MXene structures as good binders for LiPS chemisorption: M_2X MXenes (Ti_2CT_x ,²¹⁷ Ti_2NT_x ,²¹⁹ V_2CT_x ²¹⁹), M_3X_2 MXenes ($Ti_3C_2T_x$,²²⁰ $V_3C_2T_x$,²²¹ $Cr_3C_2T_x$,²²¹ $Zr_3C_2T_x$,²²¹ $Nb_3C_2T_x$,²²¹ $Hf_3C_2T_x$ ²²¹), and ordered double TM MXenes ($Mo_2TiC_2T_x$ ⁶⁷). Nazar's group determined that the LiPS species are strongly bonded to the Ti atoms in Ti_2CT_x through Lewis acid-base Ti-S bonding at the expense of Ti-OH (T_x) interactions.^{56,217} The effect of MXenes' surface chemistry on LiPS affinity was elucidated by density functional theory (DFT) calculations which concluded that $-O$ and $-F$ T_x groups act as stronger immobilizers than $-F$ in restricting LiPS diffusion in conventional electrolytes.^{219,221,222} Additionally, N-doping of $Ti_3C_2T_x$ further improved charge transport capacity and the Lewis acid-base binding strength to LiPS species.²²³ Since the MXene surface chemistry and doping character can be directly tuned by the synthetic method,^{34,43} we expect future work to utilize theory-guided calculations to screen dopants and T_x groups, to complement current synthetic methods and deliberately modulate the LiPS immobilization strength for a variety of MXenes to act as efficient S-host cathodes and separators for Li-S batteries.

Beyond the high electrical conductivity and chemical affinity to LiPS, MXenes are also mechanically robust to accommodate the large volumetric changes in the S cathode during charge/discharge cycles.¹⁴ However, MXene nanosheets have a high tendency to self-restack,⁵¹ limiting the S/LiPS loading and restricting Li^+ /electrolyte access at the S cathode. Thus, secondary materials have been integrated with MXenes as spacers to reduce MXene inter-layer re-stacking, while retaining the high electrical conductivity and LiPS binding affinity of MXenes. In this section, we highlight the use of MXene hybrids as S-host cathode and separator materials, illustrating how hybridization can augment the LiPS binding affinity to improve discharge capacity and impede capacity decay beyond that demonstrated by bare MXenes.

MXenes have been hybridized with TM chalcogenides²²⁴ and oxides^{105,208,225} to chemically interact with LiPS and expedite their catalytic conversion to Li₂S (**Figure 9a**). Zhang *et al.* electrostatically self-assembled a 3D S/MnO₂@Ti₃C₂T_x hybrid, taking advantage of the high surface area and conductivity of delaminated Ti₃C₂T_x sheets, and the high chemical affinity of MnO₂ to LiPS.²⁰⁸ The 3D mesoporous conductive network enabled a high S loading of $\approx 70\%$ and could readily accommodate volumetric changes during charge/discharge cycles. Moreover, the intense O-Ti-S and O-S peaks in the O 1s XPS spectrum validated the strong MnO₂-MXene integration and LiPS retention ability of MnO₂. The S/MnO₂@Ti₃C₂T_x cathode had a higher initial discharge capacity (1140 mAh g_S⁻¹, 0.05C) than the unhybridized components, which implies higher S utilization. The high cathode stability was demonstrated in the hybrid's respectable specific capacity of 501 mAh g_S⁻¹ after 500 cycles at 1C, with a minor 0.06% decay/cycle. Compared to the individual components (S/MnO₂ and S/Ti₃C₂T_x), the S/MnO₂@Ti₃C₂T_x hybrid's superior LiPS absorption was visually confirmed by the faintest coloration in the electrolyte after 4 h of cycling, indicating minimal LiPS dissolution into the electrolyte (**Figure 9b**).

Separately, the high LiPS binding affinity to other TM compounds such as TiO₂^{105,225} and MoS₂²²⁴ was validated experimentally. When used as symmetric cell electrodes in an electrolyte with Li₂S_x species, Ti₃C₂T_x/1T-2H MoS₂-C hybrid afforded the highest redox current density, and hence the fastest rate of catalytic LiPS conversion, as compared to their separate components (Ti₃C₂T_x and 2H-MoS₂) and the Ti₃C₂T_x/2H MoS₂-C hybrid (**Figure 9c**).²²⁴ This highlighted the importance of higher electrical conductivity (in 1T/2H-MoS₂) to facilitate electron transfer for LiPS redox conversion, as compared to using semiconducting 2H-MoS₂ for hybridization with MXenes. The 1T/2H-MoS₂ also contained a high concentration of edge defects and positively

charged S vacancies to bind strongly to negatively charged LiPS and facilitate electron transfer for rapid LiPS redox conversion.

Beyond TM compounds, C-based materials^{56,64,218} have also been hybridized with MXenes to further improve the cathode's electronic conductivity⁵⁶ for more efficient S utilization, and provide large surface areas to physically confine LiPS species.²¹⁸ Interweaving Ti-based MXene nanosheets ($\text{Ti}_3\text{C}_2\text{T}_x$, Ti_2CT_x , and $\text{Ti}_3(\text{CN})\text{T}_x$) with CNTs inhibited MXene inter-layer restacking to maximize Ti-S interactions for LiPS absorption, which led to stable cycling performances with high S loading of up to 5.5 mg cm^{-2} for high energy density Li-S batteries.⁵⁶ Separately, Zhou *et al.* treated $\text{Ti}_3\text{C}_2\text{T}_x$ sheets with molten KOH to produce $\text{Ti}_3\text{C}_2\text{T}_x/\text{C}$ hybrids with an expanded inter-layer spacing and significantly increased surface area (from 3.5 to $150 \text{ m}^2 \text{ g}^{-1}$).²¹⁸ Hybridization with disordered C also reduced the charge transfer resistance by five-folds to accelerate LiPS conversion, increasing the calculated Li_2S precipitation capacity from 95 to 226 mAh g^{-1} .²¹⁸ Since TiO_2 was previously reported to improve LiPS binding efficiency,^{105,225} we predict that the partial oxidation of Ti-based MXenes to MXene/ TiO_2/C hybrids⁹² (similar to those for PC HER applications) may significantly enhance LiPS absorption and redox conversion kinetics, while providing a conductive, large-area support for LiPS deposition.

MXenes and their hybrids have also been incorporated in Li-S battery separators. As some MXenes are known to have high LiPS binding affinity, MXene-containing separators can immobilize parasitic LiPS shuttling between electrodes, thus limiting the internal short circuit effect and prolonging cycling stability.^{209,210,226} Similar to the cathode designs, MXenes have been hybridized with TM oxides (with high LiPS adsorption affinity)²²⁷ and C-based materials^{210,226} to act as efficient physical barriers at the separator facing the cathode. For example, Jiao *et al.* produced $\text{TiO}_2@\text{Ti}_3\text{C}_2\text{T}_x$ hybrids from controlled partial oxidation of $\text{Ti}_3\text{C}_2\text{T}_x$, to be mixed with

graphene and coated on a commercial Celgard polymer separator (**Figure 9a**).²²⁷ From the LiPS permeation test (**Figure 9d**), no significant darkening in the electrolyte was observed when the optimized (4 h oxidation) graphene-TiO₂@Ti₃C₂T_x-polymer separator was used, in contrast to the untreated and graphene-coated separators. This validated the use of TiO₂ as LiPS adsorption centers, while MXenes provided a conductive large-area support to facilitate rapid LiPS conversion. When the separator was incorporated into a Li-S cell, only a minor 0.028% capacity fade/cycle was observed over 1000 cycles at 2C (red curve, **Figure 9e**), with stable cycling also observed for over 200 cycles at a higher 7.3 mg cm⁻² S loading.

Summary, specific challenges, and outlook of metal-sulfur batteries. The discovery of a strong Ti (MXene)-S (LiPS) bond,⁵⁶ coupled with high metallic conductivity and mechanical flexibility, have enabled Ti-based MXenes to serve as large-area S-host materials in Li-S cathodes and separators. By hybridizing MXenes with other secondary materials with high affinity toward LiPS absorption, MXene hybrids have successfully enhanced LiPS capture and redox conversion kinetics to improve the discharge capacity and cycling stability. While not discussed in this section, MXenes have also been utilized as S-host materials for Na-S batteries,²²⁸ and have shown promise as alkali metal hosts to impede dendrite formation at the anode.^{229–232} We thus expect efforts to be made in the theoretical screening of potential MXene hybrid combinations, especially with conductive non-Ti-based MXenes, for LiPS binding affinity and catalytic conversion to Li₂S. Combined with advanced synthetic designs in phase, defect, doping, and structural engineering of secondary materials on MXenes, future MXene hybrids could be applied in the cathode, anode, and separator to realize industrially relevant Li-S batteries with high discharge capacities, cycling stability, and S loading.

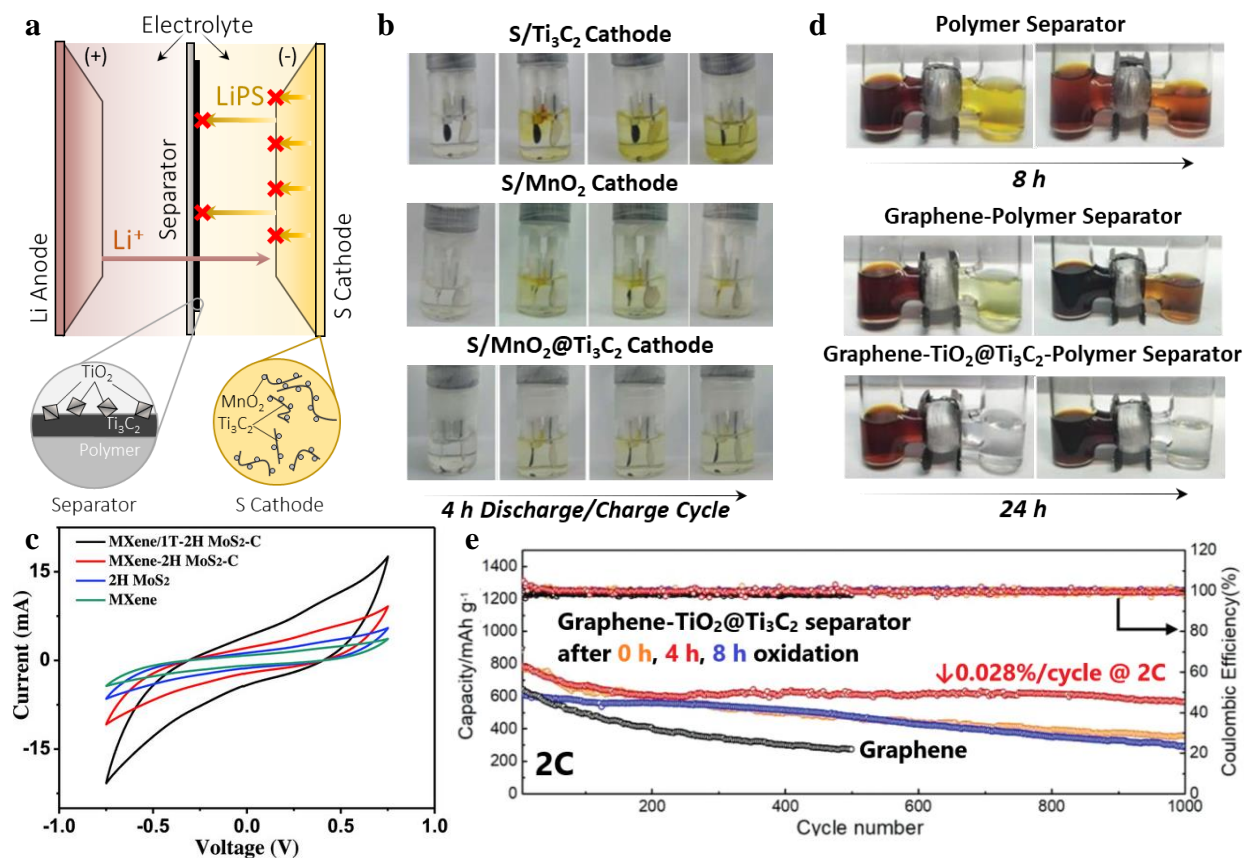


Figure 9. MXene hybrids as S cathodes and separators for (a) Li-S batteries. (b) Photographs of S/Mn₃O₄@Ti₃C₂T_x S cathode during 4 h of charge-discharge (yellow colouration indicates LiPS leeching into the electrolyte). Adapted from ref ²⁰⁸. Copyright 2018 American Chemical Society. (c) Symmetric cell cyclic voltammetry (CV) cycling using the MXene hybrids for both electrodes. Adapted from ref ²²⁴. Copyright 2018 WILEY-VCH. (d) Visual LiPS permeation test with graphene-TiO₂@Ti₃C₂T_x-polymer separator (yellow/brown colouration on the right side of the cell indicates LiPS permeating through the separator) and (e) long-term cycling of graphene-TiO₂@Ti₃C₂T_x separators (with different oxidation durations) at 2C. Adapted from ref ²²⁷. Copyright 2019 WILEY-VCH.

MXENE HYBRIDS FOR EMERGING EC, PC, AND PEC REACTIONS OF INTEREST

TM carbides and nitrides have a long history in catalyzing hydrogenation (or dehydrogenation) reactions due to their suitable surface interactions with the relevant reaction intermediates.^{233,234} With growing research interest in sustainable catalytic reactions, it was discovered that TM carbides and nitrides are also active in the catalytic conversion of abundant and stable moieties like CO₂ or N₂ to higher value-added chemicals.²³⁵ Sharing similarities to the bulk 3D crystalline TM carbide and nitride forms, MXenes are also anticipated to be catalytically active for CO₂ and N₂ activation due to their suitable adsorption sites^{236,237} and favorable adsorbate interactions.²³⁸ Having recently demonstrated promising nitrogen and carbon catalysis on MXenes,^{25,239} MXene hybrids have been predicted to expand the platform even further to enhance catalytic activity and catalyze other important reactions in the future. Here, we analyze the current strategies and pathways in which MXenes hybrids have been used to enhance important PC, EC, and PEC reactions of CO₂, N₂, and their related moieties.

MXene hybrids and composites for electrocatalytic/photocatalytic (EC/PC) carbon dioxide reduction (CO₂RR). MXenes synthesized to date are similar to the bulk 3D crystalline non-MXene TM carbides and nitrides in terms of high electronic conductivity.^{152,240} Additionally, the MXenes' basal planes are terminated with T_x groups in ambient conditions or electrolytes.²⁴¹ These T_x groups usually comprise of electronegative elements (F, O, Cl) that can alter the MXenes' effective work function^{242,243} and bring about unique MXene-intermediate molecule adsorbate interactions.^{23,244,245} In CO₂RR, these unusual interactions render alternative thermodynamic pathways that were previously and commonly unfavorable on TM catalysts, feasible, providing a means to circumvent the scaled binding energy relations.²⁴⁶ Beyond providing active sites for CO₂RR intermediates, Chen *et al.* described an interesting possibility of MXenes' T_x groups being

involved in the catalysis process.²² The DFT scheme in **Figure 10a** describes how H atoms in the T_x termination group can be “borrowed” by the intermediate during some of the proton-electron transfer steps, before being regenerated in the last three proton coupled electron transfer steps.

Despite encouraging theoretical simulations, EC CO₂RR catalysis by bare MXenes in aqueous electrolytes have yet to be reported, possibly due to the weaker CO₂RR intermediate-MXenes binding strength, and severe competition from HER as a side-reaction.¹⁸ Handoko *et al.* recently reported EC CO₂RR on Ti₂CT_x and Mo₂CT_x MXenes in a mixture of acetonitrile, water, and 1-Butyl-3-methylimidazolium tetrafluoroborate (BMIMBF₄).²⁵ Formic acid (HCOOH) was the main product, with peak HCOOH Faradaic efficiency (FE_{HCOOH}, see **Vocabulary** for definition of FE) of 56% at -1.8 V (vs. standard hydrogen electrode, SHE) on Ti₂CT_x synthesized with KF-HCl (**Figure 10b**). Interestingly, higher activity and an earlier CO₂RR onset potential was observed for MXenes with lower -F T_x content. This observation is explained by DFT calculations, which revealed that the critical step involving the *COOH intermediate is more adversely affected by an increasing presence of -F T_x groups (**Figure 10c**).

As such, we believe that MXene hybrids can offer a viable value proposition. In addition to their excellent electronic conductivity, thin MXene layers would be a superior catalyst support choice compared to other C-based materials, due to stronger metal-support interactions.²⁴⁷ Furthermore, the possibility of intermetallic compound formation has been reported,²⁴⁸ revealing an active surface with a unique electronic structure that is more resistant to agglomeration.²⁴⁹ For example, Mo₂CO₂ MXene has been predicted as a good Pd support.²⁵⁰ Specifically, a more active Pd dimer species that allows for partial methane oxidation to methanol can be stabilized on Mo₂CO₂ MXenes.²⁵⁰

In addition, MXenes have also been demonstrated to be suitable substrates for single atom catalysts (an emerging active frontier in heterogeneous catalysis²⁵¹) such as Pt, Ru and Rh, through a simple self-reduction reaction at room temperature.²⁵² The single atom nature of PGMs substituting the Ti positions in $\text{Ti}_3\text{C}_2\text{T}_x$ MXene was demonstrated with extended X-ray absorption fine structure (EXAFS, **Figure 10d**) spectroscopy and high-angular annular dark-field (HAADF) scanning transmission electron microscopy (STEM) imaging (**Figure 10e**).²⁵² In particular, $\text{Pt}_1/\text{Ti}_{3-\delta}\text{C}_2\text{T}_x$ structures were reported to be active for CO_2 activation with amines and silane into formamide at 140 °C with near-complete conversion and selectivity.²⁵²

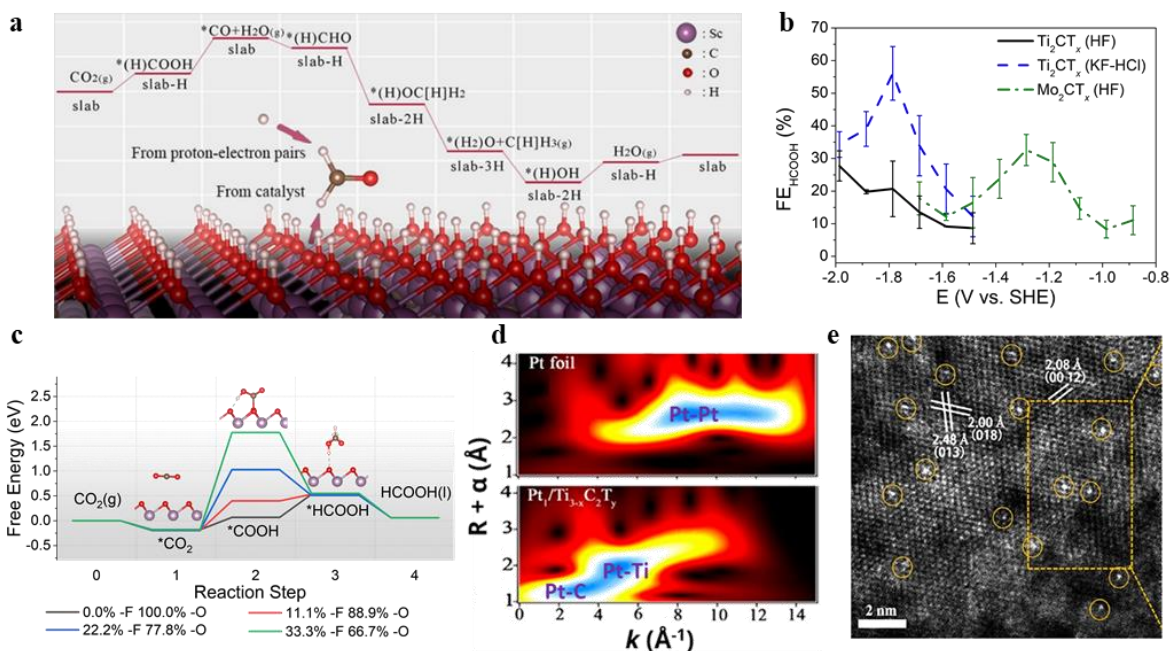


Figure 10. MXenes for CO_2 RR. (a) DFT scheme showing the possible involvement of T_x atoms in CO_2 RR to CH_4 . Adapted with permission from ref ²². Copyright 2019 American Chemical Society. (b) Comparison of FE for CO_2 RR to formic acid on Ti_2CT_x and Mo_2CT_x . Error bars represent one standard deviation of three independent measurements. (c) Calculated free energy diagram at 0 V applied potential for CO_2 RR to formic acid on Mo_2CT_x MXenes with varying fractions of -F and -O surface T_x groups. Purple, red, brown and white spheres represent Mo, O, C and H atoms respectively. Adapted with permission from ref ²⁵. Copyright 2020 The Authors. (d) Two-dimensional wavelet transformation of Pt K-edge EXAFS (radial distance information in the y-axis and energy dependence k -space in the x-axis) and (e) HAADF STEM of $\text{Pt}_1/\text{Ti}_{3-\delta}\text{C}_2\text{T}_x$.

which clearly demonstrates the absence of Pt-Pt bond in the single atom Pt-on-Ti₃C₂T_x MXene. Adapted with permission from ref ²⁵². Copyright 2019 American Chemical Society.

We note that most experimental CO₂RR on MXenes or their hybrids were conducted using PC/PEC instead of EC. This is intriguing, as apart from the photophysical processes, PC should share many commonalities with EC.²⁵³ Discrepancies between the measured activities of the same TM catalyst (or co-catalyst) species in EC and PC approaches have been reported.²⁵⁴ These discrepancies can be partly attributed to the attenuated work function under steady state illumination and interfacial voltage loss,²⁵⁵ limited cathodic potential range (*i.e.* conduction band position),²⁵⁶ and temporal discontinuity between the photo-generated carrier lifetime (fs to ms) and reaction kinetics (ms to s).^{256,257} Besides impacting catalytic activity, we believe that these differences may enhance the selectivity in PC CO₂RR, as the diverse intermediate stability in CO₂RR and rate of competitive HER is sensitive to the applied potential.²⁰²

A commonly adopted hybrid combination for PC CO₂RR is MXenes coupled with a wider bandgap photo-absorber. MXenes made to date are metallic and some are predicted to have narrow bandgaps,²⁵⁸ thus hybridization with a wider bandgap photo-absorber is the only way to generate sufficient photo-carriers for catalysis. A notable example is the Ti₃C₂T_x/g-C₃N₄ hybrid which produced 2.24–5.19 and 0.04–0.05 μmol g⁻¹ h⁻¹ of CO and CH₄ respectively.^{259,260} Although g-C₃N₄ is a very good photo-absorber with high quantum yield even at visible wavelengths ($\lambda > 395$ nm),²⁶¹ it is limited by rapid charge recombination.²⁶² The role of Ti₃C₂T_x in the hybrid is likely that of a charge separator, as their work function position is suitably positioned to accept electrons from the g-C₃N₄ conduction band, thus enhancing the photo-generated carrier lifetime (**Figure 11a**).²⁵⁹ The activity of Ti₃C₂T_x/g-C₃N₄ was further enhanced considerably by depositing Pd on the hybrid structure, which produced formate and methanol at a rate of 905 and 350 μmol g⁻¹ h⁻¹, respectively, in a PEC setting.²⁶³ Pd is a very interesting co-catalyst choice, because it is known to

bind very strongly to adsorbed *CO in EC CO₂RR,²⁶⁴ which often leads to catalyst deactivation. The authors attributed the high activity of the Ti₃C₂T_x/g-C₃N₄/Pd hybrid to electron trapping by protonic species on the Pd surface, but we speculate that the stronger binding may allow the key *CO intermediate to persist longer, allowing for photo-electron accumulation and transfer.

Depending on the relative band positions, hybridization of metals (*i.e.* MXenes) with semiconductors often results in a built-in Schottky junction. This increases the electronic transport resistance and it is thus generally undesired. However, in PC, the Schottky barrier junction may actually improve the overall carrier lifetime by minimizing the electron losses associated with back injections. One example of the adoption of this strategy is reported in Ti₃C₂T_x/CeO₂, which produced up to 40.2 μmol g⁻¹ h⁻¹ of CO.²⁶⁵ The built-in junction may also exist in many other examples, especially in hybrids involving wide-bandgap *n*-type semiconductors such as TiO₂,⁸⁵ Bi₂WO₆,¹⁰¹ or CsPbBr₃,¹²⁵ although this is hard to ascertain as the MXenes' work function varies²⁴³ depending on the actual T_x composition in the reaction environment. Hybridization with these semiconductors generally yield modest CO₂RR activity (**Table S4a**), of up to 28 μmol g⁻¹ h⁻¹ products for Ti₃C₂T_x/P25/TiO₂.²⁶⁶ While a slightly higher activity was observed for Ti₃C₂T_x/CsPbBr₃ (32 μmol g⁻¹ h⁻¹ CO and 14 μmol g⁻¹ h⁻¹ CH₄), the perovskite's (CsPbBr₃) instability in aqueous solutions necessitated the use of ethyl acetate as the electrolyte.¹²⁵

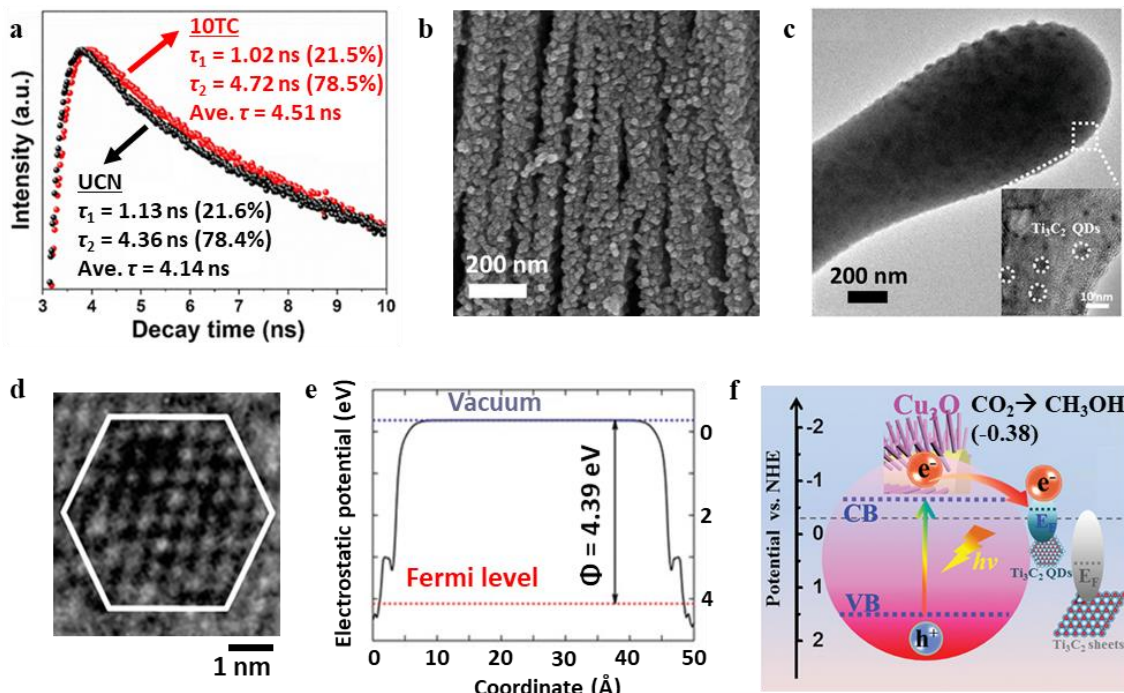


Figure 11. MXene hybrids for PC/PEC CO₂RR. (a) Transient PL spectroscopy showing a longer photo-generated carrier lifetime for $\text{Ti}_3\text{C}_2\text{T}_x/g\text{-C}_3\text{N}_4$ (10TC), compared to bare $g\text{-C}_3\text{N}_4$ (UCN). Adapted with permission from ref ²⁵⁹. Copyright 2020 Elsevier B.V. (b) Morphology of $\text{Ti}_3\text{C}_2\text{T}_x/\text{TiO}_2$ after controlled calcination of $\text{Ti}_3\text{C}_2\text{T}_x$ at 550°C. Adapted with permission from ref ⁸⁵. Copyright 2018 Elsevier Inc. (c) TEM image of $\text{Ti}_3\text{C}_2\text{T}_x$ QD/Cu₂O and (d) HRTEM image of $\text{Ti}_3\text{C}_2\text{T}_x$ QDs, showing hexagonal units. (e) DFT calculated Fermi level and (f) band diagram of $\text{Ti}_3\text{C}_2\text{T}_x$ QD/Cu₂O. Adapted with permission from ref ¹²¹. Copyright 2018 WILEY-VCH.

$\text{TiO}_2/\text{Ti}_3\text{C}_2\text{T}_x$ is another popular MXene hybrid for PC CO₂RR, since TiO_2 can be naturally grown from *in-situ* conversion of Ti-based MXenes *via* partial oxidation. Under the right synthesis conditions, hierarchical hybrids were produced while retaining the conductive $\text{Ti}_3\text{C}_2\text{T}_x$ backbone (**Figure 11b**).⁸⁵ The *in-situ* grown $\text{TiO}_2/\text{Ti}_3\text{C}_2\text{T}_x$ hybrid, combined with Pd co-catalysts, is possibly the most active MXene hybrid for PEC CO₂RR, yielding a cocktail of products (formate, methanol, and ethanol) at a high total hydrocarbon yield of 1840 $\mu\text{mol g}^{-1} \text{h}^{-1}$.⁹² Separately, a different approach hybridized $\text{Ti}_3\text{C}_2\text{T}_x$ with Cu_2O (**Figure 11c**).¹²¹ Instead of using large MXenes flakes directly, tiny $\text{Ti}_3\text{C}_2\text{T}_x$ QDs were prepared by rigorous sonication in inert argon. These MXene QDs were then treated with positively charged polyethylenimine to aid their electrostatic self-assembly with negatively charged polystyrene sulfonate-coated Cu_2O nanorods. The theoretical Fermi level

of the hexagonal $\text{Ti}_3\text{C}_2\text{T}_x$ QDs was estimated to be significantly lower than the “bulk” $\text{Ti}_3\text{C}_2\text{T}_x$ sheets (**Figures 11d and 11e**), which resulted in more facile electron transfer from the Cu_2O photo-absorber, at a potential above the thermodynamic requirement for CO_2RR to methanol (-0.81 V vs. RHE, **Figure 11f**).²⁰² The $\text{Ti}_3\text{C}_2\text{T}_x$ QD/ Cu_2O hybrid supplied $78.5\ \mu\text{mol g}^{-1}\text{ h}^{-1}$ of methanol.

Beyond CO_2RR , $\text{CdS}/\text{Ti}_3\text{C}_2\text{T}_x$ was also shown to be active in the PC reduction of 4-nitroaniline to *p*-phenylenediamine (PPD),²⁶⁷ an important synthetic intermediate for dyes and aramid fibers. While the PC activity of CdS in reducing aromatic nitro-compounds is not surprising, hybridization with MXenes significantly enhanced their activity and photo-stability. It was proposed that hybridization with CdS formed a Janus-like structure, characterized by the strong metallic adsorption of Cd onto $\text{Ti}_3\text{C}_2\text{T}_x$,²⁶⁸ thus limiting the dissolution of CdS. Similar strategies may therefore be extended to other TM chalcogenides for enhancing CO_2RR activity.

MXenes hybrids and composites for electrocatalytic/photocatalytic (EC/PC) nitrogen reduction (N_2RR). The abundance of N_2 in the air has attracted many attempts to convert them to nitrate and ammonium compounds for agricultural applications. Combined with steam reforming of natural gas, the Haber-Bosch process is still widely used in modern ammonia production plants worldwide today. Although the Haber-Bosch process is an exothermic reaction overall, it still requires a massive energy input to drive the $\text{N}\equiv\text{N}$ bond dissociation ($941\ \text{kJ mol}^{-1}$) through the dissociative pathway over a suitable catalyst (**Figure 12a**).²⁶⁹

EC/PC N_2RR offers an attractive alternative to the Haber-Bosch process. With the ability to be conducted under ambient conditions, N_2RR is potentially safer, cleaner, and a more sustainable way to produce NH_3 with a smaller plant footprint when coupled with sustainable energy inputs. Unlike the Haber-Bosch process with a kinetically²⁷⁰ (or thermodynamically,²⁷¹

depending on the substrate) limited $\text{N}\equiv\text{N}$ dissociation step, PC/EC N_2RR preferentially undergoes the associative pathway, whereby the adsorbed N_2 molecule first undergoes stepwise protonation.²⁶⁹ The associative N_2RR pathway diverges to three main pathways depending on the initial N_2 adsorption geometry (**Figure 12b**): alternating and distal protonation mechanisms operate when N_2 is adsorbed end-on, while the enzymatic mechanism operates after N_2 is adsorbed side-on.^{272,273} There are also possibilities of pathway inter-mixing, depending on the thermodynamic and kinetic barriers.²⁷⁴ Side-on N_2 adsorption is more favorable on the basal planes of bare M_2C MXenes,^{24,275,276} M_3C_2 MXenes with group 14 “M” elements (**Figure 12d**),²⁷⁷ and ordered double TM $\text{Mo}_2\text{TiC}_2\text{T}_x$ MXenes.²⁷⁸ Conversely, distal adsorption is preferred on M_3C_2 MXenes with group 15 and 16 “M” elements.²⁷⁷ However, it should be noted that bare MXenes are unlikely to be stable under N_2RR operating conditions,²⁴ and it is important to include the relevant T_x species when performing theoretical calculations. The T_x groups generally cause N_2 adsorption on MXenes to be more difficult,²⁴ although alternative adsorption sites can be provided by exposed “M” sites at the edges (**Figure 12e**),²⁷⁹ or on single atom dopants.²⁷⁴

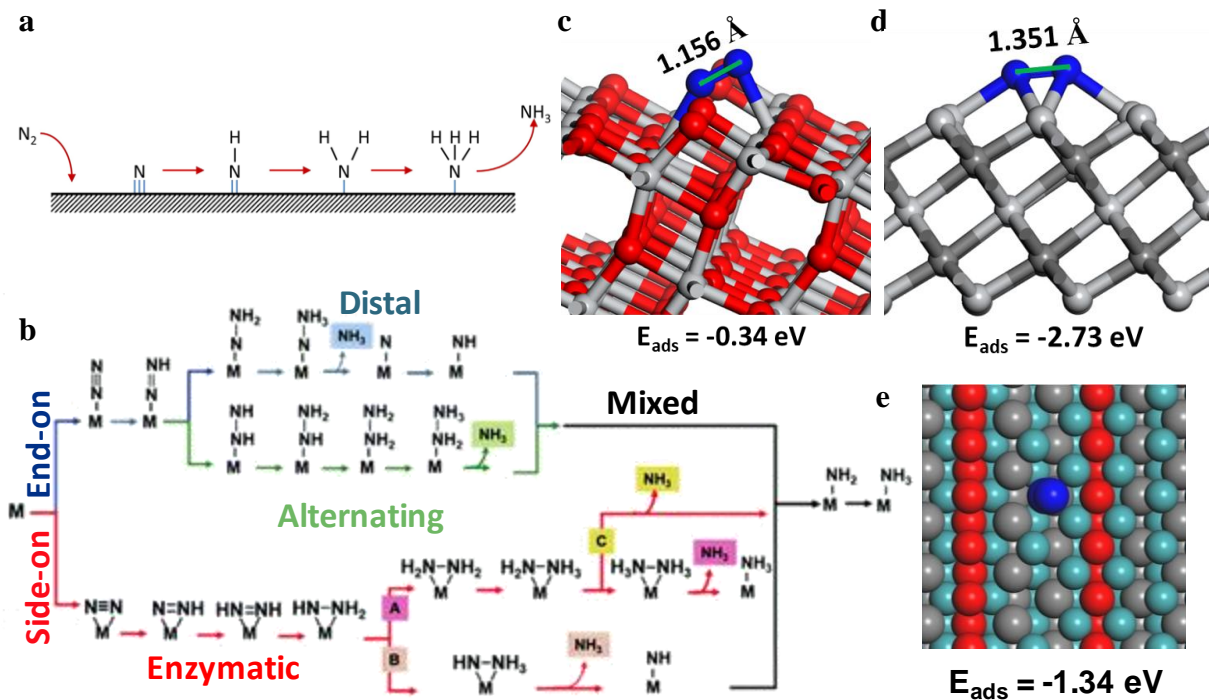


Figure 12. N_2 RR mechanistic study. (a) Dissociative N_2 reduction to NH_3 . Adapted with permission from ref ²⁶⁹. Copyright 2016 Elsevier B.V. (b) Associative N_2 reduction to NH_3 , with diverging pathways depending on the adsorption geometry of the N_2 molecule. Adapted with permission from ref ²⁷⁵. Copyright 2020 Royal Society of Chemistry. Schematics of side-on N_2 adsorption on (c) defective (101) TiO_2 surface with O-vacancy and on (d) $Ti_3C_2T_x$ MXene. Dark grey, red, light grey and blue balls represent C, O, Ti and N respectively. Adapted with permission from ref ²⁸⁰. Copyright 2020 Elsevier B.V. (e) Alternative end-on N_2 adsorption on the exposed Ti site on $Ti_3C_2O_2$ MXene edges. Gray, red, sky blue and blue balls represent C, O, Ti and N respectively. Adapted with permission from ref ²⁷⁹. Copyright 2018 Elsevier Inc.

Before discussing the catalytic N_2 RR activity of MXenes and their hybrids, it is imperative that we discuss the best activity reporting practices. A recurring issue in most PC/EC N_2 RR research is that the quantity of NH_3 product produced is very small, in the range of 10 to 1000 nmol,²⁸¹ and thus very susceptible to contamination and false positives. Therefore, establishing a suitable NH_3 detection protocol with robust control measurements is vital. There are two commonly adopted methods to quantify the produced NH_3 in solution: (1) colorimetric assays, including Nessler's reagent (Nessler) or Berthelot's reagent (*e.g.* indophenol blue, IB), and (2) ion chromatography (IC). While both methods generally work well in detecting low concentrations of

NH_3 ($<500 \mu\text{g L}^{-1}$),²⁸² any impurities that result in false strong absorption in the detection wavelength, such as methanol and carbon particles, must be avoided in colorimetric-based methods. We note that the IB-based colorimetric assays are unsuitable for use at $>500 \mu\text{g L}^{-1}$ NH_3 , or in acidic media, due to higher deviations.²⁸² Finally, rigorous experimentation, including statistical reproducibility and confirmation that the NH_3 originated from N_2RR , requires the use of isotopically labeled $^{15}\text{N}_2$. Detection of $^{15}\text{NH}_3$ can be achieved using mass spectrometry, infrared, or nuclear magnetic resonance (NMR) spectroscopy.²⁸³ For the reader's benefit, we report the NH_3 detection method, and whether ^{15}N isotope labeling control was performed in summary **Table S4b**.

$\text{Ti}_3\text{C}_2\text{T}_x$ is the most commonly used MXene for PC/EC N_2RR due to their stability²⁸⁴ and close structural relationship with the popular TiO_2 photocatalyst. $\text{Ti}_3\text{C}_2\text{T}_x$ has been reported to perform EC N_2RR with modest NH_3 yields ($157\text{--}522 \mu\text{mol g}^{-1} \text{h}^{-1}$) and FE at relatively low cathodic potentials (-0.1 to -0.4 V vs. RHE), with electrochemical and structural stability.^{239,279} Investigations into MXene hybrids, especially through the use of single atom dopants, have predicted attractive N_2RR activity, as the single atom dopants provide more favorable N_2 adsorption sites and correspondingly lower activation barriers. A range of *in-silico* single atom modifications (boron²⁷⁴ and various TMs^{271,285,286}) have been studied, with Ru, Mo, Ti, and Fe commonly identified as promising dopants with the least negative N_2RR limiting potentials. Apart from calculating the lowest energy pathway from N_2 to NH_3 , it is also critical to evaluate the formation energy and the stability of the hybrid through first principle calculations, or from more realistic kinetic stability studies.²⁸⁷

Experimentally, $\text{Ti}_3\text{C}_2\text{T}_x$ has been used to support metallic N_2RR electrocatalysts such as Ru ($2321 \mu\text{mol g}^{-1} \text{h}^{-1}$ and 13% FE)²⁸⁸ and fine ($<10 \text{ nm}$) Au NPs ($1761 \mu\text{mol g}^{-1} \text{h}^{-1}$ and 18.3% FE),²⁸⁹ with up to 14 times higher N_2RR activity than bare $\text{Ti}_3\text{C}_2\text{T}_x$. Enhanced N_2 adsorption and

*N₂ coverage was a reason for the high catalytic activity on fine Au NPs/Ti₃C₂T_x, as shown in the desorption profile (**Figure 13a**). Despite numerous encouraging predictions of N₂RR on single-atom/MXene hybrids, only one example was reported experimentally, using Ru single atoms/Mo₂CT_x.²⁹⁰ This hybrid electrocatalyst is highly N₂RR active, yielding 2382 μmol g⁻¹ h⁻¹ NH₃ at a significant 25.7% FE. The N₂RR active site was investigated using *operando* Ru K-edge X-ray absorption near edge structure (XANES). A slight increase in the Ru oxidation state to +3.56 was observed when N₂ was introduced without bias (at open circuit potential, OCP) compared to the baseline measurement in Ar (+3.27), attributed to the electron back-donation when the Ru-N₂ bond was formed. The oxidation state reduces back to +3.15 when a N₂RR-relevant potential (-0.3 V *vs.* RHE) was applied, indicating N₂RR. This phenomenon was also observed in the Fourier transformed-XANES (FT-XANES, **Figure 13b**). A discernible shift in the first neighbor peak to a shorter apparent distance of 1.51 Å was seen when N₂ was introduced, which reverted back to 1.56 Å during N₂RR, possibly due to Ru-N coordination during adsorption.

Beyond metallic catalysts, Ti₃C₂T_x was also combined with TM oxide catalysts such as Mn_xO_y.²⁹¹ Manganese oxides are N₂RR active, but exist in many structures with poor conductivity that limit their EC N₂RR performance. Hybridizing MnO₂ with Ti₃C₂T_x MXenes yielded up to 2003 μmol g⁻¹ h⁻¹ NH₃ (11.39% FE) and traces of N₂H₂ at -0.55 V *vs.* RHE.²⁹¹ The superior N₂RR activity of Ti₃C₂T_x/MnO₂ was ascribed to multiple advantages provided by the Ti₃C₂T_x support: (1) prevention of MnO₂ aggregation, (2) facilitation of electron transfer to MnO₂ and avoidance of parasitic current loss, and (3) larger surface area with favorable adsorption and active sites.

As discussed earlier, Ti₃C₂T_x is a good precursor for *in-situ* conversion to Ti₃C₂T_x/TiO₂ hybrids. It is interesting that Ti₃C₂T_x/TiO₂ hybrids can display EC N₂RR activity with modest NH₃ yield (1545–1889 μmol g⁻¹ h⁻¹) and FE (8.42–16.07%) in aqueous solutions,^{91,292} despite potential

competition from HER and the poor conductivity of TiO₂. Expectedly, there are many more examples of Ti₃C₂T_x/TiO₂ hybrids reported for PC than EC N₂RR to utilize TiO₂ as a photocatalyst. The highest PC NH₃ yield using MXene hybrids so far is reported by Hou *et al.* (422 μmol g⁻¹ h⁻¹).⁸⁶ This recent work demonstrated that the hybrid's photo-response extends up to the near-infrared region. A significant yield (82 μmol g⁻¹ h⁻¹) was still detectible at 740 nm irradiation, corresponding to an apparent quantum efficiency (AQE) of 0.07% (**Figure 13c**).⁸⁶ Liao *et al.* recently investigated the role of Ti₃C₂T_x in enhancing TiO₂ N₂RR activity.²⁸⁰ In this work, the authors mixed P25 TiO₂ (80% anatase and 20% rutile phase) with Ti₃C₂T_x and treated them in N₂ atmosphere. Interestingly, the hybridization process introduced significant O-vacancies in TiO₂, as indicated by the broadening of the Raman peak around 1500 cm⁻¹, and a strong low temperature electron spin resonance (ESR) signal (**Figure 13d**). The defective TiO₂ sites acted as an alternative adsorption site (**Figure 12c**) alongside Ti₃C₂ (**Figure 12d**), which enabled a higher coverage of adsorbed *N₂. At the optimum Ti₃C₂T_x loading of 6%, the NH₃ yield of the hybrid was 10.74 μmol g⁻¹ h⁻¹ without any sacrificial reagents. The NH₃ yield was further enhanced to 43.44 μmol g⁻¹ h⁻¹ after 0.02 M CH₃OH was added as a sacrificial electron donor (**Figure 13e**), indicating that the anodic reaction (water oxidation) is still a significant bottleneck.

Alternatively, the oxidation of Ti₃C₂T_x to TiO₂ can be fully completed, resulting in a unique MXene-derived TiO₂ structure with many Ti³⁺ sites, which are inherently more active catalytically.²⁹³ These MXene-derived hybrids were used for EC and PC N₂RR. Using *in-situ* oxidation, a more complex MXene-derived hybrid of TiO₂@C/g-C₃N₄ was also produced from Ti₃C₂T_x for PC N₂RR.²⁹³ This structure was demonstrated to be an efficient and stable N₂RR photocatalyst with an NH₃ production rate of 250.6 μmol g⁻¹ h⁻¹. The outstanding NH₃ production

performance was attributed to the abundance of surface defects, efficient electron-donation, suitable light harvesting, small transition impedance, and strong N₂ adsorption.

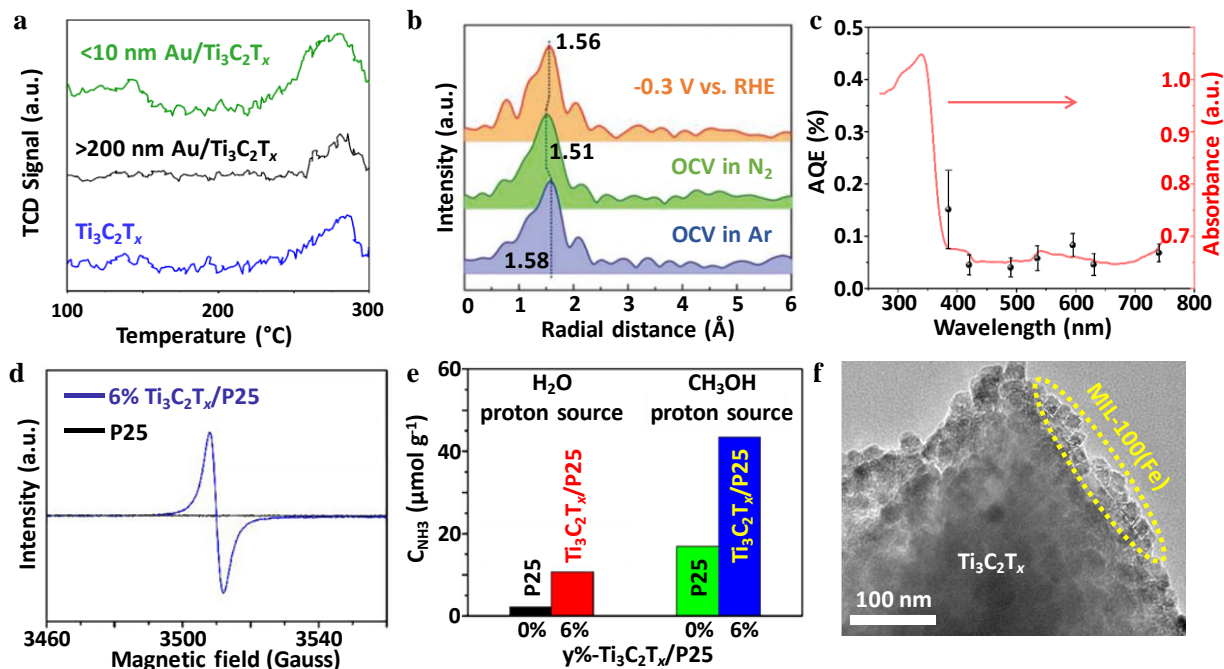


Figure 13. MXene hybrids for N₂RR. (a) N₂ temperature programmed desorption profile of Ti₃C₂T_x, <10 nm Au/Ti₃C₂T_x hybrid, and >200 nm Au/Ti₃C₂T_x hybrid. A broad peak around 130 °C signifies N₂ physisorption, while the band closer to 280 °C represents N₂ chemisorption. Adapted with permission from ref ²⁸⁹. Copyright 2019 American Chemical Society. (b) FT-EXAFS spectra derived from the normalized *operando* Ru K-edge XANES spectra for single atom Ru-Mo₂CT_x under various applied voltages vs. RHE in 0.5 M K₂SO₄. Adapted with permission from ref ²⁹⁰. Copyright 2020 WILEY-VCH. (c) AQEs for N₂ fixation on Ti₃C₂T_x/TiO₂ under monochromatic light irradiation. Adapted with permission from ref ⁸⁶. Copyright 2020 Elsevier B.V. (d) ESR spectra of bare P25 and 6% Ti₃C₂T_x/P25 hybrid, (e) NH₃ yield after 1 h N₂RR on 0% (bare P25) and 6% Ti₃C₂T_x/P25 hybrid, in H₂O and with 0.2 M CH₃OH. Adapted with permission from ref ²⁸⁰. Copyright 2020 Elsevier B.V. (f) HRTEM of 15%-Ti₃C₂T_x/MIL-100(Fe) hybrid. Adapted with permission from ref ²⁹⁴. Copyright 2019 American Chemical Society.

Apart from N₂RR, NO oxidation is another pathway for nitrogen fixation and air pollution elimination, since NO accounts for 95% of all the NO_x contaminations in air.²⁹⁴ Wang *et al.* reported the PC oxidation of NO by the Ti₃C₂T_x/MIL-100(Fe) MOF hybrid (**Figure 13f**). This work found that 58% NO was eliminated by the hybrid containing 15 wt% Ti₃C₂T_x, which was 2.8 and 4.1 times more efficient than the bare MIL-100(Fe) MOF and Ti₃C₂T_x MXene, respectively.

The enhanced NO oxidation was due to synergistic effects in the as-formed Schottky junction: $\text{Ti}_3\text{C}_2\text{T}_x$ acted as an electron conductor and accumulated electrons on surface to promote O_2RR and form $\cdot\text{O}_2^-$. Both the generated $\cdot\text{O}_2^-$ and h^+ active species on the surface of MIL-100(Fe) then oxidized NO to NO_3^- in the presence of water.

Summary, specific challenges, and outlook for EC/PC CO_2RR and N_2RR . Thus far, we have elaborated on how MXene hybrids have found their way into emerging catalytic reactions (of CO_2 , N_2 and related compounds), functioning either as support or active materials. Although the use of MXenes in these emerging catalytic reactions is nascent and has yet to result in record performance metrics, it provides a variety of different reaction pathways and is a welcome addition as an alternative catalyst support choice. We predict that the role of MXenes in these emerging reactions will continue to grow as we discover more MXene hybrids and learn more about their unique interactions with reaction intermediates and other co-catalysts. A summary table of performance metrics for various MXene hybrids in EC/PC CO_2RR and N_2RR is provided in **Tables S4a and S4b** respectively.

Specifically, we identify that the MXene/single atom hybrid is a worthwhile opportunity to pursue due to the many encouraging computational predictions but minimal experimental demonstrations. Single atom catalysis is a rapidly expanding field whereby methods of synthesizing and stabilizing these single atoms are quickly being developed.²⁵¹ Related to this point, mechanistic studies into MXene/single atom hybrids have not been established and is thus open for investigation, especially on the dynamic behavior of these single atom catalysts during catalytic reactions. Although the evidences so far suggest that single atom dopants are the active species, the catalytic action may also rely on the adsorbate interactions with the MXene catalyst support, for example through stepwise or cascading reactions. We foresee that *operando*

techniques capable of discerning transient catalyst state and surface adsorbates, such as resonant inelastic X-ray scattering and SECM, will play an important role here.

Another interesting research opportunity lies in bridging the gap in understanding between the PC and EC operating modes of CO₂RR and N₂RR on MXenes and their hybrids. We note that most direct experimental CO₂RR on MXene hybrids have been reported on PC compared to EC, possibly pointing to the direction of an indirect electron transfer driven reaction. In PC reactions, HER appears to be less severe a problem, even if these reactions (CO₂RR, N₂RR) are conducted in aqueous electrolytes. Although it is possible to run EC CO₂RR or N₂RR in non-aqueous electrolytes,²⁵ it is still important to improve our understanding on how to limit the HER side-reaction and run EC CO₂RR or N₂RR more economically in aqueous solutions. Some strategies for theoretical and experimental investigations are thus required (*e.g.* decoupling the lifetime of photo-generated carriers with the reaction dynamics). Additionally, studying how to tune the Fermi level of MXenes with different T_x groups and the coupled co-catalyst is important to ensure the efficient photo-carrier movement towards the desired surface.

We also see a huge opportunity from MXene-derived materials in catalysis. Although this class of material does not fit the MXene hybrids category strictly, we recognize that the resulting MXene-derived materials behave differently and are much more active than those obtained using conventional methods. While many examples of TiO₂ hybrids have been derived from Ti-based MXenes, far fewer have reported using other MXenes. In particular, group 14, 15, and 16 TM MXene-derived materials could hold interesting properties for CO₂RR and N₂RR.

CONCLUDING REMARKS AND FUTURE OUTLOOK

In this review, we discussed the design rules behind MXene hybrids for catalytic energy storage and conversion applications. We summarized the different classes of secondary materials hybridized with MXenes and their synthesis methods, highlighting their differences. By carefully considering the MXenes' properties (T_x groups, basal plane defects, edge charges, and identity of the outer metal surface), a variety of secondary materials can be chemically coupled with MXenes to form MXene hybrids with varying architectures, from vertically-aligned nanomaterials on MXenes to lateral coverages of MXenes and even more complex 3D mesoporous structures.

In general, MXenes and their hybrids are susceptible to oxidative degradation in environments containing water and/or oxygen,¹⁹³ and under applied anodic potentials in aqueous media,²⁹ both of which are common in catalysis. The MXenes' instability should thus be thoughtfully considered when designing MXene hybrids for energy storage and conversion. This can be circumvented through recent advances in the synthesis (F-free²⁹⁵ and/or aqueous-free^{296,297}), storage,^{193,298} and stabilization (in thin films²⁹⁹ or colloids³⁰⁰) of MXenes. These breakthroughs also offer greater flexibility and control of surface T_x groups for targeted hybrid assembly. This can be translated to the preparation of stable MXenes and their hybrids for water-sensitive applications, such as non-polar organic composites, polymer inks for additive manufacturing, and organic electrolytes for supercapacitors and batteries,^{301,302} and are also highly relevant for communities working on flexible electronics, biomedical, and electromagnetic applications.

Additionally, we expect directed efforts to be made beyond mono-metal MXenes to synthesize multi-metal MXenes such as ordered double MXenes ($M'_2MC_2T_x$ and $M'_2M_2C_3T_x$), which have already been theoretically predicted to possess high levels of HER activity.³⁰³ Adding

to the already-growing MXenes family, disordered double TM solid solution MXenes such as $(\text{Ti,V})_2\text{CT}_x$ and $(\text{Mo,V})_4\text{C}_3\text{T}_x$ are also attractive prospects for synthesis and characterization, given the ease of tuning their electrochemical and physical properties based on their compositions.^{84,304} Another key challenge lies in the expansion of existing etching methods to ternary transition metal nitrides MAX materials to produce nitride MXenes, since only Ti_2NT_x has been produced in this manner,³⁰⁵ while $\text{Ti}_4\text{N}_3\text{T}_x$ has only been synthesized through harsh molten fluoride salt etching.^{19,201} Other Mo-containing nitride MXenes are instead produced through ammoniating their corresponding carbide MXenes with NH_3 gas at a similarly high temperature of 600°C .³⁰⁶ Additionally, closely related 2D MXene-like TM nitrides, such as MoN, have also been reported to be catalytically active for energy storage and conversion applications.^{307–309} Investigating these layered 2D MXene-like TM nitrides can potentially reveal important insights into the predicted stability and chemical reactivity of MXene nitrides. In all, expanding the MXenes family can create more possibilities in advanced MXene hybrid design to realize theoretically predicted properties and competitive performances as multi-functional MXene hybrids and composites.

For each of the industrially relevant catalytic energy storage (metal-air/sulfur batteries) and conversion (water splitting, HER, OER, CO_2RR and N_2RR) applications, we clarified the roles of each material component in the MXene hybrids – a conductive support, co-catalyst, electronic structure modulator, photo-carrier generator and phase stabilizer, to name a few. More importantly, we described how strong chemical and electronic coupling within the hybrid can induce directed morphological growth, alter the electronic structure, and create more catalytically active motifs for synergistic enhancement in catalytic activity and stability. By combining T_x control, doping and hybridization to modulate the electronic density and intrinsic activity of active site, coupled with nanostructuring to increase the density and accessibility of those active sites, many MXene hybrids

have outperformed their separate individual components in both catalytic activity and stability. We also provide application-specific challenges and our outlook at the end of each application section for readers working on those applications. A summary of key performance metrics for HER, OER, ORR, CO₂RR and N₂RR is provided in **Tables S2–S4** for the reader's convenience.

MXene hybrids and composites have achieved superior catalytic energy storage and conversion performances compared to traditional materials, and we anticipate further advances as the chemical and electronic nature of the MXene hybrid interfaces are elucidated using a powerful combination of *in-situ/operando* experiments and theoretical modelling.^{21,202,238} A better understanding of the dynamics at the MXenes' hybrid surface and interface in the presence of reactive species, solvent, and applied potential is indispensable toward building a more realistic and multi-scale MXene hybrid model that incorporates the effects of electrochemical potential, solvation, and micro-kinetics into the current purely atomistic view of DFT, as recently demonstrated on metallic catalysts.^{310–312} So far, *operando* measurements demonstrated on bare MXenes¹⁹ have clarified our fundamental understanding of the localized electrochemical activity and electronic structure at the catalytic surface. For this purpose, it is not unreasonable to use MXene-like surrogate structures that can be synthesized using bottom-up approaches with atomic precision (CVD and ALD) for such fundamental studies.^{65,66,148}

Finally, efforts can be undertaken in the development of mild and scalable top-down MXene synthesis and hybridization techniques to (1) minimize MXene oxidation and mechanical damage during processing especially at high temperatures,^{192,193} (2) enable greater control over the chemical composition, morphology and distribution of the secondary material grown on MXenes, and (3) realize highly porous and 3D MXene hybrid networks for efficient mass and long-range charge transport to further enhance catalytic activity.¹⁶⁹ Given the rapid rise in interest amongst

MXene hybrids and composites, we expect an increase in both experimental and theoretical efforts towards developing MXene hybrids for clean energy and related applications in the near future.

ASSOCIATED CONTENT

The authors declare no competing financial interests.

Supporting Information.

Detailed data entries (categorization of MXene hybrid publications, electrocatalytic HER/OER/ORR performances, photocatalytic HER performances, photo/electrocatalytic CO₂RR/N₂RR performances) is available free of charge in the Supporting Information online.

AUTHOR INFORMATION

Corresponding Author

*Z. W. Seh: sehzw@imre.a-star.edu.sg

*B. Anasori: banasori@iupui.edu

Author Contributions

The manuscript was written through contributions of all authors. All authors have given approval to the final version of the manuscript.

ACKNOWLEDGEMENT

This work was supported by the Singapore National Research Foundation (NRF-NRFF2017-04). B.A. acknowledges startup funding from the Department of Mechanical and Energy Engineering and Purdue School of Engineering and Technology of IUPUI. H.-Y.J. acknowledges the National Natural Science Foundation of China (NSFC, No. 21703170) and Key Research and Development Program of Shaanxi (Program No. 2020GY-244). J.T. acknowledges the RS International

Exchanges 2017 Cost Share Award (IEC\NSFC\170342) and the Leverhulme Trust (RPG-2017-122).

VOCABULARY

MXene hybrid/composite, a material fabricated by combining MXenes with another at least one other non-MXene material (metal, semiconductor or insulator) to form at least one interface. A hybrid/composite material is a more general classification than a heterostructure (see definition for heterostructure below).

MXene heterostructure, a material fabricated by growing at least one non-MXene material on MXenes in a repetitive layered manner, which forms more than one MXene-other material interface that repeats itself *i.e.* MXene-other material-MXene-other material-... and so on.

(Photo)electrocatalyst, a material that reduces the activation energy and overpotential (see definition for overpotential below) to drive an electrochemical reaction of interest, such as HER, OER, ORR, CO₂RR and N₂RR.

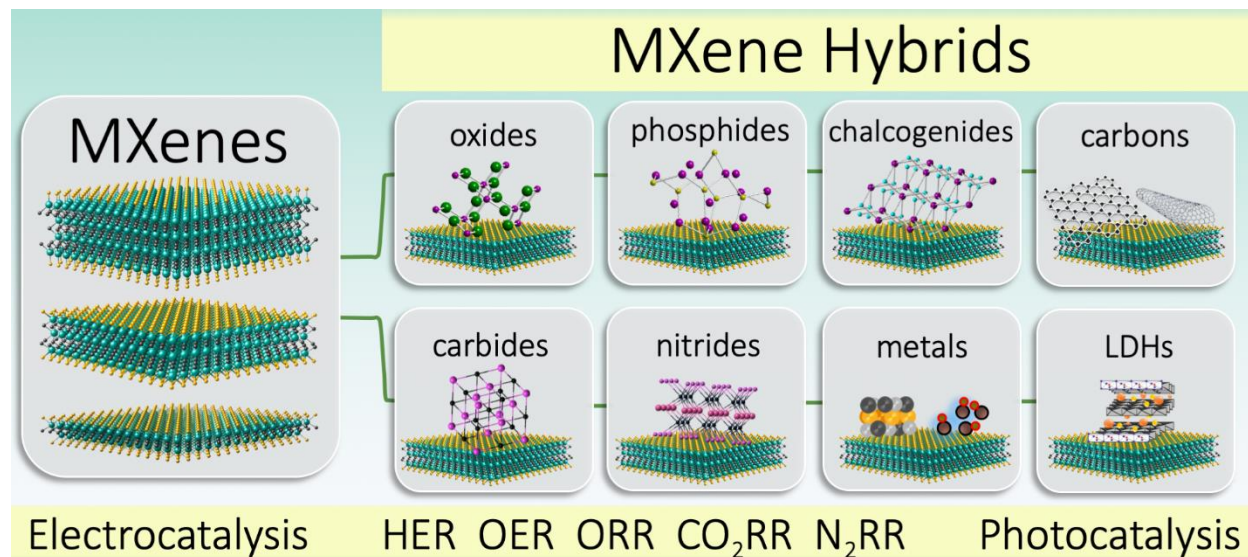
Overpotential (at -10 mA cm⁻² current density) $\eta_{j=10}$, the additional potential difference (voltage) beyond the thermodynamically determined redox potential to drive an electrochemical redox half-cell reaction at a specific current density.

Tafel slope, the amount of increase in overpotential required to increase the current density produced for an electrochemical redox half-cell reaction by a factor of ten.

Metal-air/sulfur battery, two different battery architectures for energy storage. Metal-air/sulfur batteries use a metal anode and an air/sulfur cathode. The redox half-cell reactions occurring at the cathode are OER/ORR for metal-air batteries and S-redox reactions for metal-sulfur batteries.

Faradaic efficiency, the ratio of the number of electrons used to produce the desired electrochemical product compared to the total number of electrons added into the system. For example, a 70% Faradaic efficiency in CO₂RR to CH₄ indicates that 70% of the electrons added are used to reduce CO₂ to CH₄ while the other 30% of electrons added are used to reduce CO₂ to other products.

TOC FIGURE (can be rescaled to 9 cm width × 4 cm height)



REFERENCES

- (1) Chu, S.; Majumdar, A. Opportunities and Challenges for a Sustainable Energy Future. *Nature* **2012**, *488*, 294–303.
- (2) Armstrong, R. C.; Wolfram, C.; de Jong, K. P.; Gross, R.; Lewis, N. S.; Boardman, B.; Ragauskas, A. J.; Ehrhardt-Martinez, K.; Crabtree, G.; Ramana, M. V. The Frontiers of Energy. *Nat. Energy* **2016**, *1*, 15020.
- (3) Seh, Z. W.; Kibsgaard, J.; Dickens, C. F.; Chorkendorff, I.; Nørskov, J. K.; Jaramillo, T. F. Combining Theory and Experiment in Electrocatalysis: Insights into Materials Design. *Science* **2017**, *355*, eaad4998.
- (4) Di, J.; Yan, C.; Handoko, A. D.; Seh, Z. W.; Li, H.; Liu, Z. Ultrathin Two-Dimensional Materials for Photo- and Electrocatalytic Hydrogen Evolution. *Mater. Today* **2018**, *21*, 749–770.
- (5) Chia, X.; Pumera, M. Characteristics and Performance of Two-Dimensional Materials for Electrocatalysis. *Nat. Catal.* **2018**, *1*, 909–921.
- (6) Pomerantseva, E.; Bonaccorso, F.; Feng, X.; Cui, Y.; Gogotsi, Y. Energy Storage: The Future Enabled by Nanomaterials. *Science* **2019**, *366*, ean8285.
- (7) Sun, Y.; Liu, N.; Cui, Y. Promises and Challenges of Nanomaterials for Lithium-Based Rechargeable Batteries. *Nat. Energy* **2016**, *1*, 16071.
- (8) Li, Y.; Dai, H. Recent Advances in Zinc–Air Batteries. *Chem. Soc. Rev.* **2014**, *43*, 5257–5275.
- (9) Greeley, J.; Stephens, I. E. L.; Bondarenko, A. S.; Johansson, T. P.; Hansen, H. A.; Jaramillo, T. F.; Rossmeisl, J.; Chorkendorff, I.; Nørskov, J. K. Alloys of Platinum and Early Transition Metals as Oxygen Reduction Electrocatalysts. *Nat. Chem.* **2009**, *1*, 552–556.
- (10) Greeley, J.; Jaramillo, T. F.; Bonde, J.; Chorkendorff, I.; Nørskov, J. K. Computational High-Throughput Screening of Electrocatalytic Materials for Hydrogen Evolution. *Nat. Mater.* **2006**, *5*, 909–913.
- (11) Montoya, J. H.; Seitz, L. C.; Chakthranont, P.; Vojvodic, A.; Jaramillo, T. F.; Nørskov, J. K. Materials for Solar Fuels and Chemicals. *Nat. Mater.* **2017**, *16*, 70–81.
- (12) Naguib, M.; Kurtoglu, M.; Presser, V.; Lu, J.; Niu, J.; Heon, M.; Hultman, L.; Gogotsi, Y.; Barsoum, M. W. Two-Dimensional Nanocrystals Produced by Exfoliation of Ti_3AlC_2 . *Adv. Mater.* **2011**, *23*, 4248–4253.
- (13) Gogotsi, Y.; Anasori, B. The Rise of MXenes. *ACS Nano* **2019**, *13*, 8491–8494.
- (14) Anasori, B.; Gogotsi, Y. Introduction to 2D Transition Metal Carbides and Nitrides (MXenes). In *2D Metal Carbides and Nitrides (MXenes): Structure, Properties and Applications*; Springer International Publishing: Cham, 2019; pp 3–12.
- (15) Li, Z.; Wu, Y. 2D Early Transition Metal Carbides (MXenes) for Catalysis. *Small* **2019**, *15*, 1804736.
- (16) Naguib, M.; Mochalin, V. N.; Barsoum, M. W.; Gogotsi, Y. 25th Anniversary Article: MXenes: A New Family of Two-Dimensional Materials. *Adv. Mater.* **2014**, *26*, 992–1005.
- (17) Seh, Z. W.; Fredrickson, K. D.; Anasori, B.; Kibsgaard, J.; Strickler, A. L.; Lukatskaya, M. R.; Gogotsi, Y.; Jaramillo, T. F.; Vojvodic, A. Two-Dimensional Molybdenum Carbide

- (MXene) as an Efficient Electrocatalyst for Hydrogen Evolution. *ACS Energy Lett.* **2016**, *1*, 589–594.
- (18) Handoko, A. D.; Fredrickson, K. D.; Anasori, B.; Convey, K. W.; Johnson, L. R.; Gogotsi, Y.; Vojvodic, A.; Seh, Z. W. Tuning the Basal Plane Functionalization of Two-Dimensional Metal Carbides (MXenes) To Control Hydrogen Evolution Activity. *ACS Appl. Energy Mater.* **2018**, *1*, 173–180.
- (19) Djire, A.; Wang, X.; Xiao, C.; Nwamba, O. C.; Mirkin, M. V.; Neale, N. R. Basal Plane Hydrogen Evolution Activity from Mixed Metal Nitride MXenes Measured by Scanning Electrochemical Microscopy. *Adv. Funct. Mater.* **2020**, 2001136.
- (20) Jaramillo, T. F.; Jorgensen, K. P.; Bonde, J.; Nielsen, J. H.; Horch, S.; Chorkendorff, I. Identification of Active Edge Sites for Electrochemical H₂ Evolution from MoS₂ Nanocatalysts. *Science* **2007**, *317*, 100–102.
- (21) Zhan, C.; Sun, W.; Xie, Y.; Jiang, D.; Kent, P. R. C. Computational Discovery and Design of MXenes for Energy Applications: Status, Successes, and Opportunities. *ACS Appl. Mater. Interfaces* **2019**, *11*, 24885–24905.
- (22) Chen, H.; Handoko, A. D.; Xiao, J.; Feng, X.; Fan, Y.; Wang, T.; Legut, D.; Seh, Z. W.; Zhang, Q. Catalytic Effect on CO₂ Electroreduction by Hydroxyl-Terminated Two-Dimensional MXenes. *ACS Appl. Mater. Interfaces* **2019**, *11*, 36571–36579.
- (23) Handoko, A. D.; Khoo, K. H.; Tan, T. L.; Jin, H.; Seh, Z. W. Establishing New Scaling Relations on Two-Dimensional MXenes for CO₂ Electroreduction. *J. Mater. Chem. A* **2018**, *6*, 21885–21890.
- (24) Johnson, L. R.; Sridhar, S.; Zhang, L.; Fredrickson, K. D.; Raman, A. S.; Jang, J.; Leach, C.; Padmanabhan, A.; Price, C. C.; Frey, N. C.; Raizada, A.; Rajaraman, V.; Saiprasad, S. A.; Tang, X.; Vojvodic, A. MXene Materials for the Electrochemical Nitrogen Reduction—Functionalized or Not? *ACS Catal.* **2020**, *10*, 253–264.
- (25) Handoko, A. D.; Chen, H.; Lum, Y.; Zhang, Q.; Anasori, B.; Seh, Z. W. Two-Dimensional Titanium and Molybdenum Carbide MXenes as Electrocatalysts for CO₂ Reduction. *iScience* **2020**, *23*, 101181.
- (26) Deysler, G.; Shuck, C. E.; Hantanasirisakul, K.; Frey, N. C.; Foucher, A. C.; Maleski, K.; Sarycheva, A.; Shenoy, V. B.; Stach, E. A.; Anasori, B.; Gogotsi, Y. Synthesis of Mo₄VAIC₄ MAX Phase and Two-Dimensional Mo₄VC₄ MXene with Five Atomic Layers of Transition Metals. *ACS Nano* **2020**, *14*, 204–217.
- (27) Naguib, M.; Mashtalir, O.; Carle, J.; Presser, V.; Lu, J.; Hultman, L.; Gogotsi, Y.; Barsoum, M. W. Two-Dimensional Transition Metal Carbides. *ACS Nano* **2012**, *6*, 1322–1331.
- (28) Halim, J.; Kota, S.; Lukatskaya, M. R.; Naguib, M.; Zhao, M.-Q.; Moon, E. J.; Pitoock, J.; Nanda, J.; May, S. J.; Gogotsi, Y.; Barsoum, M. W. Synthesis and Characterization of 2D Molybdenum Carbide (MXene). *Adv. Funct. Mater.* **2016**, *26*, 3118–3127.
- (29) Anasori, B.; Lukatskaya, M. R.; Gogotsi, Y. 2D Metal Carbides and Nitrides (MXenes) for Energy Storage. *Nat. Rev. Mater.* **2017**, *2*, 16098.
- (30) Srivastava, P.; Mishra, A.; Mizuseki, H.; Lee, K.-R.; Singh, A. K. Mechanistic Insight into the Chemical Exfoliation and Functionalization of Ti₃C₂ MXene. *ACS Appl. Mater. Interfaces* **2016**, *8*, 24256–24264.

- (31) Naguib, M.; Gogotsi, Y. Synthesis of Two-Dimensional Materials by Selective Extraction. *Acc. Chem. Res.* **2015**, *48*, 128–135.
- (32) Shuck, C. E.; Sarycheva, A.; Anayee, M.; Levitt, A.; Zhu, Y.; Uzun, S.; Balitskiy, V.; Zahorodna, V.; Gogotsi, O.; Gogotsi, Y. Scalable Synthesis of $Ti_3C_2T_x$ MXene. *Adv. Eng. Mater.* **2020**, *22*, 1901241.
- (33) Verger, L.; Natu, V.; Carey, M.; Barsoum, M. W. MXenes: An Introduction of Their Synthesis, Select Properties, and Applications. *Trends Chem.* **2019**, *1*, 656–669.
- (34) Alhabeab, M.; Maleski, K.; Anasori, B.; Lelyukh, P.; Clark, L.; Sin, S.; Gogotsi, Y. Guidelines for Synthesis and Processing of Two-Dimensional Titanium Carbide ($Ti_3C_2T_x$ MXene). *Chem. Mater.* **2017**, *29*, 7633–7644.
- (35) Halim, J.; Lukatskaya, M. R.; Cook, K. M.; Lu, J.; Smith, C. R.; Näslund, L.-Å.; May, S. J.; Hultman, L.; Gogotsi, Y.; Eklund, P.; Barsoum, M. W. Transparent Conductive Two-Dimensional Titanium Carbide Epitaxial Thin Films. *Chem. Mater.* **2014**, *26*, 2374–2381.
- (36) Sun, W.; Shah, S. A.; Chen, Y.; Tan, Z.; Gao, H.; Habib, T.; Radovic, M.; Green, M. J. Electrochemical Etching of Ti_2AlC to Ti_2CT_x (MXene) in Low-Concentration Hydrochloric Acid Solution. *J. Mater. Chem. A* **2017**, *5*, 21663–21668.
- (37) Li, P.; Zhu, J.; Handoko, A. D.; Zhang, R.; Wang, H.; Legut, D.; Wen, X.; Fu, Z.; Seh, Z. W.; Zhang, Q. High-Throughput Theoretical Optimization of the Hydrogen Evolution Reaction on MXenes by Transition Metal Modification. *J. Mater. Chem. A* **2018**, *6*, 4271–4278.
- (38) Naguib, M.; Unocic, R. R.; Armstrong, B. L.; Nanda, J. Large-Scale Delamination of Multi-Layers Transition Metal Carbides and Carbonitrides “MXenes.” *Dalton Trans.* **2015**, *44*, 9353–9358.
- (39) Mashtalir, O.; Naguib, M.; Mochalin, V. N.; Dall’Agnese, Y.; Heon, M.; Barsoum, M. W.; Gogotsi, Y. Intercalation and Delamination of Layered Carbides and Carbonitrides. *Nat. Commun.* **2013**, *4*, 1716.
- (40) Fu, Z.; Wang, N.; Legut, D.; Si, C.; Zhang, Q.; Du, S.; Germann, T. C.; Francisco, J. S.; Zhang, R. Rational Design of Flexible Two-Dimensional MXenes with Multiple Functionalities. *Chem. Rev.* **2019**, *119*, 11980–12031.
- (41) Liu, Y.-T.; Zhu, X.-D.; Pan, L. Hybrid Architectures Based on 2D MXenes and Low-Dimensional Inorganic Nanostructures: Methods, Synergies, and Energy-Related Applications. *Small* **2018**, *14*, 1803632.
- (42) Zhan, X.; Si, C.; Zhou, J.; Sun, Z. MXene and MXene-Based Composites: Synthesis, Properties and Environment-Related Applications. *Nanoscale Horiz.* **2020**, *5*, 235–258.
- (43) Yu, H.; Wang, Y.; Jing, Y.; Ma, J.; Du, C.; Yan, Q. Surface Modified MXene-Based Nanocomposites for Electrochemical Energy Conversion and Storage. *Small* **2019**, *15*, 1901503.
- (44) Peng, J.; Chen, X.; Ong, W.-J.; Zhao, X.; Li, N. Surface and Heterointerface Engineering of 2D MXenes and Their Nanocomposites: Insights into Electro- and Photocatalysis. *Chem* **2019**, *5*, 18–50.
- (45) Wang, H.; Lee, J.-M. Recent Advances in Structural Engineering of MXene Electrocatalysts. *J. Mater. Chem. A* **2020**, *8*, 10604–10624.

- (46) Zheng, L.; Han, S.; Liu, H.; Yu, P.; Fang, X. Hierarchical MoS₂ Nanosheet@TiO₂ Nanotube Array Composites with Enhanced Photocatalytic and Photocurrent Performances. *Small* **2016**, *12*, 1527–1536.
- (47) Peng, C.; Yang, X.; Li, Y.; Yu, H.; Wang, H.; Peng, F. Hybrids of Two-Dimensional Ti₃C₂ and TiO₂ Exposing {001} Facets toward Enhanced Photocatalytic Activity. *ACS Appl. Mater. Interfaces* **2016**, *8*, 6051–6060.
- (48) Wang, H.; Wu, Y.; Xiao, T.; Yuan, X.; Zeng, G.; Tu, W.; Wu, S.; Lee, H. Y.; Tan, Y. Z.; Chew, J. W. Formation of Quasi-Core-Shell In₂S₃/Anatase TiO₂@metallic Ti₃C₂T_x Hybrids with Favorable Charge Transfer Channels for Excellent Visible-Light-Photocatalytic Performance. *Appl. Catal. B: Environ.* **2018**, *233*, 213–225.
- (49) Kong, F.; He, X.; Liu, Q.; Qi, X.; Sun, D.; Zheng, Y.; Wang, R.; Bai, Y. Further Surface Modification by Carbon Coating for *In-Situ* Growth of Fe₃O₄ Nanoparticles on MXene Ti₃C₂ Multilayers for Advanced Li-Ion Storage. *Electrochim. Acta* **2018**, *289*, 228–237.
- (50) Zuo, D.; Song, S.; An, C.; Tang, L.; He, Z.; Zheng, J. Synthesis of Sandwich-like Structured Sn/SnO_x@MXene Composite through *In-Situ* Growth for Highly Reversible Lithium Storage. *Nano Energy* **2019**, *62*, 401–409.
- (51) Sun, X.; Tan, K.; Liu, Y.; Zhang, J.; Denis, D. K.; Zaman, F. uz; Hou, L.; Yuan, C. A Two-Dimensional Assembly of Ultrafine Cobalt Oxide Nanocrystallites Anchored on Single-Layer Ti₃C₂T_x Nanosheets with Enhanced Lithium Storage for Li-Ion Batteries. *Nanoscale* **2019**, *11*, 16755–16766.
- (52) Li, Z.; Qi, Z.; Wang, S.; Ma, T.; Zhou, L.; Wu, Z.; Luan, X.; Lin, F.-Y.; Chen, M.; Miller, J. T.; Xin, H.; Huang, W.; Wu, Y. *In Situ* Formed Pt₃Ti Nanoparticles on a Two-Dimensional Transition Metal Carbide (MXene) Used as Efficient Catalysts for Hydrogen Evolution Reactions. *Nano Lett.* **2019**, *19*, 5102–5108.
- (53) Zhu, X.-D.; Xie, Y.; Liu, Y.-T. Exploring the Synergy of 2D MXene-Supported Black Phosphorus Quantum Dots in Hydrogen and Oxygen Evolution Reactions. *J. Mater. Chem. A* **2018**, *6*, 21255–21260.
- (54) Xu, J.; Shim, J.; Park, J.-H.; Lee, S. MXene Electrode for the Integration of WSe₂ and MoS₂ Field Effect Transistors. *Adv. Funct. Mater.* **2016**, *26*, 5328–5334.
- (55) Naguib, M.; Mashtalir, O.; Lukatskaya, M. R.; Dyatkin, B.; Zhang, C.; Presser, V.; Gogotsi, Y.; Barsoum, M. W. One-Step Synthesis of Nanocrystalline Transition Metal Oxides on Thin Sheets of Disordered Graphitic Carbon by Oxidation of MXenes. *Chem. Commun.* **2014**, *50*, 7420–7423.
- (56) Liang, X.; Rangom, Y.; Kwok, C. Y.; Pang, Q.; Nazar, L. F. Interwoven MXene Nanosheet/Carbon-Nanotube Composites as Li-S Cathode Hosts. *Adv. Mater.* **2017**, *29*, 1603040.
- (57) Venkatkarthick, R.; Rodthongkum, N.; Zhang, X.; Wang, S.; Pattananuwat, P.; Zhao, Y.; Liu, R.; Qin, J. Vanadium-Based Oxide on Two-Dimensional Vanadium Carbide MXene (V₂O_x@V₂CT_x) as Cathode for Rechargeable Aqueous Zinc-Ion Batteries. *ACS Appl. Energy Mater.* **2020**, *3*, 4677–4689.
- (58) Wang, Z.; Yu, K.; Feng, Y.; Qi, R.; Ren, J.; Zhu, Z. VO₂(p)-V₂C(MXene) Grid Structure as a Lithium Polysulfide Catalytic Host for High-Performance Li-S Battery. *ACS Appl. Mater. Interfaces* **2019**, *11*, 44282–44292.

- (59) Bai, J.; Zhao, B.; Lin, S.; Li, K.; Zhou, J.; Dai, J.; Zhu, X.; Sun, Y. Construction of Hierarchical V_4C_3 -MXene/MoS₂/C Nanohybrids for High Rate Lithium-Ion Batteries. *Nanoscale* **2020**, *12*, 1144–1154.
- (60) Wang, X.; Li, H.; Li, H.; Lin, S.; Bai, J.; Dai, J.; Liang, C.; Zhu, X.; Sun, Y.; Dou, S. Heterostructures of Ni–Co–Al Layered Double Hydroxide Assembled on V_4C_3 MXene for High-Energy Hybrid Supercapacitors. *J. Mater. Chem. A* **2019**, *7*, 2291–2300.
- (61) Butt, R.; Siddique, A. H.; Bokhari, S. W.; Jiang, S.; Lei, D.; Zhou, X.; Liu, Z. Niobium Carbide/Reduced Graphene Oxide Hybrid Porous Aerogel as High Capacity and Long-life Anode Material for Li-ion Batteries. *Int. J. Energy Res.* **2019**, *43*, 4995–5003.
- (62) Zhang, C. J.; Kim, S. J.; Ghidui, M.; Zhao, M.-Q.; Barsoum, M. W.; Nicolosi, V.; Gogotsi, Y. Layered Orthorhombic Nb₂O₅@Nb₄C₃T_x and TiO₂@Ti₃C₂T_x Hierarchical Composites for High Performance Li-Ion Batteries. *Adv. Funct. Mater.* **2016**, *26*, 4143–4151.
- (63) Qin, L.; Tao, Q.; El Ghazaly, A.; Fernandez-Rodriguez, J.; Persson, P. O. Å.; Rosen, J.; Zhang, F. High-Performance Ultrathin Flexible Solid-State Supercapacitors Based on Solution Processable Mo_{1.33}C MXene and PEDOT:PSS. *Adv. Funct. Mater.* **2018**, *28*, 1703808.
- (64) Lv, L.; Guo, C.; Sun, W.; Wang, Y. Strong Surface-Bound Sulfur in Carbon Nanotube Bridged Hierarchical Mo₂C-Based MXene Nanosheets for Lithium–Sulfur Batteries. *Small* **2018**, 1804338.
- (65) Jeon, J.; Park, Y.; Choi, S.; Lee, J.; Lim, S. S.; Lee, B. H.; Song, Y. J.; Cho, J. H.; Jang, Y. H.; Lee, S. Epitaxial Synthesis of Molybdenum Carbide and Formation of a Mo₂C/MoS₂ Hybrid Structure via Chemical Conversion of Molybdenum Disulfide. *ACS Nano* **2018**, *12*, 338–346.
- (66) Sun, W.; Wang, X.; Feng, J.; Li, T.; Huan, Y.; Qiao, J.; He, L.; Ma, D. Controlled Synthesis of 2D Mo₂C/Graphene Heterostructure on Liquid Au Substrates as Enhanced Electrocatalytic Electrodes. *Nanotechnology* **2019**, *30*, 385601.
- (67) Chen, C.; Xie, X.; Anasori, B.; Sarycheva, A.; Makaryan, T.; Zhao, M.; Urbankowski, P.; Miao, L.; Jiang, J.; Gogotsi, Y. MoS₂-on-MXene Heterostructures as Highly Reversible Anode Materials for Lithium-Ion Batteries. *Angew. Chem. Int. Ed.* **2018**, *57*, 1846–1850.
- (68) Dai, C.; Chen, Y.; Jing, X.; Xiang, L.; Yang, D.; Lin, H.; Liu, Z.; Han, X.; Wu, R. Two-Dimensional Tantalum Carbide (MXenes) Composite Nanosheets for Multiple Imaging-Guided Photothermal Tumor Ablation. *ACS Nano* **2017**, *11*, 12696–12712.
- (69) Zhang, J.; Kong, N.; Uzun, S.; Levitt, A.; Seyedin, S.; Lynch, P. A.; Qin, S.; Han, M.; Yang, W.; Liu, J.; Wang, X.; Gogotsi, Y.; Razal, J. M. Scalable Manufacturing of Free-Standing, Strong Ti₃C₂T_x MXene Films with Outstanding Conductivity. *Adv. Mater.* **2020**, *32*, 2001093.
- (70) Wu, X.; Wang, Z.; Yu, M.; Xiu, L.; Qiu, J. Stabilizing the MXenes by Carbon Nanoplatelet for Developing Hierarchical Nanohybrids with Efficient Lithium Storage and Hydrogen Evolution Capability. *Adv. Mater.* **2017**, *29*, 1607017.
- (71) Gao, Y.; Wang, L.; Zhou, A.; Li, Z.; Chen, J.; Bala, H.; Hu, Q.; Cao, X. Hydrothermal Synthesis of TiO₂/Ti₃C₂ Nanocomposites with Enhanced Photocatalytic Activity. *Mater. Lett.* **2015**, *150*, 62–64.

- (72) Zhang, H.; Dong, H.; Zhang, X.; Xu, Y.; Fransaer, J. Cu₂O Hybridized Titanium Carbide with Open Conductive Frameworks for Lithium-Ion Batteries. *Electrochim. Acta* **2016**, *202*, 24–31.
- (73) Rakhi, R. B.; Ahmed, B.; Anjum, D.; Alshareef, H. N. Direct Chemical Synthesis of MnO₂ Nanowhiskers on Transition-Metal Carbide Surfaces for Supercapacitor Applications. *ACS Appl. Mater. Interfaces* **2016**, *8*, 18806–18814.
- (74) Du, Y.; Zhang, X.; Wei, L.; Yu, B.; Wang, Y.; Wang, Y.; Ye, S. Electrodeposition of a Ni-P Composite Coating Reinforced with Ti₃C₂T_x@TiO₂/MoS₂ Particles. *Mater. Chem. Phys.* **2020**, *241*, 122448.
- (75) Mai, Y. J.; Li, Y. G.; Li, S. L.; Zhang, L. Y.; Liu, C. S.; Jie, X. H. Self-Lubricating Ti₃C₂ Nanosheets/Copper Composite Coatings. *J. Alloys Compd.* **2019**, *770*, 1–5.
- (76) Yang, Q.; Huang, Z.; Li, X.; Liu, Z.; Li, H.; Liang, G.; Wang, D.; Huang, Q.; Zhang, S.; Chen, S.; Zhi, C. A Wholly Degradable, Rechargeable Zn–Ti₃C₂ MXene Capacitor with Superior Anti-Self-Discharge Function. *ACS Nano* **2019**, *13*, 8275–8283.
- (77) Aïssa, B.; Ali, A.; Mahmoud, K. A.; Haddad, T.; Nedil, M. Transport Properties of a Highly Conductive 2D Ti₃C₂T_x MXene/Graphene Composite. *Appl. Phys. Lett.* **2016**, *109*, 043109.
- (78) Peng, C.; Wei, P.; Li, X.; Liu, Y.; Cao, Y.; Wang, H.; Yu, H.; Peng, F.; Zhang, L.; Zhang, B.; Lv, K. High Efficiency Photocatalytic Hydrogen Production over Ternary Cu/TiO₂@Ti₃C₂T_x Enabled by Low-Work-Function 2D Titanium Carbide. *Nano Energy* **2018**, *53*, 97–107.
- (79) Ahmed, B.; Anjum, D. H.; Gogotsi, Y.; Alshareef, H. N. Atomic Layer Deposition of SnO₂ on MXene for Li-Ion Battery Anodes. *Nano Energy* **2017**, *34*, 249–256.
- (80) Yu, X.; Wang, T.; Yin, W.; Zhang, Y. Ti₃C₂ MXene Nanoparticles Modified Metal Oxide Composites for Enhanced Photoelectrochemical Water Splitting. *Int. J. Hydrog. Energy* **2019**, *44*, 2704–2710.
- (81) Karlsson, L. H.; Birch, J.; Halim, J.; Barsoum, M. W.; Persson, P. O. Å. Atomically Resolved Structural and Chemical Investigation of Single MXene Sheets. *Nano Lett.* **2015**, *15*, 4955–4960.
- (82) Byeon, A.; Hatter, C. B.; Park, J. H.; Ahn, C. W.; Gogotsi, Y.; Lee, J. W. Molybdenum Oxide/Carbon Composites Derived from the CO₂ Oxidation of Mo₂CT_x (MXene) for Lithium Ion Battery Anodes. *Electrochim. Acta* **2017**, *258*, 979–987.
- (83) Yuan, W.; Cheng, L.; Zhang, Y.; Wu, H.; Lv, S.; Chai, L.; Guo, X.; Zheng, L. 2D-Layered Carbon/TiO₂ Hybrids Derived from Ti₃C₂ MXenes for Photocatalytic Hydrogen Evolution under Visible Light Irradiation. *Adv. Mater. Interfaces* **2017**, *4*, 1700577.
- (84) Yazdanparast, S.; Soltanmohammad, S.; Fash-White, A.; Tucker, G. J.; Brennecka, G. L. Synthesis and Surface Chemistry of 2D TiVC Solid-Solution MXenes. *ACS Appl. Mater. Interfaces* **2020**, *12*, 20129–20137.
- (85) Low, J.; Zhang, L.; Tong, T.; Shen, B.; Yu, J. TiO₂/MXene Ti₃C₂ Composite with Excellent Photocatalytic CO₂ Reduction Activity. *J. Catal.* **2018**, *361*, 255–266.
- (86) Hou, T.; Li, Q.; Zhang, Y.; Zhu, W.; Yu, K.; Wang, S.; Xu, Q.; Liang, S.; Wang, L. Near-Infrared Light-Driven Photofixation of Nitrogen over Ti₃C₂T_x/TiO₂ Hybrid Structures with Superior Activity and Stability. *Appl. Catal. B: Environ.* **2020**, *273*, 119072.

- (87) Li, Y.; Zhang, D.; Feng, X.; Liao, Y.; Wen, Q.; Xiang, Q. Truncated Octahedral Bipyramidal TiO₂/MXene Ti₃C₂ Hybrids with Enhanced Photocatalytic H₂ Production Activity. *Nanoscale Adv.* **2019**, *1*, 1812–1818.
- (88) Hao, C.; Liao, Y.; Wu, Y.; An, Y.; Lin, J.; Gu, Z.; Jiang, M.; Hu, S.; Wang, X. RuO₂-Loaded TiO₂-MXene as a High Performance Photocatalyst for Nitrogen Fixation. *J. Phys. Chem. Solids* **2020**, *136*, 109141.
- (89) Li, Y.; Deng, X.; Tian, J.; Liang, Z.; Cui, H. Ti₃C₂ MXene-Derived Ti₃C₂/TiO₂ Nanoflowers for Noble-Metal-Free Photocatalytic Overall Water Splitting. *Appl. Mater. Today* **2018**, *13*, 217–227.
- (90) Zheng, R.; Shu, C.; Hou, Z.; Hu, A.; Hei, P.; Yang, T.; Li, J.; Liang, R.; Long, J. *In Situ* Fabricating Oxygen Vacancy-Rich TiO₂ Nanoparticles *via* Utilizing Thermodynamically Metastable Ti Atoms on Ti₃C₂T_x MXene Nanosheet Surface To Boost Electrocatalytic Activity for High-Performance Li–O₂ Batteries. *ACS Appl. Mater. Interfaces* **2019**, *11*, 46696–46704.
- (91) Fang, Y.; Liu, Z.; Han, J.; Jin, Z.; Han, Y.; Wang, F.; Niu, Y.; Wu, Y.; Xu, Y. High-Performance Electrocatalytic Conversion of N₂ to NH₃ Using Oxygen-Vacancy-Rich TiO₂ *In Situ* Grown on Ti₃C₂T_x MXene. *Adv. Energy Mater.* **2019**, *9*, 1803406.
- (92) Xu, Y.; Wang, S.; Yang, J.; Han, B.; Nie, R.; Wang, J.; Wang, J.; Jing, H. *In-Situ* Grown Nanocrystal TiO₂ on 2D Ti₃C₂ Nanosheets for Artificial Photosynthesis of Chemical Fuels. *Nano Energy* **2018**, *51*, 442–450.
- (93) Peng, C.; Wang, H.; Yu, H.; Peng, F. (111) TiO_{2-x}/Ti₃C₂: Synergy of Active Facets, Interfacial Charge Transfer and Ti³⁺ Doping for Enhance Photocatalytic Activity. *Mater. Res. Bull.* **2017**, *89*, 16–25.
- (94) Lotfi, R.; Naguib, M.; Yilmaz, D. E.; Nanda, J.; van Duin, A. C. T. A Comparative Study on the Oxidation of Two-Dimensional Ti₃C₂ MXene Structures in Different Environments. *J. Mater. Chem. A* **2018**, *6*, 12733–12743.
- (95) Chertopalov, S.; Mochalin, V. N. Environment-Sensitive Photoresponse of Spontaneously Partially Oxidized Ti₃C₂ MXene Thin Films. *ACS Nano* **2018**, *12*, 6109–6116.
- (96) Ghassemi, H.; Harlow, W.; Mashtalir, O.; Beidaghi, M.; Lukatskaya, M. R.; Gogotsi, Y.; Taheri, M. L. *In Situ* Environmental Transmission Electron Microscopy Study of Oxidation of Two-Dimensional Ti₃C₂ and Formation of Carbon-Supported TiO₂. *J. Mater. Chem. A* **2014**, *2*, 14339.
- (97) Yuan, W.; Cheng, L.; An, Y.; Lv, S.; Wu, H.; Fan, X.; Zhang, Y.; Guo, X.; Tang, J. Laminated Hybrid Junction of Sulfur-Doped TiO₂ and a Carbon Substrate Derived from Ti₃C₂ MXenes: Toward Highly Visible Light-Driven Photocatalytic Hydrogen Evolution. *Adv. Sci.* **2018**, *5*, 1700870.
- (98) Anasori, B.; Xie, Y.; Beidaghi, M.; Lu, J.; Hosler, B. C.; Hultman, L.; Kent, P. R. C.; Gogotsi, Y.; Barsoum, M. W. Two-Dimensional, Ordered, Double Transition Metals Carbides (MXenes). *ACS Nano* **2015**, *9*, 9507–9516.
- (99) Anasori, B.; Shi, C.; Moon, E. J.; Xie, Y.; Voigt, C. A.; Kent, P. R. C.; May, S. J.; Billinge, S. J. L.; Barsoum, M. W.; Gogotsi, Y. Control of Electronic Properties of 2D Carbides (MXenes) by Manipulating Their Transition Metal Layers. *Nanoscale Horiz.* **2016**, *1*, 227–234.

- (100) Kong, X.; Gao, P.; Jiang, R.; Feng, J.; Yang, P.; Gai, S.; Chen, Y.; Chi, Q.; Xu, F.; Ye, W. Orderly Layer-by-Layered TiO₂/Carbon Superstructures Based on MXene's Defect Engineering for Efficient Hydrogen Evolution. *Appl. Catal. A: General* **2020**, *590*, 117341.
- (101) Cao, S.; Shen, B.; Tong, T.; Fu, J.; Yu, J. 2D/2D Heterojunction of Ultrathin MXene/Bi₂WO₆ Nanosheets for Improved Photocatalytic CO₂ Reduction. *Adv. Funct. Mater.* **2018**, *28*, 1800136.
- (102) Li, N.; Zhang, Y.; Jia, M.; Lv, X.; Li, X.; Li, R.; Ding, X.; Zheng, Y.-Z.; Tao, X. 1T/2H MoSe₂-on-MXene Heterostructure as Bifunctional Electrocatalyst for Efficient Overall Water Splitting. *Electrochim. Acta* **2019**, *326*, 134976.
- (103) Zhao, M.-Q.; Torelli, M.; Ren, C. E.; Ghidui, M.; Ling, Z.; Anasori, B.; Barsoum, M. W.; Gogotsi, Y. 2D Titanium Carbide and Transition Metal Oxides Hybrid Electrodes for Li-Ion Storage. *Nano Energy* **2016**, *30*, 603–613.
- (104) Xiong, J.; Pan, L.; Wang, H.; Du, F.; Chen, Y.; Yang, J.; Zhang, C. (John). Synergistically Enhanced Lithium Storage Performance Based on Titanium Carbide Nanosheets (MXene) Backbone and SnO₂ Quantum Dots. *Electrochim. Acta* **2018**, *268*, 503–511.
- (105) Gao, X.-T.; Xie, Y.; Zhu, X.-D.; Sun, K.-N.; Xie, X.-M.; Liu, Y.-T.; Yu, J.-Y.; Ding, B. Ultrathin MXene Nanosheets Decorated with TiO₂ Quantum Dots as an Efficient Sulfur Host toward Fast and Stable Li-S Batteries. *Small* **2018**, *14*, 1802443.
- (106) Li, X.; Yin, X.; Xu, H.; Han, M.; Li, M.; Liang, S.; Cheng, L.; Zhang, L. Ultralight MXene-Coated, Interconnected SiC_ns Three-Dimensional Lamellar Foams for Efficient Microwave Absorption in the X-Band. *ACS Appl. Mater. Interfaces* **2018**, *10*, 34524–34533.
- (107) Zhao, L.; Dong, B.; Li, S.; Zhou, L.; Lai, L.; Wang, Z.; Zhao, S.; Han, M.; Gao, K.; Lu, M.; Xie, X.; Chen, B.; Liu, Z.; Wang, X.; Zhang, H.; Li, H.; Liu, J.; Zhang, H.; Huang, X.; Huang, W. Interdiffusion Reaction-Assisted Hybridization of Two-Dimensional Metal–Organic Frameworks and Ti₃C₂T_x Nanosheets for Electrocatalytic Oxygen Evolution. *ACS Nano* **2017**, *11*, 5800–5807.
- (108) Byrappa, K.; Yoshimura, M. *Handbook of Hydrothermal Technology*, 2nd ed.; William Andrew: Oxford ; Waltham, Mass, 2013.
- (109) Zhao, R.; Wang, M.; Zhao, D.; Li, H.; Wang, C.; Yin, L. Molecular-Level Heterostructures Assembled from Titanium Carbide MXene and Ni–Co–Al Layered Double-Hydroxide Nanosheets for All-Solid-State Flexible Asymmetric High-Energy Supercapacitors. *ACS Energy Lett.* **2018**, *3*, 132–140.
- (110) Li, H.; Musharavati, F.; Zalenezhad, E.; Chen, X.; Hui, K. N.; Hui, K. S. Electrodeposited Ni Co Layered Double Hydroxides on Titanium Carbide as a Binder-Free Electrode for Supercapacitors. *Electrochim. Acta* **2018**, *261*, 178–187.
- (111) Huang, H.; Cui, J.; Liu, G.; Bi, R.; Zhang, L. Carbon-Coated MoSe₂/MXene Hybrid Nanosheets for Superior Potassium Storage. *ACS Nano* **2019**, *13*, 3448–3456.
- (112) Handoko, A. D.; Goh, G. K. L. Hydrothermal Synthesis of Sodium Potassium Niobate Solid Solutions at 200°C. *Green Chem.* **2010**, *12*, 680.
- (113) Gogotsi, Y. G.; Kofstad, P.; Yoshimura, M.; Nickel, K. G. Formation of Sp³-Bonded Carbon upon Hydrothermal Treatment of SiC. *Diam. Relat. Mater.* **1996**, *5*, 151–162.

- (114) Lange, F. F. Chemical Solution Routes to Single-Crystal Thin Films. *Science* **1996**, *273*, 903–909.
- (115) Handoko, A. D.; Goh, G. K. L. Hydrothermal Growth of Piezoelectrically Active Lead-Free (Na,K)NbO₃–LiTaO₃ Thin Films. *CrystEngComm* **2013**, *15*, 672–678.
- (116) Demazeau, G. Solvothermal Reactions: An Original Route for the Synthesis of Novel Materials. *J. Mater. Sci.* **2008**, *43*, 2104–2114.
- (117) Zhu, L.; Lv, J.; Yu, X.; Zhao, H.; Sun, C.; Zhou, Z.; Ying, Y.; Tan, L. Further Construction of MnO₂ Composite through *In-Situ* Growth on MXene Surface Modified by Carbon Coating with Outstanding Catalytic Properties on Thermal Decomposition of Ammonium Perchlorate. *Appl. Surf. Sci.* **2020**, *502*, 144171.
- (118) Liang, J.; Ding, C.; Liu, J.; Chen, T.; Peng, W.; Li, Y.; Zhang, F.; Fan, X. Heterostructure Engineering of Co-Doped MoS₂ Coupled with Mo₂CT_x MXene for Enhanced Hydrogen Evolution in Alkaline Media. *Nanoscale* **2019**, *11*, 10992–11000.
- (119) Cui, B.; Hu, B.; Liu, J.; Wang, M.; Song, Y.; Tian, K.; Zhang, Z.; He, L. Solution-Plasma-Assisted Bimetallic Oxide Alloy Nanoparticles of Pt and Pd Embedded within Two-Dimensional Ti₃C₂T_x Nanosheets as Highly Active Electrocatalysts for Overall Water Splitting. *ACS Appl. Mater. Interfaces* **2018**, *10*, 23858–23873.
- (120) Zou, H.; He, B.; Kuang, P.; Yu, J.; Fan, K. Metal–Organic Framework-Derived Nickel–Cobalt Sulfide on Ultrathin Mxene Nanosheets for Electrocatalytic Oxygen Evolution. *ACS Appl. Mater. Interfaces* **2018**, *10*, 22311–22319.
- (121) Zeng, Z.; Yan, Y.; Chen, J.; Zan, P.; Tian, Q.; Chen, P. Boosting the Photocatalytic Ability of Cu₂O Nanowires for CO₂ Conversion by MXene Quantum Dots. *Adv. Funct. Mater.* **2019**, *29*, 1806500.
- (122) Cai, T.; Wang, L.; Liu, Y.; Zhang, S.; Dong, W.; Chen, H.; Yi, X.; Yuan, J.; Xia, X.; Liu, C.; Luo, S. Ag₃PO₄/Ti₃C₂ MXene Interface Materials as a Schottky Catalyst with Enhanced Photocatalytic Activities and Anti-Photocorrosion Performance. *Appl. Catal. B: Environ.* **2018**, *239*, 545–554.
- (123) Li, Z.; Zhuang, Z.; Lv, F.; Zhu, H.; Zhou, L.; Luo, M.; Zhu, J.; Lang, Z.; Feng, S.; Chen, W.; Mai, L.; Guo, S. The Marriage of the FeN₄ Moiety and MXene Boosts Oxygen Reduction Catalysis: Fe 3d Electron Delocalization Matters. *Adv. Mater.* **2018**, *30*, 1803220.
- (124) Zhao, J.-H.; Liu, L.-W.; Li, K.; Li, T.; Liu, F.-T. Conductive Ti₃C₂ and MOF-Derived CoS_x Boosting the Photocatalytic Hydrogen Production Activity of TiO₂. *CrystEngComm* **2019**, *21*, 2416–2421.
- (125) Pan, A.; Ma, X.; Huang, S.; Wu, Y.; Jia, M.; Shi, Y.; Liu, Y.; Wangyang, P.; He, L.; Liu, Y. CsPbBr₃ Perovskite Nanocrystal Grown on MXene Nanosheets for Enhanced Photoelectric Detection and Photocatalytic CO₂ Reduction. *J. Phys. Chem. Lett.* **2019**, *10*, 6590–6597.
- (126) Yu, M.; Zhou, S.; Wang, Z.; Zhao, J.; Qiu, J. Boosting Electrocatalytic Oxygen Evolution by Synergistically Coupling Layered Double Hydroxide with MXene. *Nano Energy* **2018**, *44*, 181–190.

- (127) Zhang, X.; Shao, B.; Sun, Z.; Gao, Z.; Qin, Y.; Zhang, C.; Cui, F.; Yang, X. Platinum Nanoparticle-Deposited $\text{Ti}_3\text{C}_2\text{T}_x$ MXene for Hydrogen Evolution Reaction. *Ind. Eng. Chem. Res.* **2020**, *59*, 1822–1828.
- (128) Li, X.; Yin, X.; Han, M.; Song, C.; Xu, H.; Hou, Z.; Zhang, L.; Cheng, L. Ti_3C_2 MXenes Modified with *In Situ* Grown Carbon Nanotubes for Enhanced Electromagnetic Wave Absorption Properties. *J. Mater. Chem. C* **2017**, *5*, 4068–4074.
- (129) Zhang, S.; Ying, H.; Guo, R.; Yang, W.; Han, W.-Q. Vapor Deposition Red Phosphorus to Prepare Nitrogen-Doped $\text{Ti}_3\text{C}_2\text{T}_x$ MXenes Composites for Lithium-Ion Batteries. *J. Phys. Chem. Lett.* **2019**, *10*, 6446–6454.
- (130) Geng, D.; Zhao, X.; Chen, Z.; Sun, W.; Fu, W.; Chen, J.; Liu, W.; Zhou, W.; Loh, K. P. Direct Synthesis of Large-Area 2D Mo_2C on *In Situ* Grown Graphene. *Adv. Mater.* **2017**, *29*, 1700072.
- (131) Tang, Y.; Yang, C.; Yang, Y.; Yin, X.; Que, W.; Zhu, J. Three Dimensional Hierarchical Network Structure of S- NiFe_2O_4 Modified Few-Layer Titanium Carbides (MXene) Flakes on Nickel Foam as a High Efficient Electrocatalyst for Oxygen Evolution. *Electrochim. Acta* **2019**, *296*, 762–770.
- (132) Yang, L.; Zheng, W.; Zhang, P.; Chen, J.; Tian, W. B.; Zhang, Y. M.; Sun, Z. M. MXene/CNTs Films Prepared by Electrophoretic Deposition for Supercapacitor Electrodes. *J. Electroanal. Chem.* **2018**, *830–831*, 1–6.
- (133) An, X.; Wang, W.; Wang, J.; Duan, H.; Shi, J.; Yu, X. The Synergetic Effects of Ti_3C_2 MXene and Pt as Co-Catalysts for Highly Efficient Photocatalytic Hydrogen Evolution over g- C_3N_4 . *Phys. Chem. Chem. Phys.* **2018**, *20*, 11405–11411.
- (134) Luo, J.; Tao, X.; Zhang, J.; Xia, Y.; Huang, H.; Zhang, L.; Gan, Y.; Liang, C.; Zhang, W. Sn^{4+} Ion Decorated Highly Conductive Ti_3C_2 MXene: Promising Lithium-Ion Anodes with Enhanced Volumetric Capacity and Cyclic Performance. *ACS Nano* **2016**, *10*, 2491–2499.
- (135) Peng, Q.; Guo, J.; Zhang, Q.; Xiang, J.; Liu, B.; Zhou, A.; Liu, R.; Tian, Y. Unique Lead Adsorption Behavior of Activated Hydroxyl Group in Two-Dimensional Titanium Carbide. *J. Am. Chem. Soc.* **2014**, *136*, 4113–4116.
- (136) Wenderich, K.; Mul, G. Methods, Mechanism, and Applications of Photodeposition in Photocatalysis: A Review. *Chem. Rev.* **2016**, *116*, 14587–14619.
- (137) Li, J.; Qin, R.; Yan, L.; Chi, Z.; Yu, Z.; Li, N.; Hu, M.; Chen, H.; Shan, G. Plasmonic Light Illumination Creates a Channel To Achieve Fast Degradation of $\text{Ti}_3\text{C}_2\text{T}_x$ Nanosheets. *Inorg. Chem.* **2019**, *58*, 7285–7294.
- (138) Shen, S.; Ke, T.; Rajavel, K.; Yang, K.; Lin, D. Dispersibility and Photochemical Stability of Delaminated MXene Flakes in Water. *Small* **2020**, 2002433.
- (139) Ma, T. Y.; Cao, J. L.; Jaroniec, M.; Qiao, S. Z. Interacting Carbon Nitride and Titanium Carbide Nanosheets for High-Performance Oxygen Evolution. *Angew. Chem. Int. Ed.* **2016**, *55*, 1138–1142.
- (140) Sambyal, P.; Iqbal, A.; Hong, J.; Kim, H.; Kim, M.-K.; Hong, S. M.; Han, M.; Gogotsi, Y.; Koo, C. M. Ultralight and Mechanically Robust $\text{Ti}_3\text{C}_2\text{T}_x$ Hybrid Aerogel Reinforced by Carbon Nanotubes for Electromagnetic Interference Shielding. *ACS Appl. Mater. Interfaces* **2019**, *11*, 38046–38054.

- (141) Zhao, M.-Q.; Ren, C. E.; Ling, Z.; Lukatskaya, M. R.; Zhang, C.; Van Aken, K. L.; Barsoum, M. W.; Gogotsi, Y. Flexible MXene/Carbon Nanotube Composite Paper with High Volumetric Capacitance. *Adv. Mater.* **2015**, *27*, 339–345.
- (142) Yue, Y.; Liu, N.; Ma, Y.; Wang, S.; Liu, W.; Luo, C.; Zhang, H.; Cheng, F.; Rao, J.; Hu, X.; Su, J.; Gao, Y. Highly Self-Healable 3D Microsupercapacitor with MXene–Graphene Composite Aerogel. *ACS Nano* **2018**, *12*, 4224–4232.
- (143) Li, Y.; Ding, L.; Guo, Y.; Liang, Z.; Cui, H.; Tian, J. Boosting the Photocatalytic Ability of G-C₃N₄ for Hydrogen Production by Ti₃C₂ MXene Quantum Dots. *ACS Appl. Mater. Interfaces* **2019**, *11*, 41440–41447.
- (144) Yan, J.; Ren, C. E.; Maleski, K.; Hatter, C. B.; Anasori, B.; Urbankowski, P.; Sarycheva, A.; Gogotsi, Y. Flexible MXene/Graphene Films for Ultrafast Supercapacitors with Outstanding Volumetric Capacitance. *Adv. Funct. Mater.* **2017**, *27*, 1701264.
- (145) Yu, P.; Cao, G.; Yi, S.; Zhang, X.; Li, C.; Sun, X.; Wang, K.; Ma, Y. Binder-Free 2D Titanium Carbide (MXene)/Carbon Nanotube Composites for High-Performance Lithium-Ion Capacitors. *Nanoscale* **2018**, *10*, 5906–5913.
- (146) Yang, C.; Jiang, Q.; Li, W.; He, H.; Yang, L.; Lu, Z.; Huang, H. Ultrafine Pt Nanoparticle-Decorated 3D Hybrid Architectures Built from Reduced Graphene Oxide and MXene Nanosheets for Methanol Oxidation. *Chem. Mater.* **2019**, *31*, 9277–9287.
- (147) Gu, H.; Xing, Y.; Xiong, P.; Tang, H.; Li, C.; Chen, S.; Zeng, R.; Han, K.; Shi, G. Three-Dimensional Porous Ti₃C₂T_x MXene–Graphene Hybrid Films for Glucose Biosensing. *ACS Appl. Nano Mater.* **2019**, *2*, 6537–6545.
- (148) Yang, L.; Chen, W.; Yang, R.; Chen, A.; Zhang, H.; Sun, Y.; Jia, Y.; Li, X.; Tang, Z.; Gui, X. Fabrication of MoO_x/Mo₂C-Layered Hybrid Structures by Direct Thermal Oxidation of Mo₂C. *ACS Appl. Mater. Interfaces* **2020**, *12*, 10755–10762.
- (149) Yu, M.; Wang, Z.; Liu, J.; Sun, F.; Yang, P.; Qiu, J. A Hierarchically Porous and Hydrophilic 3D Nickel–Iron/MXene Electrode for Accelerating Oxygen and Hydrogen Evolution at High Current Densities. *Nano Energy* **2019**, *63*, 103880.
- (150) Hope, M. A.; Forse, A. C.; Griffith, K. J.; Lukatskaya, M. R.; Ghidui, M.; Gogotsi, Y.; Grey, C. P. NMR Reveals the Surface Functionalisation of Ti₃C₂ MXene. *Phys. Chem. Chem. Phys.* **2016**, *18*, 5099–5102.
- (151) Wu, X.; Zhou, S.; Wang, Z.; Liu, J.; Pei, W.; Yang, P.; Zhao, J.; Qiu, J. Engineering Multifunctional Collaborative Catalytic Interface Enabling Efficient Hydrogen Evolution in All pH Range and Seawater. *Adv. Energy Mater.* **2019**, *9*, 1901333.
- (152) Hantanasirisakul, K.; Gogotsi, Y. Electronic and Optical Properties of 2D Transition Metal Carbides and Nitrides (MXenes). *Adv. Mater.* **2018**, *30*, 1804779.
- (153) Hao, C.; Wu, Y.; An, Y.; Cui, B.; Lin, J.; Li, X.; Wang, D.; Jiang, M.; Cheng, Z.; Hu, S. Interface-Coupling of CoFe-LDH on MXene as High-Performance Oxygen Evolution Catalyst. *Mater. Today Energy* **2019**, *12*, 453–462.
- (154) Pandey, M.; Thygesen, K. S. Two-Dimensional MXenes as Catalysts for Electrochemical Hydrogen Evolution: A Computational Screening Study. *J. Phys. Chem. C* **2017**, *121*, 13593–13598.
- (155) Gao, G.; O’Mullane, A. P.; Du, A. 2D MXenes: A New Family of Promising Catalysts for the Hydrogen Evolution Reaction. *ACS Catal.* **2017**, *7*, 494–500.

- (156) Zheng, J.; Sun, X.; Qiu, C.; Yan, Y.; Yao, Z.; Deng, S.; Zhong, X.; Zhuang, G.; Wei, Z.; Wang, J. High-Throughput Screening of Hydrogen Evolution Reaction Catalysts in MXene Materials. *J. Phys. Chem. C* **2020**, *124*, 13695–13705.
- (157) Yuan, W.; Cheng, L.; An, Y.; Wu, H.; Yao, N.; Fan, X.; Guo, X. MXene Nanofibers as Highly Active Catalysts for Hydrogen Evolution Reaction. *ACS Sustainable Chem. Eng.* **2018**, *6*, 8976–8982.
- (158) Yang, X.; Gao, N.; Zhou, S.; Zhao, J. MXene Nanoribbons as Electrocatalysts for the Hydrogen Evolution Reaction with Fast Kinetics. *Phys. Chem. Chem. Phys.* **2018**, *20*, 19390–19397.
- (159) Zhang, J.; Zhao, Y.; Guo, X.; Chen, C.; Dong, C.-L.; Liu, R.-S.; Han, C.-P.; Li, Y.; Gogotsi, Y.; Wang, G. Single Platinum Atoms Immobilized on an MXene as an Efficient Catalyst for the Hydrogen Evolution Reaction. *Nat. Catal.* **2018**, *1*, 985–992.
- (160) Kuznetsov, D. A.; Chen, Z.; Kumar, P. V.; Tsoukalou, A.; Kierzkowska, A.; Abdala, P. M.; Safonova, O. V.; Fedorov, A.; Müller, C. R. Single Site Cobalt Substitution in 2D Molybdenum Carbide (MXene) Enhances Catalytic Activity in the Hydrogen Evolution Reaction. *J. Am. Chem. Soc.* **2019**, *141*, 17809–17816.
- (161) Ramalingam, V.; Varadhan, P.; Fu, H.; Kim, H.; Zhang, D.; Chen, S.; Song, L.; Ma, D.; Wang, Y.; Alshareef, H. N.; He, J. Heteroatom-Mediated Interactions between Ruthenium Single Atoms and an MXene Support for Efficient Hydrogen Evolution. *Adv. Mater.* **2019**, *31*, 1903841.
- (162) Li, Z.; Cui, Y.; Wu, Z.; Milligan, C.; Zhou, L.; Mitchell, G.; Xu, B.; Shi, E.; Miller, J. T.; Ribeiro, F. H.; Wu, Y. Reactive Metal–Support Interactions at Moderate Temperature in Two-Dimensional Niobium-Carbide-Supported Platinum Catalysts. *Nat. Catal.* **2018**, *1*, 349–355.
- (163) Le, T. A.; Bui, Q. V.; Tran, N. Q.; Cho, Y.; Hong, Y.; Kawazoe, Y.; Lee, H. Synergistic Effects of Nitrogen Doping on MXene for Enhancement of Hydrogen Evolution Reaction. *ACS Sustainable Chem. Eng.* **2019**, *7*, 16879–16888.
- (164) Qu, G.; Zhou, Y.; Wu, T.; Zhao, G.; Li, F.; Kang, Y.; Xu, C. Phosphorized MXene-Phase Molybdenum Carbide as an Earth-Abundant Hydrogen Evolution Electrocatalyst. *ACS Appl. Energy Mater.* **2018**, *1*, 7206–7212.
- (165) Yoon, Y.; Tiwari, A. P.; Choi, M.; Novak, T. G.; Song, W.; Chang, H.; Zyung, T.; Lee, S. S.; Jeon, S.; An, K. Precious-Metal-Free Electrocatalysts for Activation of Hydrogen Evolution with Nonmetallic Electron Donor: Chemical Composition Controllable Phosphorous Doped Vanadium Carbide MXene. *Adv. Funct. Mater.* **2019**, *29*, 1903443.
- (166) He, Y.; He, Q.; Wang, L.; Zhu, C.; Golani, P.; Handoko, A. D.; Yu, X.; Gao, C.; Ding, M.; Wang, X.; Liu, F.; Zeng, Q.; Yu, P.; Guo, S.; Yakobson, B. I.; Wang, L.; Seh, Z. W.; Zhang, Z.; Wu, M.; Wang, Q. J.; Zhang, H.; Liu, Z. Self-Gating in Semiconductor Electrocatalysis. *Nat. Mater.* **2019**, *18*, 1098–1104.
- (167) Du, C.-F.; Dinh, K. N.; Liang, Q.; Zheng, Y.; Luo, Y.; Zhang, J.; Yan, Q. Self-Assemble and *In Situ* Formation of Ni_{1-x}Fe_xPS₃ Nanomosaic-Decorated MXene Hybrids for Overall Water Splitting. *Adv. Energy Mater.* **2018**, *8*, 1801127.

- (168) Yue, Q.; Sun, J.; Chen, S.; Zhou, Y.; Li, H.; Chen, Y.; Zhang, R.; Wei, G.; Kang, Y. Hierarchical Mesoporous MXene–NiCoP Electrocatalyst for Water-Splitting. *ACS Appl. Mater. Interfaces* **2020**, *12*, 18570–18577.
- (169) Xiu, L.; Wang, Z.; Yu, M.; Wu, X.; Qiu, J. Aggregation-Resistant 3D MXene-Based Architecture as Efficient Bifunctional Electrocatalyst for Overall Water Splitting. *ACS Nano* **2018**, *12*, 8017–8028.
- (170) Selvam, N. C. S.; Lee, J.; Choi, G. H.; Oh, M. J.; Xu, S.; Lim, B.; Yoo, P. J. MXene Supported Co_xA_y (A = OH, P, Se) Electrocatalysts for Overall Water Splitting: Unveiling the Role of Anions in Intrinsic Activity and Stability. *J. Mater. Chem. A* **2019**, *7*, 27383–27393.
- (171) Wang, H.; Lin, Y.; Liu, S.; Li, J.; Bu, L.; Chen, J.; Xiao, X.; Choi, J.-H.; Gao, L.; Lee, J.-M. Confined Growth of Pyridinic N– Mo_2C Sites on MXenes for Hydrogen Evolution. *J. Mater. Chem. A* **2020**, *8*, 7109–7116.
- (172) Attanayake, N. H.; Abeyweera, S. C.; Thenuwara, A. C.; Anasori, B.; Gogotsi, Y.; Sun, Y.; Strongin, D. R. Vertically Aligned MoS_2 on Ti_3C_2 (MXene) as an Improved HER Catalyst. *J. Mater. Chem. A* **2018**, *6*, 16882–16889.
- (173) Liu, J.; Liu, Y.; Xu, D.; Zhu, Y.; Peng, W.; Li, Y.; Zhang, F.; Fan, X. Hierarchical “Nanoroll” like $\text{MoS}_2/\text{Ti}_3\text{C}_2\text{T}_x$ Hybrid with High Electrocatalytic Hydrogen Evolution Activity. *Appl. Catal. B: Environ.* **2019**, *241*, 89–94.
- (174) Kuang, P.; He, M.; Zhu, B.; Yu, J.; Fan, K.; Jaroniec, M. 0D/2D NiS_2/V -MXene Composite for Electrocatalytic H_2 Evolution. *J. Catal.* **2019**, *375*, 8–20.
- (175) Jiang, H.; Wang, Z.; Yang, Q.; Tan, L.; Dong, L.; Dong, M. Ultrathin $\text{Ti}_3\text{C}_2\text{T}_x$ (MXene) Nanosheet-Wrapped NiSe_2 Octahedral Crystal for Enhanced Supercapacitor Performance and Synergistic Electrocatalytic Water Splitting. *Nano-Micro Lett.* **2019**, *11*, 31.
- (176) Wang, Z.; Xu, W.; Yu, K.; Feng, Y.; Zhu, Z. 2D Heterogeneous Vanadium Compound Interfacial Modulation Enhanced Synergistic Catalytic Hydrogen Evolution for Full PH Range Seawater Splitting. *Nanoscale* **2020**, *12*, 6176–6187.
- (177) Du, C.; Sun, X.; Yu, H.; Liang, Q.; Dinh, K. N.; Zheng, Y.; Luo, Y.; Wang, Z.; Yan, Q. Synergy of Nb Doping and Surface Alloy Enhanced on Water–Alkali Electrocatalytic Hydrogen Generation Performance in Ti-Based MXene. *Adv. Sci.* **2019**, 1900116.
- (178) Zhao, G.; Rui, K.; Dou, S. X.; Sun, W. Boosting Electrochemical Water Oxidation: The Merits of Heterostructured Electrocatalysts. *J. Mater. Chem. A* **2020**, *8*, 6393–6405.
- (179) Li, N.; Wei, S.; Xu, Y.; Liu, J.; Wu, J.; Jia, G.; Cui, X. Synergistic Enhancement of Oxygen Evolution Reaction by $\text{Ti}_3\text{C}_2\text{T}_x$ Nanosheets Supported Amorphous FeOOH Quantum Dots. *Electrochim. Acta* **2018**, *290*, 364–368.
- (180) Wu, Z.; Wang, H.; Xiong, P.; Li, G.; Qiu, T.; Gong, W.-B.; Zhao, F.; Li, C.; Li, Q.; Wang, G.; Geng, F. Molecularly Thin Nitride Sheets Stabilized by Titanium Carbide as Efficient Bifunctional Electrocatalysts for Fiber-Shaped Rechargeable Zinc-Air Batteries. *Nano Lett.* **2020**, *20*, 2892–2898.
- (181) Hao, N.; Wei, Y.; Wang, J.; Wang, Z.; Zhu, Z.; Zhao, S.; Han, M.; Huang, X. *In Situ* Hybridization of an MXene/ TiO_2 / NiFeCo -Layered Double Hydroxide Composite for Electrochemical and Photoelectrochemical Oxygen Evolution. *RSC Adv.* **2018**, *8*, 20576–20584.

- (182) Zhang, Y.; Jiang, H.; Lin, Y.; Liu, H.; He, Q.; Wu, C.; Duan, T.; Song, L. *In Situ* Growth of Cobalt Nanoparticles Encapsulated Nitrogen-Doped Carbon Nanotubes among $\text{Ti}_3\text{C}_2\text{T}_x$ (MXene) Matrix for Oxygen Reduction and Evolution. *Adv. Mater. Interfaces* **2018**, *5*, 1800392.
- (183) Liu, J.; Chen, T.; Juan, P.; Peng, W.; Li, Y.; Zhang, F.; Fan, X. Hierarchical Cobalt Borate/MXenes Hybrid with Extraordinary Electrocatalytic Performance in Oxygen Evolution Reaction. *ChemSusChem* **2018**, *11*, 3758–3765.
- (184) Deng, S.; Yang, F.; Zhang, Q.; Zhong, Y.; Zeng, Y.; Lin, S.; Wang, X.; Lu, X.; Wang, C.-Z.; Gu, L.; Xia, X.; Tu, J. Phase Modulation of (1T-2H)- MoSe_2/TiC -C Shell/Core Arrays *via* Nitrogen Doping for Highly Efficient Hydrogen Evolution Reaction. *Adv. Mater.* **2018**, *30*, 1802223.
- (185) Chen, Y.; Lai, Z.; Zhang, X.; Fan, Z.; He, Q.; Tan, C.; Zhang, H. Phase Engineering of Nanomaterials. *Nat. Rev. Chem.* **2020**, *4*, 243–256.
- (186) Benchakar, M.; Bilyk, T.; Garner, C.; Loupias, L.; Morais, C.; Pacaud, J.; Canaff, C.; Chartier, P.; Morisset, S.; Guignard, N.; Mauchamp, V.; Célérier, S.; Habrioux, A. MXene Supported Cobalt Layered Double Hydroxide Nanocrystals: Facile Synthesis Route for a Synergistic Oxygen Evolution Reaction Electrocatalyst. *Adv. Mater. Interfaces* **2019**, *6*, 1901328.
- (187) Ran, J.; Gao, G.; Li, F.-T.; Ma, T.-Y.; Du, A.; Qiao, S.-Z. Ti_3C_2 MXene Co-Catalyst on Metal Sulfide Photo-Absorbers for Enhanced Visible-Light Photocatalytic Hydrogen Production. *Nat. Commun.* **2017**, *8*, 13907.
- (188) Sun, Y.; Meng, X.; Dall’Agnese, Y.; Dall’Agnese, C.; Duan, S.; Gao, Y.; Chen, G.; Wang, X.-F. 2D MXenes as Co-Catalysts in Photocatalysis: Synthetic Methods. *Nano-Micro Lett.* **2019**, *11*, 79.
- (189) Lin, J.; Yu, Y.; Zhang, Z.; Gao, F.; Liu, S.; Wang, W.; Li, G. A Novel Approach for Achieving High-Efficiency Photoelectrochemical Water Oxidation in InGaN Nanorods Grown on Si System: MXene Nanosheets as Multifunctional Interfacial Modifier. *Adv. Funct. Mater.* **2020**, *30*, 1910479.
- (190) Kong, X.; Peng, Z.; Jiang, R.; Jia, P.; Feng, J.; Yang, P.; Chi, Q.; Ye, W.; Xu, F.; Gao, P. Nanolayered Heterostructures of N-Doped TiO_2 and N-Doped Carbon for Hydrogen Evolution. *ACS Appl. Nano Mater.* **2020**, *3*, 1373–1381.
- (191) Jia, G.; Wang, Y.; Cui, X.; Zheng, W. Highly Carbon-Doped TiO_2 Derived from MXene Boosting the Photocatalytic Hydrogen Evolution. *ACS Sustainable Chem. Eng.* **2018**, *6*, 13480–13486.
- (192) Xia, F.; Lao, J.; Yu, R.; Sang, X.; Luo, J.; Li, Y.; Wu, J. Ambient Oxidation of Ti_3C_2 MXene Initialized by Atomic Defects. *Nanoscale* **2019**, *11*, 23330–23337.
- (193) Chae, Y.; Kim, S. J.; Cho, S.-Y.; Choi, J.; Maleski, K.; Lee, B.-J.; Jung, H.-T.; Gogotsi, Y.; Lee, Y.; Ahn, C. W. An Investigation into the Factors Governing the Oxidation of Two-Dimensional Ti_3C_2 MXene. *Nanoscale* **2019**, *11*, 8387–8393.
- (194) Su, T.; Peng, R.; Hood, Z. D.; Naguib, M.; Ivanov, I. N.; Keum, J. K.; Qin, Z.; Guo, Z.; Wu, Z. One-Step Synthesis of $\text{Nb}_2\text{O}_5/\text{C}/\text{Nb}_2\text{C}$ (MXene) Composites and Their Use as Photocatalysts for Hydrogen Evolution. *ChemSusChem* **2018**, *11*, 688–699.

- (195) Tian, Y.; An, Y.; Wei, H.; Wei, C.; Tao, Y.; Li, Y.; Xi, B.; Xiong, S.; Feng, J.; Qian, Y. Micron-Sized Nanoporous Vanadium Pentoxide Arrays for High-Performance Gel Zinc-Ion Batteries and Potassium Batteries. *Chem. Mater.* **2020**, *32*, 4054–4064.
- (196) Li, Y.; Yin, Z.; Ji, G.; Liang, Z.; Xue, Y.; Guo, Y.; Tian, J.; Wang, X.; Cui, H. 2D/2D/2D Heterojunction of Ti_3C_2 MXene/ MoS_2 Nanosheets/ TiO_2 Nanosheets with Exposed (001) Facets toward Enhanced Photocatalytic Hydrogen Production Activity. *Appl. Catal. B: Environ.* **2019**, *246*, 12–20.
- (197) Cheng, L.; Chen, Q.; Li, J.; Liu, H. Boosting the Photocatalytic Activity of CdLa_2S_4 for Hydrogen Production Using Ti_3C_2 MXene as a Co-Catalyst. *Appl. Catal. B: Environ.* **2020**, *267*, 118379.
- (198) Wang, H.; Sun, Y.; Wu, Y.; Tu, W.; Wu, S.; Yuan, X.; Zeng, G.; Xu, Z. J.; Li, S.; Chew, J. W. Electrical Promotion of Spatially Photoinduced Charge Separation *via* Interfacial-Built-in Quasi-Alloying Effect in Hierarchical $\text{Zn}_2\text{In}_2\text{S}_5/\text{Ti}_3\text{C}_2(\text{O}, \text{OH})_x$ Hybrids toward Efficient Photocatalytic Hydrogen Evolution and Environmental Remediation. *Appl. Catal. B: Environ.* **2019**, *245*, 290–301.
- (199) Su, T.; Hood, Z. D.; Naguib, M.; Bai, L.; Luo, S.; Rouleau, C. M.; Ivanov, I. N.; Ji, H.; Qin, Z.; Wu, Z. 2D/2D Heterojunction of $\text{Ti}_3\text{C}_2/\text{g-C}_3\text{N}_4$ Nanosheets for Enhanced Photocatalytic Hydrogen Evolution. *Nanoscale* **2019**, *11*, 8138–8149.
- (200) Ren, J.; Zong, H.; Sun, Y.; Gong, S.; Feng, Y.; Wang, Z.; Hu, L.; Yu, K.; Zhu, Z. 2D Organ-like Molybdenum Carbide (MXene) Coupled with MoS_2 Nanoflowers Enhances the Catalytic Activity in the Hydrogen Evolution Reaction. *CrystEngComm* **2020**, *22*, 1395–1403.
- (201) Djire, A.; Zhang, H.; Liu, J.; Miller, E. M.; Neale, N. R. Electrocatalytic and Optoelectronic Characteristics of the Two-Dimensional Titanium Nitride $\text{Ti}_4\text{N}_3\text{T}_x$ MXene. *ACS Appl. Mater. Interfaces* **2019**, *11*, 11812–11823.
- (202) Handoko, A. D.; Wei, F.; Jenndy; Yeo, B. S.; Seh, Z. W. Understanding Heterogeneous Electrocatalytic Carbon Dioxide Reduction through *Operando* Techniques. *Nat. Catal.* **2018**, *1*, 922–934.
- (203) Jiang, L.; Duan, J.; Zhu, J.; Chen, S.; Antonietti, M. Iron-Cluster-Directed Synthesis of 2D/2D Fe–N–C/MXene Superlattice-like Heterostructure with Enhanced Oxygen Reduction Electrocatalysis. *ACS Nano* **2020**, *14*, 2436–2444.
- (204) Chen, J.; Yuan, X.; Lyu, F.; Zhong, Q.; Hu, H.; Pan, Q.; Zhang, Q. Integrating MXene Nanosheets with Cobalt-Tipped Carbon Nanotubes for an Efficient Oxygen Reduction Reaction. *J. Mater. Chem. A* **2019**, *7*, 1281–1286.
- (205) Ostadhosseini, A.; Guo, J.; Simeski, F.; Ihme, M. Functionalization of 2D Materials for Enhancing OER/ORR Catalytic Activity in Li–Oxygen Batteries. *Commun. Chem.* **2019**, *2*, 95.
- (206) Zeng, Z.; Fu, G.; Yang, H. B.; Yan, Y.; Chen, J.; Yu, Z.; Gao, J.; Gan, L. Y.; Liu, B.; Chen, P. Bifunctional N-CoSe₂/3D-MXene as Highly Efficient and Durable Cathode for Rechargeable Zn–Air Battery. *ACS Materials Lett.* **2019**, *1*, 432–439.
- (207) Xue, Q.; Pei, Z.; Huang, Y.; Zhu, M.; Tang, Z.; Li, H.; Huang, Y.; Li, N.; Zhang, H.; Zhi, C. Mn_3O_4 Nanoparticles on Layer-Structured Ti_3C_2 MXene towards the Oxygen Reduction Reaction and Zinc–Air Batteries. *J. Mater. Chem. A* **2017**, *5*, 20818–20823.

- (208) Zhang, H.; Qi, Q.; Zhang, P.; Zheng, W.; Chen, J.; Zhou, A.; Tian, W.; Zhang, W.; Sun, Z. Self-Assembled 3D MnO₂ Nanosheets@Delaminated-Ti₃C₂ Aerogel as Sulfur Host for Lithium–Sulfur Battery Cathodes. *ACS Appl. Energy Mater.* **2019**, *2*, 705–714.
- (209) Wang, J.; Zhai, P.; Zhao, T.; Li, M.; Yang, Z.; Zhang, H.; Huang, J. Laminar MXene-Nafion-Modified Separator with Highly Inhibited Shuttle Effect for Long-Life Lithium–Sulfur Batteries. *Electrochim. Acta* **2019**, *320*, 134558.
- (210) Guo, D.; Ming, F.; Su, H.; Wu, Y.; Wahyudi, W.; Li, M.; Hedhili, M. N.; Sheng, G.; Li, L.-J.; Alshareef, H. N.; Li, Y.; Lai, Z. MXene Based Self-Assembled Cathode and Antifouling Separator for High-Rate and Dendrite-Inhibited Li–S Battery. *Nano Energy* **2019**, *61*, 478–485.
- (211) Wang, H.-F.; Xu, Q. Materials Design for Rechargeable Metal–Air Batteries. *Matter* **2019**, *1*, 565–595.
- (212) Li, Y.; Fu, J.; Zhong, C.; Wu, T.; Chen, Z.; Hu, W.; Amine, K.; Lu, J. Recent Advances in Flexible Zinc-Based Rechargeable Batteries. *Adv. Energy Mater.* **2019**, *9*, 1802605.
- (213) Wang, H.-F.; Tang, C.; Zhang, Q. A Review of Precious-Metal-Free Bifunctional Oxygen Electrocatalysts: Rational Design and Applications in Zn–Air Batteries. *Adv. Funct. Mater.* **2018**, *28*, 1803329.
- (214) Wen, Y.; Ma, C.; Wei, Z.; Zhu, X.; Li, Z. FeNC/MXene Hybrid Nanosheet as an Efficient Electrocatalyst for Oxygen Reduction Reaction. *RSC Adv.* **2019**, *9*, 13424–13430.
- (215) Wang, Z.; Chen, X.; Shen, F.; Hang, X.; Niu, C. TiC MXene High Energy Density Cathode for Lithium-Air Battery. *Adv. Theory Simul.* **2018**, *1*, 1800059.
- (216) Seh, Z. W.; Sun, Y.; Zhang, Q.; Cui, Y. Designing High-Energy Lithium–Sulfur Batteries. *Chem. Soc. Rev.* **2016**, *45*, 5605–5634.
- (217) Liang, X.; Garsuch, A.; Nazar, L. F. Sulfur Cathodes Based on Conductive MXene Nanosheets for High-Performance Lithium-Sulfur Batteries. *Angew. Chem. Int. Ed.* **2015**, *54*, 3907–3911.
- (218) Zhou, H.-Y.; Sui, Z.-Y.; Amin, K.; Lin, L.-W.; Wang, H.-Y.; Han, B.-H. Investigating the Electrocatalysis of a Ti₃C₂/Carbon Hybrid in Polysulfide Conversion of Lithium–Sulfur Batteries. *ACS Appl. Mater. Interfaces* **2020**, *12*, 13904–13913.
- (219) Liang, P.; Zhang, L.; Wang, D.; Man, X.; Shu, H.; Wang, L.; Wan, H.; Du, X.; Wang, H. First-Principles Explorations of Li₂S@V₂CT_x Hybrid Structure as Cathode Material for Lithium-sulfur Battery. *Appl. Surf. Sci.* **2019**, *489*, 677–683.
- (220) Bao, W.; Su, D.; Zhang, W.; Guo, X.; Wang, G. 3D Metal Carbide@Mesoporous Carbon Hybrid Architecture as a New Polysulfide Reservoir for Lithium-Sulfur Batteries. *Adv. Funct. Mater.* **2016**, *26*, 8746–8756.
- (221) Li, N.; Meng, Q.; Zhu, X.; Li, Z.; Ma, J.; Huang, C.; Song, J.; Fan, J. Lattice Constant-Dependent Anchoring Effect of MXenes for Lithium–Sulfur (Li–S) Batteries: A DFT Study. *Nanoscale* **2019**, *11*, 8485–8493.
- (222) Sim, E. S.; Yi, G. S.; Je, M.; Lee, Y.; Chung, Y.-C. Understanding the Anchoring Behavior of Titanium Carbide-Based MXenes Depending on the Functional Group in Li-S Batteries: A Density Functional Theory Study. *J. Power Sources* **2017**, *342*, 64–69.

- (223) Bao, W.; Liu, L.; Wang, C.; Choi, S.; Wang, D.; Wang, G. Facile Synthesis of Crumpled Nitrogen-Doped MXene Nanosheets as a New Sulfur Host for Lithium-Sulfur Batteries. *Adv. Energy Mater.* **2018**, *8*, 1702485.
- (224) Zhang, Y.; Mu, Z.; Yang, C.; Xu, Z.; Zhang, S.; Zhang, X.; Li, Y.; Lai, J.; Sun, Z.; Yang, Y.; Chao, Y.; Li, C.; Ge, X.; Yang, W.; Guo, S. Rational Design of MXene/1T-2H MoS₂-C Nanohybrids for High-Performance Lithium-Sulfur Batteries. *Adv. Funct. Mater.* **2018**, *28*, 1707578.
- (225) Du, C.; Wu, J.; Yang, P.; Li, S.; Xu, J.; Song, K. Embedding S@TiO₂ Nanospheres into MXene Layers as High Rate Cyclability Cathodes for Lithium-Sulfur Batteries. *Electrochim. Acta* **2019**, *295*, 1067–1074.
- (226) Liu, P.; Qu, L.; Tian, X.; Yi, Y.; Xia, J.; Wang, T.; Nan, J.; Yang, P.; Wang, T.; Fang, B.; Li, M.; Yang, B. Ti₃C₂T_x/Graphene Oxide Free-Standing Membranes as Modified Separators for Lithium-Sulfur Batteries with Enhanced Rate Performance. *ACS Appl. Energy Mater.* **2020**, *3*, 2708–2718.
- (227) Jiao, L.; Zhang, C.; Geng, C.; Wu, S.; Li, H.; Lv, W.; Tao, Y.; Chen, Z.; Zhou, G.; Li, J.; Ling, G.; Wan, Y.; Yang, Q. Capture and Catalytic Conversion of Polysulfides by *In Situ* Built TiO₂-MXene Heterostructures for Lithium-Sulfur Batteries. *Adv. Energy Mater.* **2019**, *9*, 1900219.
- (228) Bao, W.; Shuck, C. E.; Zhang, W.; Guo, X.; Gogotsi, Y.; Wang, G. Boosting Performance of Na-S Batteries Using Sulfur-Doped Ti₃C₂T_x MXene Nanosheets with a Strong Affinity to Sodium Polysulfides. *ACS Nano* **2019**, *13*, 11500–11509.
- (229) Li, B.; Zhang, D.; Liu, Y.; Yu, Y.; Li, S.; Yang, S. Flexible Ti₃C₂ MXene-Lithium Film with Lamellar Structure for Ultrastable Metallic Lithium Anodes. *Nano Energy* **2017**, *39*, 654–661.
- (230) Shi, H.; Yue, M.; Zhang, C. J.; Dong, Y.; Lu, P.; Zheng, S.; Huang, H.; Chen, J.; Wen, P.; Xu, Z.; Zheng, Q.; Li, X.; Yu, Y.; Wu, Z.-S. 3D Flexible, Conductive, and Recyclable Ti₃C₂T_x MXene-Melamine Foam for High-Areal-Capacity and Long-Lifetime Alkali-Metal Anode. *ACS Nano* **2020**, *14*, 8678–8688.
- (231) Luo, J.; Matios, E.; Wang, H.; Tao, X.; Li, W. Interfacial Structure Design of MXene-based Nanomaterials for Electrochemical Energy Storage and Conversion. *InfoMat* **2020**.
- (232) Luo, J.; Wang, C.; Wang, H.; Hu, X.; Matios, E.; Lu, X.; Zhang, W.; Tao, X.; Li, W. Pillared MXene with Ultralarge Interlayer Spacing as a Stable Matrix for High Performance Sodium Metal Anodes. *Adv. Funct. Mater.* **2019**, *29*, 1805946.
- (233) Orita, M.; Kojima, I.; Miyazaki, E. Catalysis by Transition-Metal Carbides. VII. Kinetic and XPS Studies of the Decomposition of Methanol on TiC, TaC, Mo₂C, WC, and W₂C. *Bull. Chem. Soc. Jpn.* **1986**, *59*, 689–695.
- (234) Wang, S.; Ge, H.; Sun, S.; Zhang, J.; Liu, F.; Wen, X.; Yu, X.; Wang, L.; Zhang, Y.; Xu, H.; Neuefeind, J. C.; Qin, Z.; Chen, C.; Jin, C.; Li, Y.; He, D.; Zhao, Y. A New Molybdenum Nitride Catalyst with Rhombohedral MoS₂ Structure for Hydrogenation Applications. *J. Am. Chem. Soc.* **2015**, *137*, 4815–4822.
- (235) Wang, S.; Temel, B.; Shen, J.; Jones, G.; Grabow, L. C.; Studt, F.; Bligaard, T.; Abild-Pedersen, F.; Christensen, C. H.; Nørskov, J. K. Universal Brønsted-Evans-Polanyi

- Relations for C–C, C–O, C–N, N–O, N–N, and O–O Dissociation Reactions. *Catal. Lett.* **2011**, *141*, 370–373.
- (236) Khaledialidusti, R.; Mishra, A. K.; Barnoush, A. Atomic Defects in Monolayer Ordered Double Transition Metal Carbide ($\text{Mo}_2\text{TiC}_2\text{T}_x$) MXene and CO_2 Adsorption. *J. Mater. Chem. C* **2020**, *8*, 4771–4779.
- (237) Morales-García, Á.; Fernández-Fernández, A.; Viñes, F.; Illas, F. CO_2 Abatement Using Two-Dimensional MXene Carbides. *J. Mater. Chem. A* **2018**, *6*, 3381–3385.
- (238) Handoko, A. D.; Steinmann, S. N.; Seh, Z. W. Theory-Guided Materials Design: Two-Dimensional MXenes in Electro- and Photocatalysis. *Nanoscale Horiz.* **2019**, *4*, 809–827.
- (239) Zhao, J.; Zhang, L.; Xie, X.-Y.; Li, X.; Ma, Y.; Liu, Q.; Fang, W.-H.; Shi, X.; Cui, G.; Sun, X. $\text{Ti}_3\text{C}_2\text{T}_x$ (T = F, OH) MXene Nanosheets: Conductive 2D Catalysts for Ambient Electrohydrogenation of N_2 to NH_3 . *J. Mater. Chem. A* **2018**, *6*, 24031–24035.
- (240) Williams, W. S. Transition Metal Carbides, Nitrides, and Borides for Electronic Applications. *JOM* **1997**, *49*, 38–42.
- (241) Harris, K. J.; Bugnet, M.; Naguib, M.; Barsoum, M. W.; Goward, G. R. Direct Measurement of Surface Termination Groups and Their Connectivity in the 2D MXene V_2CT_x Using NMR Spectroscopy. *J. Phys. Chem. C* **2015**, *119*, 13713–13720.
- (242) Schultz, T.; Frey, N. C.; Hantanasirisakul, K.; Park, S.; May, S. J.; Shenoy, V. B.; Gogotsi, Y.; Koch, N. Surface Termination Dependent Work Function and Electronic Properties of $\text{Ti}_3\text{C}_2\text{T}_x$ MXene. *Chem. Mater.* **2019**, *31*, 6590–6597.
- (243) Liu, Y.; Xiao, H.; Goddard, W. A. Schottky-Barrier-Free Contacts with Two-Dimensional Semiconductors by Surface-Engineered MXenes. *J. Am. Chem. Soc.* **2016**, *138*, 15853–15856.
- (244) Li, N.; Chen, X.; Ong, W.-J.; MacFarlane, D. R.; Zhao, X.; Cheetham, A. K.; Sun, C. Understanding of Electrochemical Mechanisms for CO_2 Capture and Conversion into Hydrocarbon Fuels in Transition-Metal Carbides (MXenes). *ACS Nano* **2017**, *11*, 10825–10833.
- (245) Zhang, X.; Zhang, Z.; Li, J.; Zhao, X.; Wu, D.; Zhou, Z. Ti_2CO_2 MXene: A Highly Active and Selective Photocatalyst for CO_2 Reduction. *J. Mater. Chem. A* **2017**, *5*, 12899–12903.
- (246) Abild-Pedersen, F.; Greeley, J.; Studt, F.; Rossmeisl, J.; Munter, T. R.; Moses, P. G.; Skúlason, E.; Bligaard, T.; Nørskov, J. K. Scaling Properties of Adsorption Energies for Hydrogen-Containing Molecules on Transition-Metal Surfaces. *Phys. Rev. Lett.* **2007**, *99*, 016105.
- (247) Li, Z.; Yu, L.; Milligan, C.; Ma, T.; Zhou, L.; Cui, Y.; Qi, Z.; Libretto, N.; Xu, B.; Luo, J.; Shi, E.; Wu, Z.; Xin, H.; Delgass, W. N.; Miller, J. T.; Wu, Y. Two-Dimensional Transition Metal Carbides as Supports for Tuning the Chemistry of Catalytic Nanoparticles. *Nat. Commun.* **2018**, *9*, 5258.
- (248) Penner, S.; Armbrüster, M. Formation of Intermetallic Compounds by Reactive Metal-Support Interaction: A Frequently Encountered Phenomenon in Catalysis. *ChemCatChem* **2015**, *7*, 374–392.
- (249) Tackett, B. M.; Sheng, W.; Chen, J. G. Opportunities and Challenges in Utilizing Metal-Modified Transition Metal Carbides as Low-Cost Electrocatalysts. *Joule* **2017**, *1*, 253–263.

- (250) Sun, X.; Gao, Y.; Zhao, C.; Deng, S.; Zhong, X.; Zhuang, G.; Wei, Z.; Wang, J. Palladium Dimer Supported on Mo₂CO₂ (MXene) for Direct Methane to Methanol Conversion. *Adv. Theory Simul.* **2019**, *2*, 1800158.
- (251) Wang, A.; Li, J.; Zhang, T. Heterogeneous Single-Atom Catalysis. *Nat. Rev. Chem.* **2018**, *2*, 65–81.
- (252) Zhao, D.; Chen, Z.; Yang, W.; Liu, S.; Zhang, X.; Yu, Y.; Cheong, W.-C.; Zheng, L.; Ren, F.; Ying, G.; Cao, X.; Wang, D.; Peng, Q.; Wang, G.; Chen, C. MXene (Ti₃C₂) Vacancy-Confining Single-Atom Catalyst for Efficient Functionalization of CO₂. *J. Am. Chem. Soc.* **2019**, *141*, 4086–4093.
- (253) Wu, J.; Huang, Y.; Ye, W.; Li, Y. CO₂ Reduction: From the Electrochemical to Photochemical Approach. *Adv. Sci.* **2017**, *4*, 1700194.
- (254) Maeda, K.; Teramura, K.; Saito, N.; Inoue, Y.; Domen, K. Improvement of Photocatalytic Activity of (Ga_{1-x}Zn_x)(N_{1-x}O_x) Solid Solution for Overall Water Splitting by Co-Loading Cr and Another Transition Metal. *J. Catal.* **2006**, *243*, 303–308.
- (255) Sels, B. F.; Voorde, M. H. van de. *Nanotechnology in Catalysis: Applications in the Chemical Industry, Energy Development, and Environment Protection*, 1st edition.; Nanotechnology innovation & applications; Wiley-VCH Verlag GmbH & Co. KGaA: Weinheim, 2017.
- (256) Fresno, F.; Villar-García, I. J.; Collado, L.; Alfonso-González, E.; Reñones, P.; Barawi, M.; de la Peña O’Shea, V. A. Mechanistic View of the Main Current Issues in Photocatalytic CO₂ Reduction. *J. Phys. Chem. Lett.* **2018**, *9*, 7192–7204.
- (257) Takanabe, K. Photocatalytic Water Splitting: Quantitative Approaches toward Photocatalyst by Design. *ACS Catal.* **2017**, *7*, 8006–8022.
- (258) Zhang, Y.; Xia, W.; Wu, Y.; Zhang, P. Prediction of MXene Based 2D Tunable Band Gap Semiconductors: GW Quasiparticle Calculations. *Nanoscale* **2019**, *11*, 3993–4000.
- (259) Yang, C.; Tan, Q.; Li, Q.; Zhou, J.; Fan, J.; Li, B.; Sun, J.; Lv, K. 2D/2D Ti₃C₂ MXene/g-C₃N₄ Nanosheets Heterojunction for High Efficient CO₂ Reduction Photocatalyst: Dual Effects of Urea. *Appl. Catal. B: Environ.* **2020**, *268*, 118738.
- (260) Tang, Q.; Sun, Z.; Deng, S.; Wang, H.; Wu, Z. Decorating G-C₃N₄ with Alkalinized Ti₃C₂ MXene for Promoted Photocatalytic CO₂ Reduction Performance. *J. Colloid Interface Sci.* **2020**, *564*, 406–417.
- (261) Martin, D. J.; Qiu, K.; Shevlin, S. A.; Handoko, A. D.; Chen, X.; Guo, Z.; Tang, J. Highly Efficient Photocatalytic H₂ Evolution from Water Using Visible Light and Structure-Controlled Graphitic Carbon Nitride. *Angew. Chem. Int. Ed.* **2014**, *53*, 9240–9245.
- (262) Jiang, J.; Mu, Z.; Zhao, P.; Wang, H.; Lin, Y. Photogenerated Charge Behavior of BiOI/g-C₃N₄ Photocatalyst in Photoreduction of Cr (VI): A Novel Understanding for High-Performance. *Mater. Chem. Phys.* **2020**, *252*, 123194.
- (263) Xu, Y.; Wang, S.; Yang, J.; Han, B.; Nie, R.; Wang, J.; Dong, Y.; Yu, X.; Wang, J.; Jing, H. Highly Efficient Photoelectrocatalytic Reduction of CO₂ on the Ti₃C₂/g-C₃N₄ Heterojunction with Rich Ti³⁺ and Pyri-N Species. *J. Mater. Chem. A* **2018**, *6*, 15213–15220.
- (264) Liu, X.; Xiao, J.; Peng, H.; Hong, X.; Chan, K.; Nørskov, J. K. Understanding Trends in Electrochemical Carbon Dioxide Reduction Rates. *Nat. Commun.* **2017**, *8*, 15438.

- (265) Shen, J.; Shen, J.; Zhang, W.; Yu, X.; Tang, H.; Zhang, M.; Zulfiqar; Liu, Q. Built-in Electric Field Induced CeO₂/Ti₃C₂-MXene Schottky-Junction for Coupled Photocatalytic Tetracycline Degradation and CO₂ Reduction. *Ceram. Int.* **2019**, *45*, 24146–24153.
- (266) Ye, M.; Wang, X.; Liu, E.; Ye, J.; Wang, D. Boosting the Photocatalytic Activity of P25 for Carbon Dioxide Reduction by Using a Surface-Alkalinized Titanium Carbide MXene as Cocatalyst. *ChemSusChem* **2018**, *11*, 1606–1611.
- (267) Xie, X.; Zhang, N.; Tang, Z.-R.; Anpo, M.; Xu, Y.-J. Ti₃C₂T_x MXene as a Janus Cocatalyst for Concurrent Promoted Photoactivity and Inhibited Photocorrosion. *Appl. Catal. B: Environ.* **2018**, *237*, 43–49.
- (268) Guo, J.; Peng, Q.; Fu, H.; Zou, G.; Zhang, Q. Heavy-Metal Adsorption Behavior of Two-Dimensional Alkalinization-Intercalated MXene by First-Principles Calculations. *J. Phys. Chem. C* **2015**, *119*, 20923–20930.
- (269) Shipman, M. A.; Symes, M. D. Recent Progress towards the Electrosynthesis of Ammonia from Sustainable Resources. *Catal. Today* **2017**, *286*, 57–68.
- (270) Honkala, K. Ammonia Synthesis from First-Principles Calculations. *Science* **2005**, *307*, 555–558.
- (271) Gao, Y.; Zhuo, H.; Cao, Y.; Sun, X.; Zhuang, G.; Deng, S.; Zhong, X.; Wei, Z.; Wang, J. A Theoretical Study of Electrocatalytic Ammonia Synthesis on Single Metal Atom/MXene. *Chin. J. Catal.* **2019**, *40*, 152–159.
- (272) Yao, Y.; Zhu, S.; Wang, H.; Li, H.; Shao, M. A Spectroscopic Study on the Nitrogen Electrochemical Reduction Reaction on Gold and Platinum Surfaces. *J. Am. Chem. Soc.* **2018**, *140*, 1496–1501.
- (273) Zhao, J.; Chen, Z. Single Mo Atom Supported on Defective Boron Nitride Monolayer as an Efficient Electrocatalyst for Nitrogen Fixation: A Computational Study. *J. Am. Chem. Soc.* **2017**, *139*, 12480–12487.
- (274) Zheng, S.; Li, S.; Mei, Z.; Hu, Z.; Chu, M.; Liu, J.; Chen, X.; Pan, F. Electrochemical Nitrogen Reduction Reaction Performance of Single-Boron Catalysts Tuned by MXene Substrates. *J. Phys. Chem. Lett.* **2019**, *10*, 6984–6989.
- (275) Wang, S.; Li, B.; Li, L.; Tian, Z.; Zhang, Q.; Chen, L.; Zeng, X. C. Highly Efficient N₂ Fixation Catalysts: Transition-Metal Carbides M₂C (MXenes). *Nanoscale* **2020**, *12*, 538–547.
- (276) Shao, M.; Shao, Y.; Chen, W.; Ao, K. L.; Tong, R.; Zhu, Q.; Chan, I. N.; Ip, W. F.; Shi, X.; Pan, H. Efficient Nitrogen Fixation to Ammonia on MXenes. *Phys. Chem. Chem. Phys.* **2018**, *20*, 14504–14512.
- (277) Azofra, L. M.; Li, N.; MacFarlane, D. R.; Sun, C. Promising Prospects for 2D d²-d⁴ M₃C₂ Transition Metal Carbides (MXenes) in N₂ Capture and Conversion into Ammonia. *Energy Environ. Sci.* **2016**, *9*, 2545–2549.
- (278) Gao, Y.; Cao, Y.; Zhuo, H.; Sun, X.; Gu, Y.; Zhuang, G.; Deng, S.; Zhong, X.; Wei, Z.; Li, X.; Wang, J. Mo₂TiC₂ MXene: A Promising Catalyst for Electrocatalytic Ammonia Synthesis. *Catal. Today* **2020**, *339*, 120–126.
- (279) Luo, Y.; Chen, G.-F.; Ding, L.; Chen, X.; Ding, L.-X.; Wang, H. Efficient Electrocatalytic N₂ Fixation with MXene under Ambient Conditions. *Joule* **2019**, *3*, 279–289.

- (280) Liao, Y.; Qian, J.; Xie, G.; Han, Q.; Dang, W.; Wang, Y.; Lv, L.; Zhao, S.; Luo, L.; Zhang, W.; Jiang, H.-Y.; Tang, J. 2D-Layered Ti_3C_2 MXenes for Promoted Synthesis of NH_3 on P25 Photocatalysts. *Appl. Catal. B: Environ.* **2020**, *273*, 119054.
- (281) Suryanto, B. H. R.; Du, H.-L.; Wang, D.; Chen, J.; Simonov, A. N.; MacFarlane, D. R. Challenges and Prospects in the Catalysis of Electroreduction of Nitrogen to Ammonia. *Nat. Catal.* **2019**, *2*, 290–296.
- (282) Zhao, Y.; Shi, R.; Bian, X.; Zhou, C.; Zhao, Y.; Zhang, S.; Wu, F.; Waterhouse, G. I. N.; Wu, L.; Tung, C.; Zhang, T. Ammonia Detection Methods in Photocatalytic and Electrocatalytic Experiments: How to Improve the Reliability of NH_3 Production Rates? *Adv. Sci.* **2019**, *6*, 1802109.
- (283) Andersen, S. Z.; Čolić, V.; Yang, S.; Schwalbe, J. A.; Nielander, A. C.; McEnaney, J. M.; Enemark-Rasmussen, K.; Baker, J. G.; Singh, A. R.; Rohr, B. A.; Statt, M. J.; Blair, S. J.; Mezzavilla, S.; Kibsgaard, J.; Vesborg, P. C. K.; Cargnello, M.; Bent, S. F.; Jaramillo, T. F.; Stephens, I. E. L.; Nørskov, J. K.; Chorkendorff, I. A Rigorous Electrochemical Ammonia Synthesis Protocol with Quantitative Isotope Measurements. *Nature* **2019**, *570*, 504–508.
- (284) Habib, T.; Zhao, X.; Shah, S. A.; Chen, Y.; Sun, W.; An, H.; Lutkenhaus, J. L.; Radovic, M.; Green, M. J. Oxidation Stability of $\text{Ti}_3\text{C}_2\text{T}_x$ MXene Nanosheets in Solvents and Composite Films. *npj 2D Mater. Appl.* **2019**, *3*, 8.
- (285) Li, L.; Wang, X.; Guo, H.; Yao, G.; Yu, H.; Tian, Z.; Li, B.; Chen, L. Theoretical Screening of Single Transition Metal Atoms Embedded in MXene Defects as Superior Electrocatalyst of Nitrogen Reduction Reaction. *Small Methods* **2019**, *3*, 1900337.
- (286) Huang, B.; Li, N.; Ong, W.-J.; Zhou, N. Single Atom-Supported MXene: How Single-Atomic-Site Catalysts Tune the High Activity and Selectivity of Electrochemical Nitrogen Fixation. *J. Mater. Chem. A* **2019**, *7*, 27620–27631.
- (287) Su, Y.-Q.; Wang, Y.; Liu, J.-X.; Filot, I. A. W.; Alexopoulos, K.; Zhang, L.; Muravev, V.; Zijlstra, B.; Vlachos, D. G.; Hensen, E. J. M. Theoretical Approach To Predict the Stability of Supported Single-Atom Catalysts. *ACS Catal.* **2019**, *9*, 3289–3297.
- (288) Liu, A.; Gao, M.; Ren, X.; Meng, F.; Yang, Y.; Yang, Q.; Guan, W.; Gao, L.; Liang, X.; Ma, T. A Two-Dimensional Ru@MXene Catalyst for Highly Selective Ambient Electrocatalytic Nitrogen Reduction. *Nanoscale* **2020**, *12*, 10933–10938.
- (289) Liu, D.; Zhang, G.; Ji, Q.; Zhang, Y.; Li, J. Synergistic Electrocatalytic Nitrogen Reduction Enabled by Confinement of Nanosized Au Particles onto a Two-Dimensional Ti_3C_2 Substrate. *ACS Appl. Mater. Interfaces* **2019**, *11*, 25758–25765.
- (290) Peng, W.; Luo, M.; Xu, X.; Jiang, K.; Peng, M.; Chen, D.; Chan, T.; Tan, Y. Spontaneous Atomic Ruthenium Doping in Mo_2CT_x MXene Defects Enhances Electrocatalytic Activity for the Nitrogen Reduction Reaction. *Adv. Energy Mater.* **2020**, *10*, 2001364.
- (291) Kong, W.; Gong, F. (Frank); Zhou, Q.; Yu, G.; Ji, L.; Sun, X.; Asiri, A. M.; Wang, T.; Luo, Y.; Xu, Y. An MnO_2 - $\text{Ti}_3\text{C}_2\text{T}_x$ MXene Nanohybrid: An Efficient and Durable Electrocatalyst toward Artificial N_2 Fixation to NH_3 under Ambient Conditions. *J. Mater. Chem. A* **2019**, *7*, 18823–18827.
- (292) Zhang, J.; Yang, L.; Wang, H.; Zhu, G.; Wen, H.; Feng, H.; Sun, X.; Guan, X.; Wen, J.; Yao, Y. *In Situ* Hydrothermal Growth of TiO_2 Nanoparticles on a Conductive $\text{Ti}_3\text{C}_2\text{T}_x$

- MXene Nanosheet: A Synergistically Active Ti-Based Nanohybrid Electrocatalyst for Enhanced N₂ Reduction to NH₃ at Ambient Conditions. *Inorg. Chem.* **2019**, *58*, 5414–5418.
- (293) Liu, Q.; Ai, L.; Jiang, J. MXene-Derived TiO₂@C/g-C₃N₄ Heterojunctions for Highly Efficient Nitrogen Photofixation. *J. Mater. Chem. A* **2018**, *6*, 4102–4110.
- (294) Wang, H.; Zhao, R.; Qin, J.; Hu, H.; Fan, X.; Cao, X.; Wang, D. MIL-100(Fe)/Ti₃C₂ MXene as a Schottky Catalyst with Enhanced Photocatalytic Oxidation for Nitrogen Fixation Activities. *ACS Appl. Mater. Interfaces* **2019**, *11*, 44249–44262.
- (295) Pang, S.-Y.; Wong, Y.-T.; Yuan, S.; Liu, Y.; Tsang, M.-K.; Yang, Z.; Huang, H.; Wong, W.-T.; Hao, J. Universal Strategy for HF-Free Facile and Rapid Synthesis of Two-Dimensional MXenes as Multifunctional Energy Materials. *J. Am. Chem. Soc.* **2019**, *141*, 9610–9616.
- (296) Li, Y.; Shao, H.; Lin, Z.; Lu, J.; Liu, L.; Duployer, B.; Persson, P. O. Å.; Eklund, P.; Hultman, L.; Li, M.; Chen, K.; Zha, X.-H.; Du, S.; Rozier, P.; Chai, Z.; Raymundo-Piñero, E.; Taberna, P.-L.; Simon, P.; Huang, Q. A General Lewis Acidic Etching Route for Preparing MXenes with Enhanced Electrochemical Performance in Non-Aqueous Electrolyte. *Nat. Mater.* **2019**, *19*, 894–899.
- (297) Natu, V.; Pai, R.; Sokol, M.; Carey, M.; Kalra, V.; Barsoum, M. W. 2D Ti₃C₂T_z MXene Synthesized by Water-Free Etching of Ti₃AlC₂ in Polar Organic Solvents. *Chem* **2020**, *6*, 616–630.
- (298) Zhang, C. J.; Pinilla, S.; McEvoy, N.; Cullen, C. P.; Anasori, B.; Long, E.; Park, S.-H.; Seral-Ascaso, A.; Shmeliov, A.; Krishnan, D.; Morant, C.; Liu, X.; Duesberg, G. S.; Gogotsi, Y.; Nicolosi, V. Oxidation Stability of Colloidal Two-Dimensional Titanium Carbides (MXenes). *Chem. Mater.* **2017**, *29*, 4848–4856.
- (299) Chen, H.; Wen, Y.; Qi, Y.; Zhao, Q.; Qu, L.; Li, C. Pristine Titanium Carbide MXene Films with Environmentally Stable Conductivity and Superior Mechanical Strength. *Adv. Funct. Mater.* **2020**, *30*, 1906996.
- (300) Zhao, X.; Vashisth, A.; Prehn, E.; Sun, W.; Shah, S. A.; Habib, T.; Chen, Y.; Tan, Z.; Lutkenhaus, J. L.; Radovic, M.; Green, M. J. Antioxidants Unlock Shelf-Stable Ti₃C₂T_x (MXene) Nanosheet Dispersions. *Matter* **2019**, *1*, 513–526.
- (301) Maleski, K.; Mochalin, V. N.; Gogotsi, Y. Dispersions of Two-Dimensional Titanium Carbide MXene in Organic Solvents. *Chem. Mater.* **2017**, *29*, 1632–1640.
- (302) Kim, D.; Ko, T. Y.; Kim, H.; Lee, G. H.; Cho, S.; Koo, C. M. Nonpolar Organic Dispersion of 2D Ti₃C₂T_x MXene Flakes *via* Simultaneous Interfacial Chemical Grafting and Phase Transfer Method. *ACS Nano* **2019**, *13*, 13818–13828.
- (303) Jin, D.; Johnson, L. R.; Raman, A. S.; Ming, X.; Gao, Y.; Du, F.; Wei, Y.; Chen, G.; Vojvodic, A.; Gogotsi, Y.; Meng, X. Computational Screening of 2D Ordered Double Transition-Metal Carbides (MXenes) as Electrocatalysts for Hydrogen Evolution Reaction. *J. Phys. Chem. C* **2020**, *124*, 10584–10592.
- (304) Pinto, D.; Anasori, B.; Avireddy, H.; Shuck, C. E.; Hantanasirisakul, K.; Deysheer, G.; Morante, J. R.; Porzio, W.; Alshareef, H. N.; Gogotsi, Y. Synthesis and Electrochemical Properties of 2D Molybdenum Vanadium Carbides – Solid Solution MXenes. *J. Mater. Chem. A* **2020**, *8*, 8957–8968.

- (305) Djire, A.; Bos, A.; Liu, J.; Zhang, H.; Miller, E. M.; Neale, N. R. Pseudocapacitive Storage in Nanolayered Ti_2NT_x MXene Using Mg-Ion Electrolyte. *ACS Appl. Nano Mater.* **2019**, *2*, 2785–2795.
- (306) Urbankowski, P.; Anasori, B.; Hantanasirisakul, K.; Yang, L.; Zhang, L.; Haines, B.; May, S. J.; Billinge, S. J. L.; Gogotsi, Y. 2D Molybdenum and Vanadium Nitrides Synthesized by Ammoniation of 2D Transition Metal Carbides (MXenes). *Nanoscale* **2017**, *9*, 17722–17730.
- (307) Xiao, X.; Yu, H.; Jin, H.; Wu, M.; Fang, Y.; Sun, J.; Hu, Z.; Li, T.; Wu, J.; Huang, L.; Gogotsi, Y.; Zhou, J. Salt-Templated Synthesis of 2D Metallic MoN and Other Nitrides. *ACS Nano* **2017**, *11*, 2180–2186.
- (308) Ye, C.; Jiao, Y.; Jin, H.; Slattery, A. D.; Davey, K.; Wang, H.; Qiao, S. 2D MoN-VN Heterostructure To Regulate Polysulfides for Highly Efficient Lithium-Sulfur Batteries. *Angew. Chem. Int. Ed.* **2018**, *57*, 16703–16707.
- (309) Jin, H.; Liu, X.; Vasileff, A.; Jiao, Y.; Zhao, Y.; Zheng, Y.; Qiao, S.-Z. Single-Crystal Nitrogen-Rich Two-Dimensional Mo_5N_6 Nanosheets for Efficient and Stable Seawater Splitting. *ACS Nano* **2018**, *12*, 12761–12769.
- (310) Singh, M. R.; Goodpaster, J. D.; Weber, A. Z.; Head-Gordon, M.; Bell, A. T. Mechanistic Insights into Electrochemical Reduction of CO_2 over Ag Using Density Functional Theory and Transport Models. *Proc Natl Acad Sci USA* **2017**, *114*, E8812–E8821.
- (311) Goodpaster, J. D.; Bell, A. T.; Head-Gordon, M. Identification of Possible Pathways for C–C Bond Formation during Electrochemical Reduction of CO_2 : New Theoretical Insights from an Improved Electrochemical Model. *J. Phys. Chem. Lett.* **2016**, *7*, 1471–1477.
- (312) Cheng, T.; Wang, L.; Merinov, B. V.; Goddard, W. A. Explanation of Dramatic PH-Dependence of Hydrogen Binding on Noble Metal Electrode: Greatly Weakened Water Adsorption at High PH. *J. Am. Chem. Soc.* **2018**, *140*, 7787–7790.